

SYNTHESES AND CHARACTERIZATION OF A SERIES OF
BINUCLEAR IRIDIUM COMPLEXES

Thesis by
Terrance Patrick Smith

In Partial Fulfillment of the Requirements
for the Degree of
Doctor of Philosophy

California Institute of Technology
Pasadena, California

1982

(Submitted March 8, 1982)

TABLE OF CONTENTS

	<u>Page</u>
<u>CHAPTER 1</u> - Introduction	1
<u>CHAPTER 2</u> - Synthesis and Characterization of Ir ₂ (TMB) ₄ (BPh ₄) ₂	18
Section 1 - Introduction	19
Section 2 - Experimental	21
Section 3 - Spectroscopy	24
Section 4 - Electrochemistry	41
Section 5 - Conclusions and Prospects	48
<u>CHAPTER 3</u> - Syntheses and Characterization of Oxidative Addition Adducts of Ir ₂ (TMB) ₄ (BPh ₄) ₂	51
<u>Part A</u> - Reactivity of Ir ₂ (TMB) ₄ (BPh ₄) ₂	
Section 1 - Introduction	52
Section 2 - Experimental	54
Section 3 - Reactions with halogens and methyl iodide	57
Section 4 - Reactions with hydrogen chloride	58
Section 5 - Reactions with other small molecules	73
Section 6 - Conclusions	74
<u>Part B</u> - Physical Studies on Ir ₂ (TMB) ₄ X ₂ (BPh ₄) ₂	
Section 1 - Introduction	76
Section 2 - Experimental	77
Section 3 - Electronic Absorption Spectroscopy	80
Section 4 - Raman and FIR Studies	91

	<u>Page</u>
Section 5 - Dynamic ^1H NMR	107
Section 6 - Preliminary X-Ray Studies on Ir(TMB) $_4$ I $_2$ (BPh $_4$) $_2$	125
APPENDIX I - Spectroscopic Studies on Pyrazolyl- Bridge Binuclear Complexes	131
REFERENCES AND NOTES	146

ACKNOWLEDGEMENTS

Harry Gray is thanked for his support and input into this project. I would particularly like to thank Emily Maverick, Jan Najdzionek, Steve Milder and Ann English for help on specific experiments. Scientific discussions with John Bercau, Dick Marsh, Vinnie Miskowski, Jay Winkler, Ken Janda, and Andy Maverick were greatly appreciated.

I would also like to thank Pete Wolczanski, Steve Rice and Leslie Carey, Mark and Laurie Paffett, Jay Audett, John Buhr and Vanesse Lum, and Jimmy Mayer for some of the more interesting (non-scientific) moments at Caltech. Dan Strauss, Eric Moore, and Bob Grubbs are thanked for successfully belaying me on more than one occasion. My roommate, Eric, deserves special mention for putting up with my housekeeping for the last 4.5 years. The typing expertise of Mary Arguijo and the artistry of Valerie Purvis are ever so gratefully acknowledged.

Last, but not least, I would especially like to thank Lynn, Mom, Dad, Sean, Alyson, and Cate for making the struggle seem worthwhile.

To my parents

ABSTRACT

A binuclear iridium(I) isocyanide complex has been synthesized and its photophysics and chemistry have been investigated. The complex, $\text{Ir}_2(\text{TMB})_4^{2+}$ (TMB = 2,5-dimethyl 2,5 diisocyanohexane), possesses an intense absorption band maximizing at 625 nm in the visible region. Excitation into this feature results in two long wavelength luminescence bands at 735 nm and 1080 nm. The longer wavelength feature has been assigned as phosphorescence ($E(^3A_2) \rightarrow A_1(^1A_1)$) from the lowest electronic excited state; the lifetime of this state is 200 ns and is independent of temperature between 77 K and 298 K. In contrast, the $E(^3A_2)$ excited state of the analogous rhodium complex exhibits a dramatic temperature dependence. This difference is ascribed to the proximity of ligand field states to the lowest excited state; in the rhodium case the ligand field states are thermally accessible whereas for the iridium case they lie at much higher energy.

The d^8-d^8 iridium complex oxidatively adds a variety of small molecules (*e.g.* I_2 , Br_2 , Cl_2 , CH_3I and HCl). The reactivity is quite similar to that of the analogous rhodium system ($\text{Rh}_2(\text{TMB})_4^{2+}$). One interesting difference is the fact that the HCl adduct of $\text{Rh}_2(\text{TMB})_4^{2+}$ is directly observable only at low temperature. Nonetheless, a similar hydride species is postulated as an important

intermediate in the production of hydrogen in another binuclear rhodium system.

A number of spectroscopic methods have been employed to explore the bonding in symmetric oxidative addition adducts. A linear correlation between metal-metal force constant and intermetallic distance has been uncovered. The structure of the iodine adduct, $\text{Ir}_2(\text{TMB})_4\text{I}_2(\text{BPh}_4)_2$, has been determined; the intermetallic distance is $2.803(4) \text{ \AA}$. Also, dynamic ^1H NMR reveals that binuclear complexes containing the TMB ligand are rapidly undergoing conformation changes at ambient temperatures; the activation barriers for this process range from 12 to 15 kcal/mole.

CHAPTER 1

Introduction

The anisotropic optical and electrical behaviors exhibited by certain solids based on square planar group VIII metal complexes have fascinated researchers for over a century. Of these materials, the bronze-colored Krogman's salt, $K_2Pt(CN)_4Br_{\sim 0.3} \cdot 3H_2O(KCP)$, has received the most attention and contributed the most to our understanding of these systems. The high electrical conductivity and reflectivity of KCP are associated with the infinite columns formed by a stacking of tetracyanoplatinate units face-to-face such that the metals are aligned in a collinear fashion. The short intermetallic distance $(2.89 \text{ \AA})^1$ is indicative of a substantial metal-metal interaction. Studies on other solids derived from $Pt(CN)_4^{2-}$ have demonstrated the relationship between the extent of interaction and the physical properties. Factors that are important in controlling metal-metal distances are: the counter ion, the degree of hydration, the type and amount of oxidant. By the judicious choice of these conditions the solids can be made colorless to metallic and insulating to conducting.²

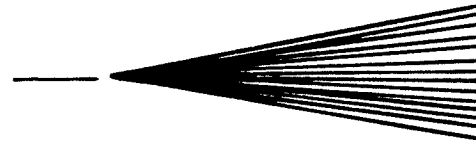
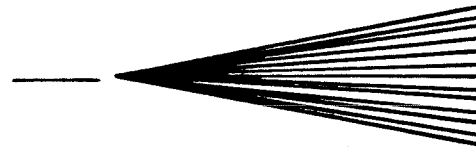
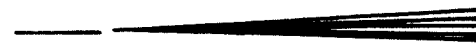
A considerable amount of theoretical and experimental work has been carried out on the electronic structures of $Pt(CN)_4^{2-}$ and of its one-dimensional derivatives. The tetracyanoplatinate ion possesses D_{4h} symmetry and the following ordering of the 5d orbitals has been proposed: $b_{2g}(xy) < e_g(xz, yz) < a_{1g}(z^2) \ll b_{1g}(x^2 - y^2)$.³ The highest occupied molecular orbital (HOMO) is the $a_{1g}(z^2)$ orbital whereas the

lowest unoccupied molecular orbital (LUMO) is predominantly ligand π -antibonding, stabilized to some extent by interaction with the $6p_z$ orbital. The lowest energy bands in the optical spectrum are therefore expected to be metal-to-ligand charge transfer transitions, assignments which have been confirmed by single crystal studies.⁴

The correlation diagram showing the effect of platinum-platinum spacing (in an infinite chain structure) on the molecular orbitals is shown in Figure 1. We note that at large separation the molecular orbitals correspond to those in the monomer but as the intermetallic distance decreases considerable overlap occurs resulting in the formation of bands. Unlike bands found in pure metals, however, these bands are associated with only the z-direction, a consequence of the extensive interaction between $5d_{z^2}$ and $6p_z$ orbitals. In Krogman's salt, some of the electrons have been removed from the valence band, decreasing the average energy of an electron and giving rise to the metallic properties.

Band formation is contingent on the presence of a sufficient number of orbitals (or monomeric units). If this condition is not met, one might expect to find materials which have properties quite unlike those in either the corresponding monomers or infinite chains. It is this type of complex which has piqued the interest of our group.

Figure 1. Qualitative diagram showing the effect of the intermetallic distance on the molecular orbitals of $\text{Pt}(\text{CN})_4^{2-}$.

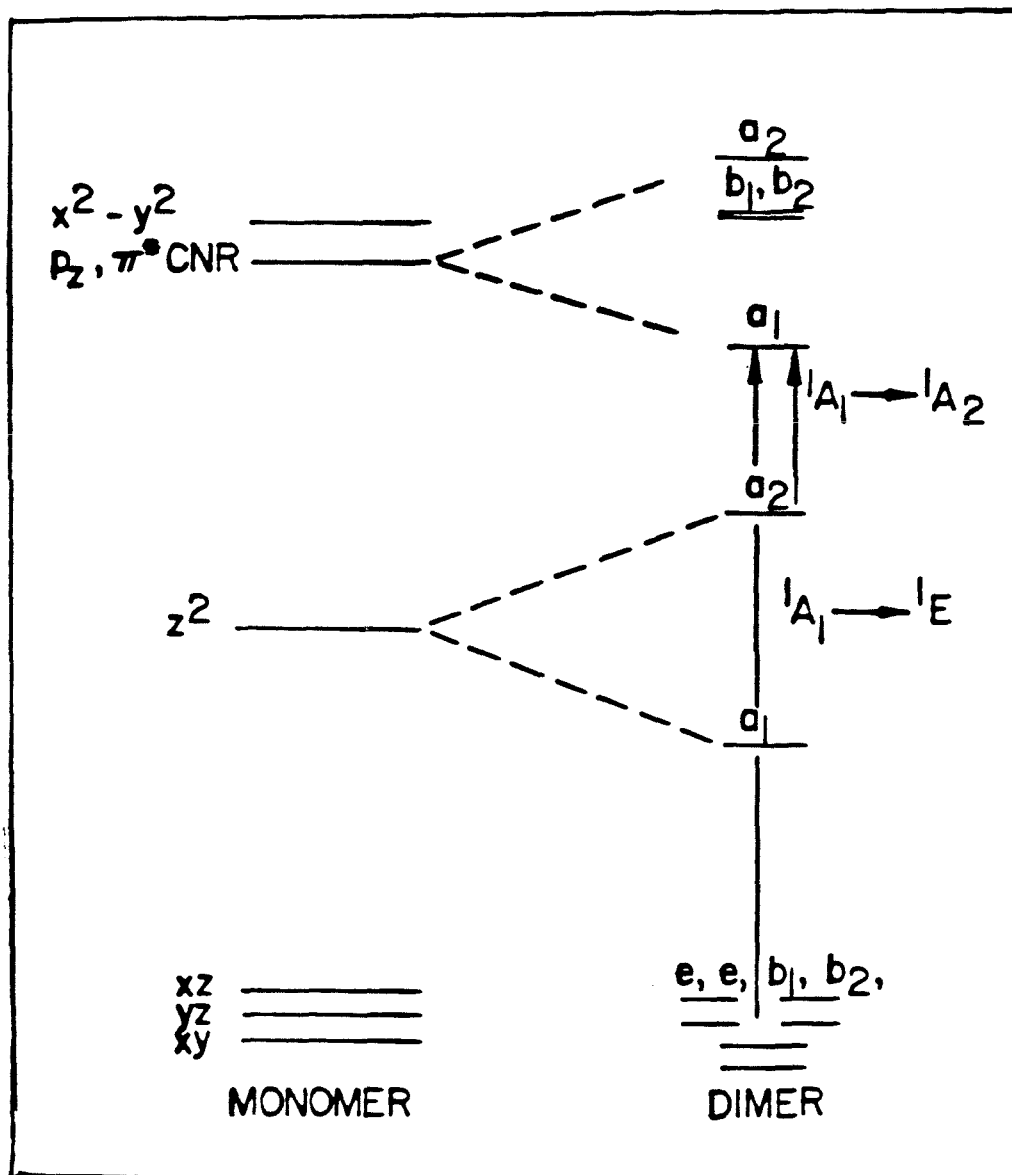
$dx^2 - y^2$ CN $\pi^* + p_z$  dz^2  dxz, dyz  xy DECREASING INTERMETALLIC
DISTANCE

For years rhodium(I) and iridium(I) isocyanide complexes have been suspected of existing as oligomers owing to their intense color, uncharacteristic of d^8 complexes possessing π -acceptor ligands.^{5,6} However, it wasn't until Mann *et al.* demonstrated that the absorbances in the visible and near-infrared region of the spectrum were not linearly related to the concentration of monomer but to some root (*e.g.* square, cube, etc.) of monomer concentration that the extent of oligomerization was realized.⁷ The existence of discrete species was later confirmed by X-ray diffraction analysis on a binuclear species.⁸

The metal-metal bonding in these oligomers cannot be explained solely on consideration of the occupied orbitals because each monomer has a closed-shell configuration. Yet, some bonding force must be present in order to overcome the electrostatic repulsion between the square planar units. We now believe that the bonding is due to a configurational interaction between the filled d_{z^2} and the empty p_z orbitals of the same symmetry which results in a net stabilization of the dimer. A molecular orbital diagram, taking into account these considerations, is shown in Figure 2. This diagram is useful in explaining a great deal of the chemistry and photophysics of these systems.

The study of the oligomers was complicated by the equilibria which exist between the various species in solution. In order to promote the formation of a single

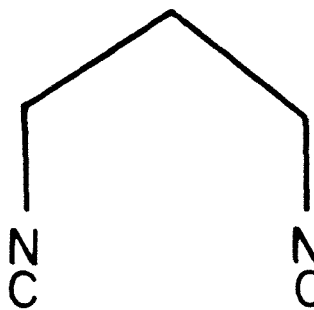
Figure 2. Molecular orbital diagram for d^8-d^8 dimers.



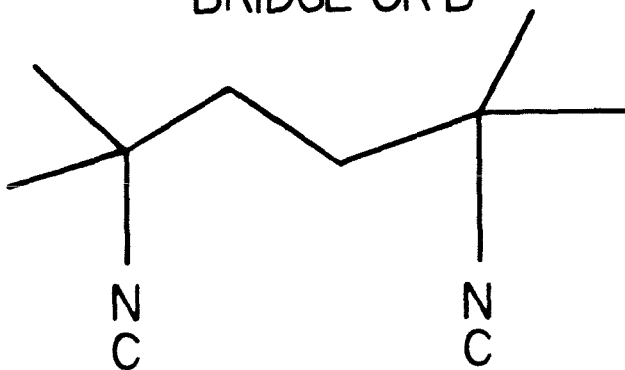
species a series of diisocyanoalkanes were synthesized. The ligands (Figure 3) were chosen to favor the formation of dimeric complexes; a strategy which has proven quite successful as only binuclear rhodium species are observed in the absence of oxidizing material. Figure 3 also shows the range of bite distances found for each of the ligands. The flexibility and steric properties of the diisocyanoalkanes have profound effects on the chemistry and photophysics of the metal complexes. By far the most demanding ligand is 1,3 diisocyanopropane (B) requiring an eclipsed geometry and possessing the smallest range of bite distance; 2,5 dimethyl 2,5-diisocyano-hexane (TMB) is somewhat more flexible and in one example has been shown to chelate.⁹ The configuration adopted by these ligands is illustrated in Figure 4 for $\text{Rh}_2(\text{B})_4^{2+}$ and $\text{Rh}_2(\text{TMB})_4^{2+}$, where the inter-metallic distances are 3.24 Å and 3.26 Å, respectively.¹⁰

The predominant mode of reactivity of monomeric rhodium(I) and iridium(I) complexes is oxidative addition. The products can be either cis or trans, depending on the substrate, and formally, the metal center is oxidized by two electrons. Not surprisingly, the binuclear complexes also undergo oxidative addition reactions. In this case, however, each metal is oxidized by one electron and only trans addition products are isolated. The two electrons which are transferred come from a metal-metal antibonding orbital (see MO diagram) and the result is formation of a

Figure 3. The diisocyanoalkane ligands and their range of bite distances.



2.84 - 3.24 Å
1,3 DIISOCYANOPROPANE
BRIDGE OR B



2.77 - 3.28 Å
2,5 DIMETHYL - 2,5 DIISOCYANOHEXANE
TMB

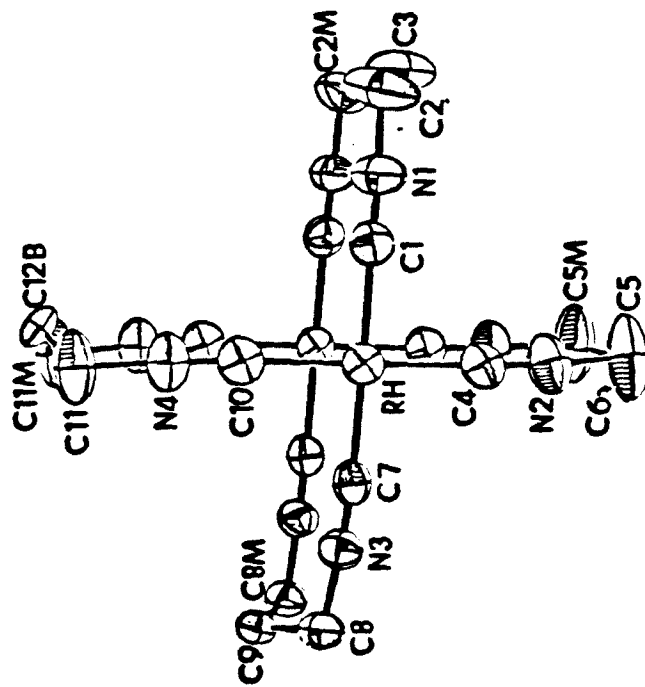


4.33 - 4.45 Å
1,8 DIISOCYANO-P-DIMETHANE
DMB

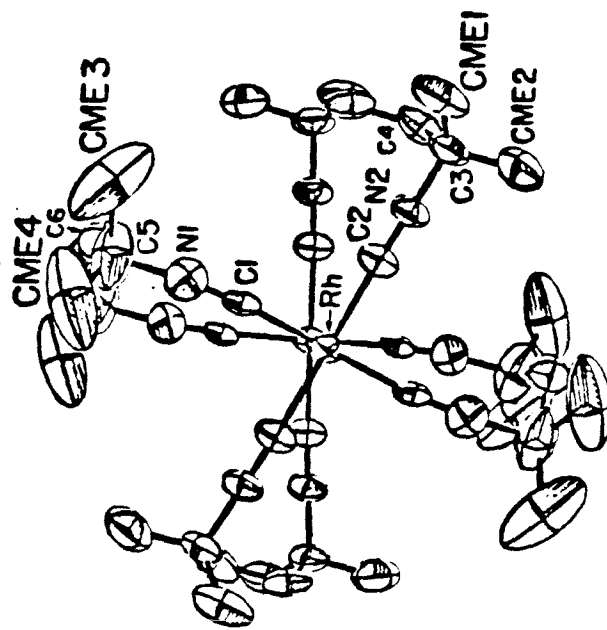
Figure 4. ORTEP drawings of $\text{Rh}_2(\text{B})_4^{2+}$ and $\text{Rh}_2(\text{TMB})_4^{2+}$.



3.24 Å



3.26 Å



single metal-metal bond. The presence of this bond has been verified by X-ray diffraction analysis of $\text{Rh}(\text{B})_4\text{Cl}_2^{2+}$ ¹¹ and $\text{Rh}_2(\text{TMB})_4\text{Cl}_2^{2+}$ ¹²; the intermetallic distances are 2.84 Å and 2.77 Å, respectively. These distances are considerably shorter (~ 0.4 Å) than those found in the corresponding rhodium(I) complexes. Other manifestation of the metal-metal bond have been observed spectroscopically. Both the Raman and uv-vis spectra have specific features that can be ascribed to the presence of a metal-metal bond.^{13,14} Furthermore, these features are very sensitive to the axial ligands, providing a valuable means of following reactions.

The rhodium(I) and rhodium(II) dimers constitute end members in a family of polynuclear complexes possessing an average oxidation state between one and two. The deep blue ion $\text{Rh}_4(\text{B})_8^{6+}$ was the first mixed-valent complex discovered and has elicited considerable study. It is produced by the reaction of $\text{Rh}_2(\text{B})_4^{2+}$ with hydrohalic acids. When $\text{Rh}_4(\text{B})_8^{6+}$ is irradiated at 580 nm in oxygen-free HCl, hydrogen and $\text{Rh}_2(\text{B})_4\text{Cl}_2^{2+}$ are formed. The tetranuclear ion can be regenerated by removing the light source, thus establishing the storage of energy. This result generated a great deal of excitement because very few photochemical systems produce hydrogen in the absence of a heterogeneous

catalysis and still are responsive to wavelengths of light prominent in the solar spectrum.¹⁵

The structure of the blue species and the average oxidation state of the rhodiums were not determined for years after its original discovery. Initially, it was thought that the mixed-valent ion was a hydrido-chloride adduct and that the anomalous color (all other oxidation products are yellow) was due to the weakening of the metal-metal bond by a trans influence exerted by the hydride.¹⁶ However, careful ^1H NMR and IR measurements failed to show any indication of a metal-hydrogen bond. Furthermore, no isotope effect was detected in the reaction that produced hydrogen. The first indication that the blue species was a tetranuclear complex came from flash photolysis studies in acid solution under conditions where no net hydrogen production was observed. In these experiments, a transient with an absorbance at ~ 400 nm was produced after micro-second irradiation into the principal absorption band of the blue species ($\lambda_{\text{max}} = 560$ nm). This transient decayed with second order kinetics and the ionic strength dependence of the decay indicated that two highly charged species ($\sim 3^+$) were recombining to form the starting complex.¹⁷

Eventually, the crystal structure of the blue ion was determined, verifying its tetranuclear nature; however, some ambiguity still remained regarding the oxidation state

of the rhodiums. This was because the crystals were grown from acidic solution and a number of water molecules were incorporated into the unit cell and the presence of hydronium ions could not be precluded.¹⁸ The average valence of 1.5 per rhodium was finally determined by an elegant series of experiments by Sigal *et al.* The first of these studies involved measuring the quantity of gas produced in the thermal reaction of $\text{Rh}_2(\text{B})_4^{2+}$ with concentrated acid; the $\text{H}_2/\text{Rh}_2(\text{B})_4^{2+}$ ratio was found to be 0.5. The electron count was also confirmed by redox titrations on the tetranuclear ion and the fully oxidized species.¹⁹

In addition to $\text{Rh}_4(\text{B})_8^{6+}$, a number of other oligomers have been found to possess non-integral oxidation states. They are produced by reacting an appropriate amount of $\text{Rh}_2(\text{B})_4^{2+}$ with $\text{Rh}_4(\text{B})_8^{6+}$. Oligomers containing up to 12 rhodiums have been characterized spectroscopically. A closely related series of complexes containing the $\text{Rh}_2(\text{TMB})_4$ moiety was also synthesized. Because of the steric hindrance provided by the methyl (of the TMB ligand) the extent of oligomerization could be more easily controlled.

The discovery of a long-lived excited state in $\text{Rh}_2(\text{B})_4^{2+}$ has been one of the most important developments in our laboratory.²¹ Milder *et al.*²² were the first to recognize that the excited triplet state ($^3\text{A}_{2u}$) was capable of undergoing bimolecular reactions. Investigations involving electron acceptors and donors have demonstrated that the

triplet state is both a powerful oxidant and a reductant. Also, whereas the photochemistry discussed on page 14 appears to be a special case, all binuclear rhodium(I) complexes possess long-lived excited states which can be quenched. The lifetimes of the $^3A_{2u}$ state are very dependent on the specific ligand, and in many cases display a marked temperature dependence; the reason for these differences is still a matter of some speculation.²³

The nature of the excited state of $Rh_2(B)_4^{2+}$ has been extensively examined. Rice and Gray²⁴ have found that there is a stronger metal-metal interaction in the excited state than in the ground state. Qualitatively, this is evidenced by the change of metal-metal stretching frequencies from a ground state value of 80 cm^{-1} to an excited state value of 140 cm^{-1} . A Franck-Condon analysis has revealed that the metal-metal contraction is substantial, $\sim 0.3\text{ \AA}$, placing the metal-metal distance close to that of the oxidized species. One of the conclusions drawn from this study was that the lowest energy transition is best described as a $\sigma^*(d_{z^2}) \rightarrow \sigma(p_z)$ transition.

The diverse chemistry displayed by the polynuclear rhodium systems encouraged us to extend our investigation to include other metals. The most promising candidates appeared to be iridium, platinum, palladium, and cobalt. This report deals with the synthesis, characterization, and general exploration of the chemistry of binuclear complexes of iridium.

CHAPTER II

Synthesis and Characterization of a Binuclear
Iridium(I) Complex

INTRODUCTION

The study of electronic excited states is an active area of research, for reasons which include:

1) On a fundamental level, excited states offer a test of our current theories on structure and bonding; 2) the high energy of these species provides an unique opportunity to explore extremely exothermic reactions; 3) in this same context, excited states can be prepared very rapidly (nanosecond or even picoseconds), allowing kinetic studies to be carried out on systems that could not be examined by conventional techniques; and 4) excited state molecules are potentially capable of mediating the conversion of radiant energy to either chemical or electrical energy.

Determining how excited states decay is one of the most challenging problems faced by today's physical chemist. Deactivation can occur by chemical reactions (*e.g.* ligand dissociation, or electron transfer); and to a large extent these processes can be understood in terms of the redistribution of electron density caused by the absorption of a photon.²⁵ Other equally important processes are emission, intersystem crossing, and internal conversion. The factors that influence these pathways tend to be more subtle and deserve more attention. The metal, obviously, exercises a critical role in determining many of the intrinsic properties of an electronic excited state. And yet, aside from the work done on the

metal-bipyridine and metal-phenanthroline systems, very few systematic investigations have been reported on this subject.^{26,27,28} Since the nature of the excited state in the binuclear rhodium(I) systems is predominantly metal-centered, we were particularly interested in exploring the photophysics of an analogous binuclear iridium(I) system. In this chapter the role of the metal in determining the rates of photochemical processes is discussed.

EXPERIMENTAL

Solvents

Spectral grade acetonitrile, acetone, and methanol were obtained from either Burdick and Jackson, or Aldrich. They were either deaerated by bubbling argon into a freshly opened bottle for at least 20 minutes and then transferred into a glovebox or, alternatively, they were degassed with five freeze-pump-thaw cycles. Tetrahydrofuran was purified by published methods.²⁹ All other solvents were reagent grade or better.

Ligands

2,5-dimethyl 2,5-diisocyano-hexane (TMB) was prepared as previously reported;³⁰ 1,8-diisocyano-p-dimethane (DMB) was synthesized in an analogous fashion. t-Butyl isocyanide was obtained from a commercial source and used without further purification.

Iridium Complexes

$[\text{IrCl}(\text{COD})]_2$ ³¹ (COD = cyclooctadiene) and $\text{Ir}(\text{CN-t-Bu})_4\text{-BPh}_4$ ³² were made by literature methods.

 $\text{Ir}_2(\text{TMB})_4(\text{BPh}_4)_2$

In a typical synthesis, 0.1 g of $[\text{IrClCOD}]_2$ and 0.1 g of TMB were dissolved in acetonitrile in separate beakers in a glovebox. Both solutions were filtered and the TMB solution was slowly added to the iridium-containing solution; the

mixture was allowed to stir for ~15 min at which time the solvent and COD were pumped-off. The resulting metallic solid was then dissolved in methanol and a filtered methanol solution of 0.11 g of sodium tetraphenylborate was added, resulting in the immediate precipitation of a turquoise solid. This solid could be recrystallized from either acetone or acetonitrile. Anal. Calcd. for $\text{Ir}_2\text{C}_{88}\text{H}_{104}\text{N}_8\text{B}_2$: C, 62.91; H, 6.24; N, 6.67. Found: C, 62.61; H, 6.43; N, 6.40

$\text{Ir}_2(\text{DMB})_4(\text{BPh}_4)_2$

This compound was prepared in a completely analogous fashion as above. Anal. Calc. for $\text{Ir}_2\text{C}_{96}\text{H}_{112}\text{N}_8\text{B}_2$: C, 64.64; H, 6.32; N, 6.31. Found: C, 63.91; H, 6.36; N, 6.28.

Other Reagents

The electrolytes, tetrabutylammonium tetraphenylborate and tetrabutylammonium triflate, were provided by J. S. Najdzionek and J. D. Buhr, respectively. Background scans indicated that there were no electroactive impurities of significant concentration in the desired region. All other materials were reagent grade or better and could be obtained from a number of commercial sources.

Instrumentation

Absorption spectra were recorded on one of the following spectrophotometers: the Cary 17 (single crystal and solution studies), the Cary 219 (solution studies) and the

HP 8450A (solution studies). Emission spectra were measured on an apparatus built at Cal Tech or on a home-made instrument built at UCSB, the designs of which have been described elsewhere.^{33,34} The spectra have been corrected for photomultiplier and grating response, unless otherwise specified. Quantum yields were measured taking the precautions noted by Demas and Crosby.³⁵ Emission lifetimes were measured on a system utilizing the frequency-doubled output of a Nd:YAG laser and a fast oscilloscope. Transient absorption spectra were obtained point by point throughout the visible range; several measurements were taken at each wavelength and then computer averaged. The transient was generated by a 337 nm pulse from a nitrogen laser (experiments were performed at UCSC). Microsecond flash photolysis experiments were done with a conventional apparatus constructed by Milder. Electrochemical studies utilized PAR model 173, 175, and 179 electronics. The best results were obtained using platinum working and counter electrodes with either an Ag/AgNO₃ or Saturated Calomel Electrode (SCE) reference electrode; all potentials have been standardized to the SCE.

SPECTROSCOPY

Electronic absorption and emission spectroscopies are the principal tools used to develop an understanding of excited states. In combination, these techniques can be used to obtain an estimate of the energy of a given state above the ground state. Also, the intensity, breadth and temperature dependence of an absorption (or emission) band, along with the Stokes shift, provide valuable information concerning the geometry and the type of excited state. And in special cases where vibrational progressions are present, it is possible to extract quantitative estimates of the distortion(s) from the ground state geometry.

A convenient place to begin this section is on the electronic spectra of a monomeric iridium(I) isocyanide complex. Geoffroy *et al.* have previously reported the uv-vis spectrum of $\text{Ir}(\text{CN-t-Bu})_4^+$,³² and found it to be similar to other iridium(I) species with π -acceptor ligands.^{36,37} There are four bands of significant intensity below 300 nm and they are listed along with their extinction coefficients and respective assignments in Table 1. All the bands are due to transitions originating from the metal d orbitals and terminating in the LUMO, and in order to account for the number of intense bands it is necessary to invoke substantial spin orbit mixing indicating the necessity

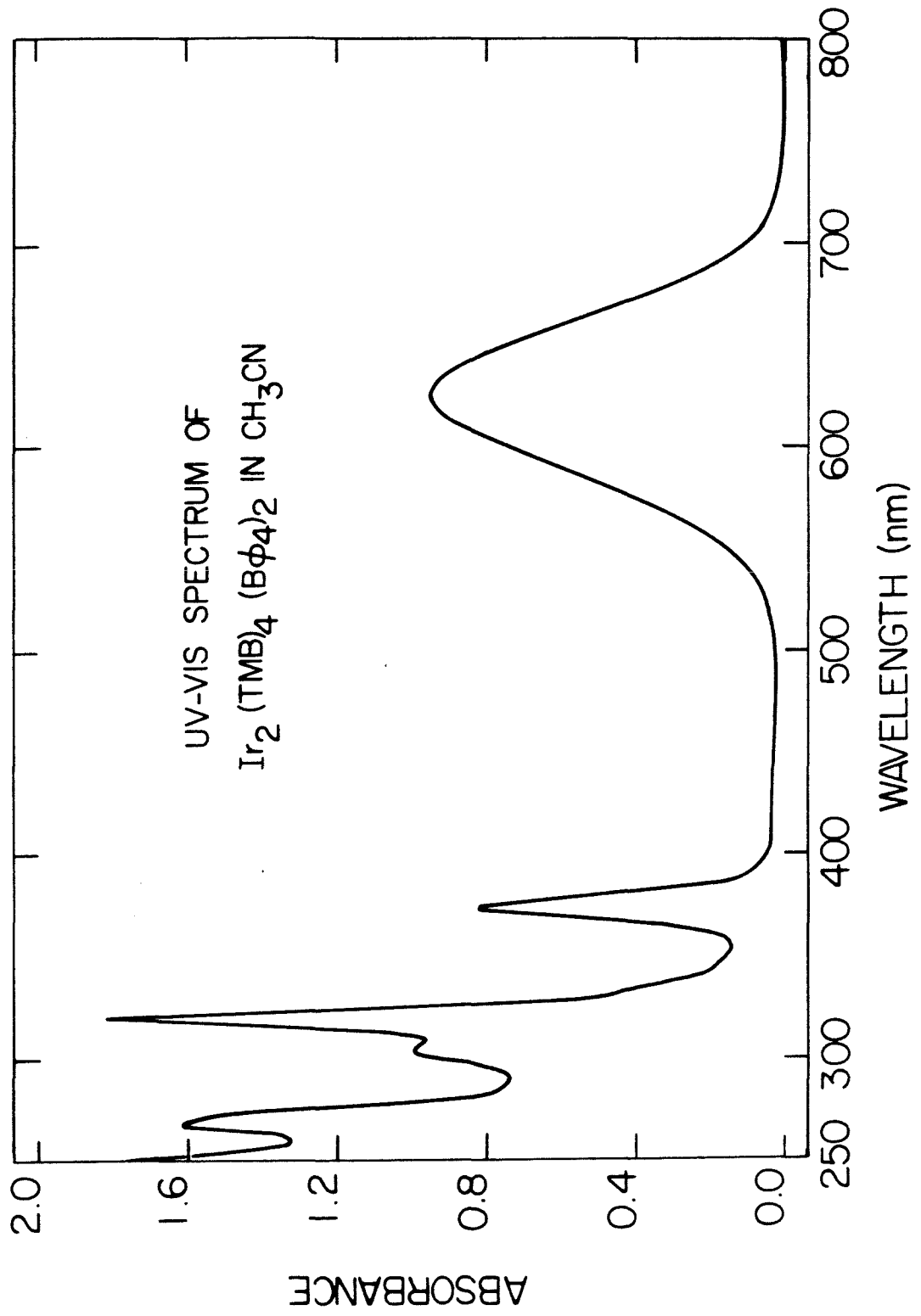
Table 1. Electronic absorption data and spectral assignments for $\text{Ir}(\text{CN-t-Bu})_4^+$.

Wavelength (nm)	Extinction Coefficients ($\text{M}^{-1} \text{cm}^{-1}$)	Assignments
309	16,787	$A_{1g}({}^1A_{1g}) \rightarrow E_u({}^1E_u)$ ($d_{xz}, d_{yz} \rightarrow p_z + \pi^*\text{CNR}$)
372	5,428	$A_{1g}({}^1A_{1g}) \rightarrow E_u({}^3E_u)$ ($d_{xz}, d_{yz} \rightarrow p_z + \pi^*\text{CNR}$)
423	4,264	$A_{1g}({}^1A_{1g}) \rightarrow A_{2u}({}^1A_{2u})$ ($d_{z^2} \rightarrow p_z + \pi^*\text{CNR}$)
490	743	$A_{1g}({}^1A_{1g}) \rightarrow E_u({}^3A_{2u})$ ($d_{z^2} \rightarrow p_z + \pi^*\text{CNR}$)

to use the \bar{D}_{4h} double group for spectral interpretation. The features maximizing at 423 nm and 490 nm are responsible for the yellow-orange color of the complex and excitation into these bands does not result in any significant luminescence, even in the solid state.

The electronic spectrum of $\text{Ir}_2(\text{TMB})_4^{2+}$ is shown in Figure 5. In contrast to the monomer, this complex is deep blue, owing to an intense absorption centered at 625 nm ($\epsilon = 11,200 \text{ M}^{-1} \text{ cm}^{-1}$). This band is logically assigned to the $A_1(^1A_1) \rightarrow A_2(^1A_2)$ ($d_{z^2} \rightarrow p_z + \pi^*\text{CNR}$) transition in analogy to a similar feature found at 515 nm ($\epsilon = 11,700 \text{ M}^{-1} \text{ cm}^{-1}$) in $\text{Rh}_2(\text{TMB})_4^{2+}$; ¹⁰ the lower energy is easily rationalized on the basis of more extensive interaction between orbitals of higher principle quantum numbers. The other intense features below 300 nm have maxima at 318 nm ($\epsilon = 22,200 \text{ M}^{-1} \text{ cm}^{-1}$) and 372 nm ($\epsilon = 9,750 \text{ M}^{-1} \text{ cm}^{-1}$); these bands are tentatively assigned to the $A_1(^1A_1) \rightarrow E(^1E)$ and $A_1(^1A_1) \rightarrow E(^3E)$ (both $d_{xz} d_{yz} \rightarrow p_z + \pi^*\text{CNR}$) transitions. It is interesting that these features are essentially identical in energy and have similar extinction coefficients to those found in $\text{Ir}(\text{CN-t-Bu})_4^+$. This assignment implies that the transitions in the dimers are essentially localized on the individual metal centers.

Figure 5. UV-VIS spectrum of $\text{Ir}_2(\text{TMB})_4(\text{BPh}_4)_2$ in acetonitrile solution.



Since almost all photochemistry originates from the lowest excited state of a given multiplicity (Kaska's rule), a detailed examination of the low energy region seemed warranted. At room temperature a shoulder was detected on the low energy side of the $A_1(^1A_1) \rightarrow A_2(^1A_2)$ transition in a single crystal sample of $Ir_2(TMB)_4(BPh_4)_2$. Upon cooling to ~ 5 K however, a distinct peak was resolved at 810 nm (Figure 6). This feature can be confidently assigned to the $A_1(^1A_1) \rightarrow E(^3A_2)$ ($d_z^2 \rightarrow p_z + \pi^*CNR$) transition. Although the extinction coefficient cannot be obtained from this sample, as the orientation of the metal-metal axis with respect to the incident light is unknown; qualitatively, it appears that the extinction coefficient is considerably reduced from the corresponding transition in the monomer. This is the result of the large energy difference between the $E(^3A_{2u})$ state and the $E(^1E)$ state which serves to mitigate any intensity stealing from the $A(^1A) \rightarrow E(^1E)$ transition.

Excitation into the 625 nm band of $Ir_2(TMB)_4^{2+}$ at room temperature in fluid solution results in two emission bands (Figure 7). The higher energy of these bands maximizes at 735 nm and is quite short-lived (< 2 ns) and accordingly it is assigned to the fluorescence $A_2(^1A_2) \rightarrow A_1(^1A_1)$. The second band is centered at 1080 nm and corresponds to a lifetime

Figure 6. Single crystal visible spectrum of $\text{Ir}_2(\text{TMB})_4(\text{BPh}_4)_2$
at ~ 5 K.

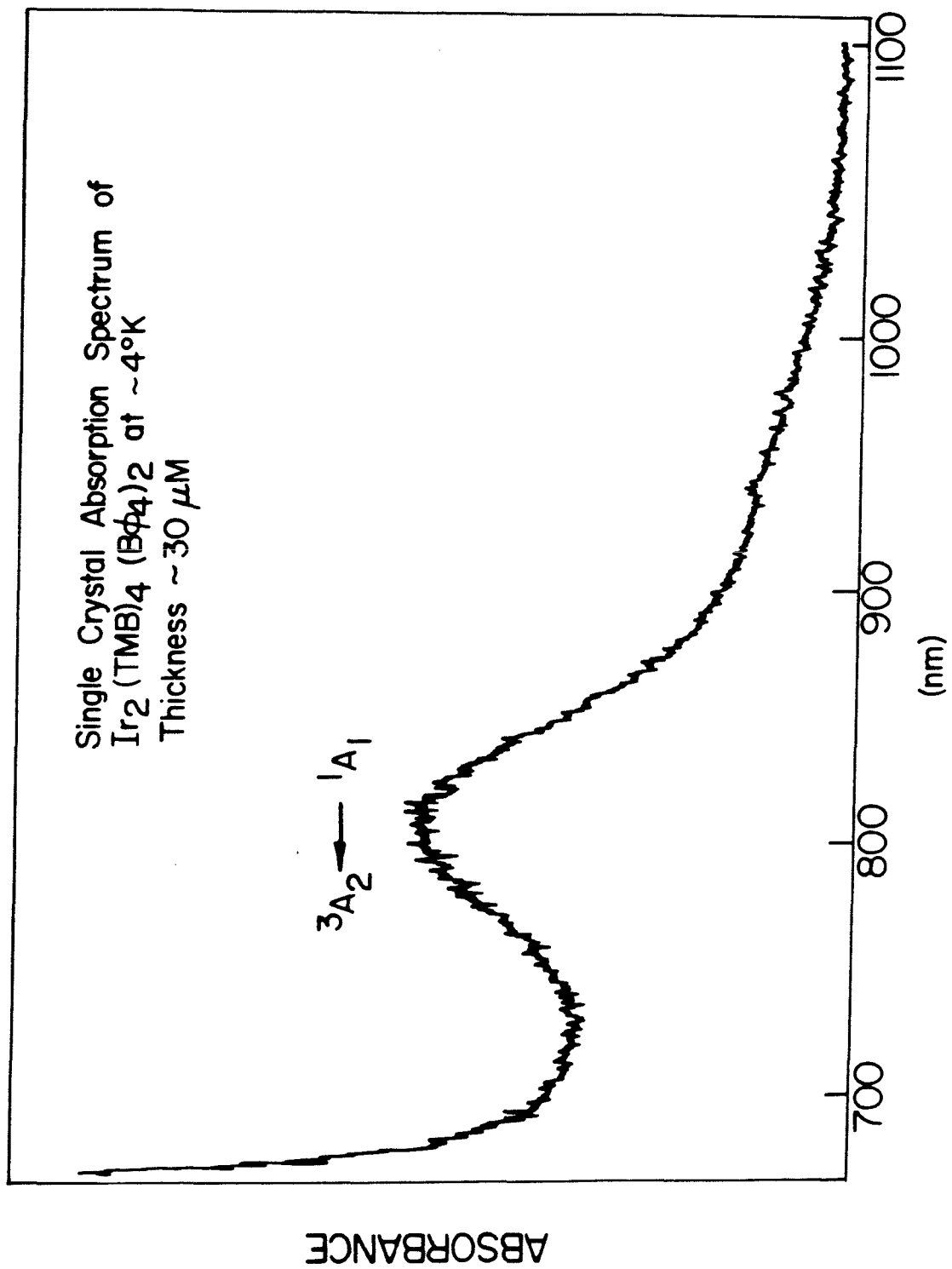
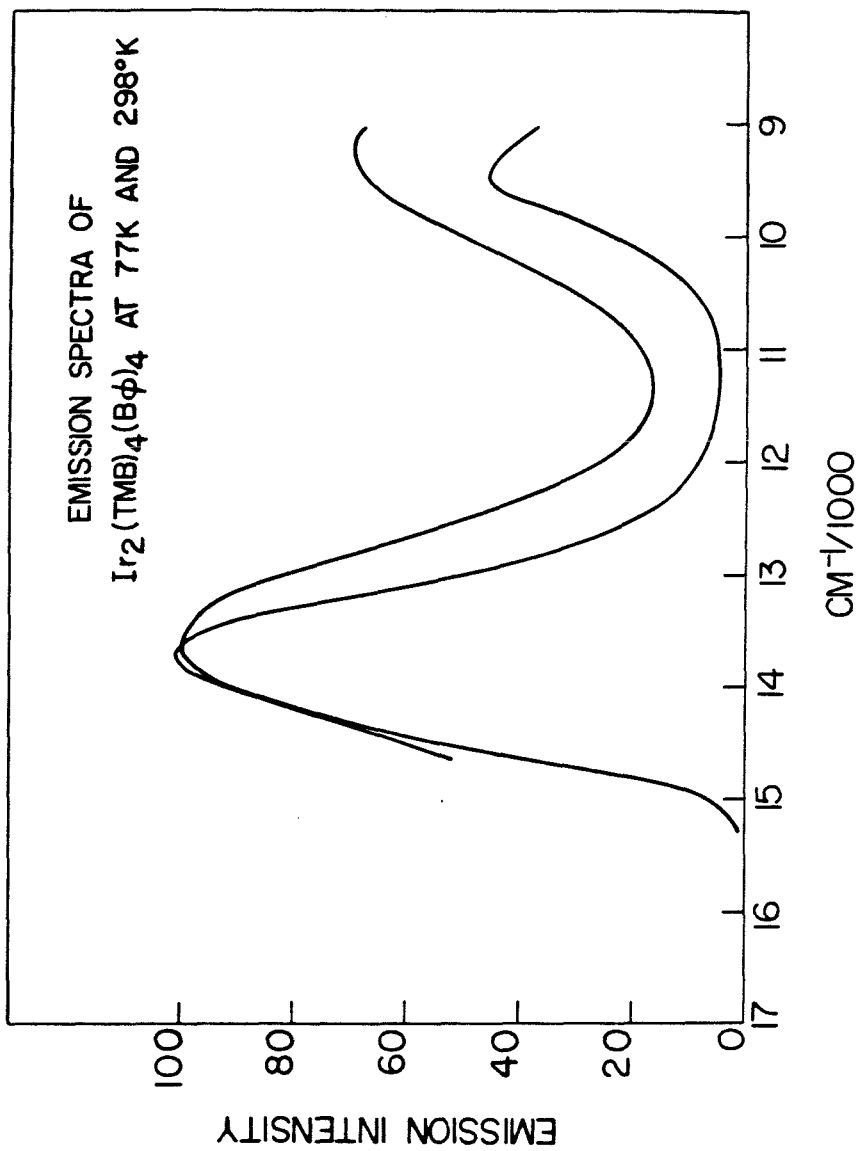


Figure 7. Emission spectra of $\text{Ir}_2(\text{TMB})_4(\text{BPh}_4)_2$.



of 200 ns and it is logically assigned to the phosphorescence $E(^3A_2) \rightarrow A(^1A_1)$; the Stokes shifts are 2400 cm^{-1} and 3200 cm^{-1} , respectively, similar to those found in the binuclear rhodium systems. The positions of the 0-0 transition for the triplet state (not observed) is estimated to be 940 nm, placing the 3A_2 state 1.31 eV above the ground state.

The quantum yields for fluorescence and phosphorescence are $2.4 \times 10^{-3} \pm 25\%$ and $1 \times 10^{-3} \pm 75\%$, respectively. The greater error associated with the phosphorescence measurement is due to the larger corrections needed for photomultiplier and grating responses in the infrared region of the spectrum. The quantum yields for $\text{Ir}_2(\text{TMB})_4^{2+}$ are roughly an order of magnitude lower than the quantum yields measured for $\text{Rh}_2(\text{B})_4^{2+}$,²¹ demonstrating the greater influence of non-radiative processes in the photophysics of the heavier metal system. It is interesting to note that radiative processes account for <1% of the absorbed radiation.

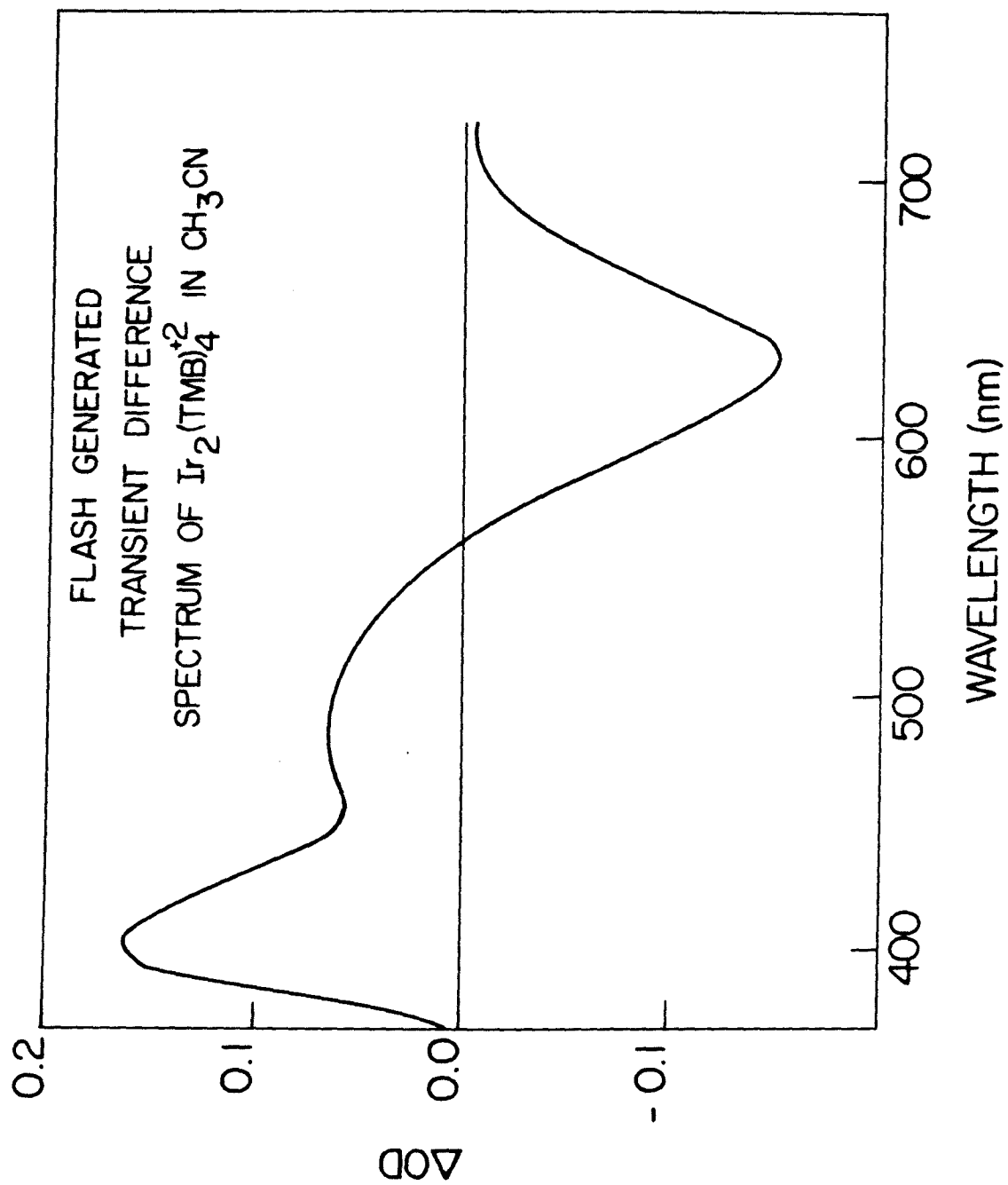
Initially, owing to the difficulties associated with detection of a relatively weak emission signal at >900 nm, the presence of a long-lived excited state was detected by a transient difference experiment. In this experiment, a transient is produced by a pulse from a laser (in this case a N_2 laser), and the change in absorbance is monitored wavelength by wavelength at a given interval after the pulse. The transient absorption spectrum of $\text{Ir}_2(\text{TMB})_4^{2+}$ is shown in Figure 8. The transient has a lifetime of $185 \pm 15 \text{ ns}$

in good agreement with the lifetime of the 3A_2 state obtained by measuring the decay of the phosphorescence signal. The decrease in absorbance at 625 nm is due to the disappearance of the ground state, whereas the two new bands at 400 nm and 510 nm can be attributed to absorption by the 3A_2 state.

The similarities to the spectra of the corresponding oxidized species (Chapter 3) are quite striking, making it tempting to assign the high energy, more intense feature to $d_{z^2} \rightarrow d_{z^2}^*$ ($\sigma \rightarrow \sigma^*$) and the other band to $d_{xz}, d_{yz} \rightarrow d_{z^2}^*$ ($d\pi \rightarrow \sigma^*$).³⁸

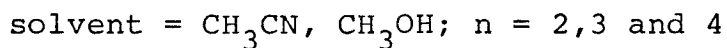
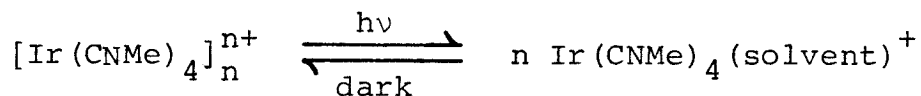
The lifetime of the ${}^3A_{2u}$ state in $\text{Ir}_2(\text{TMB})_4^{2+}$ is essentially temperature independent, varying from 193 ns at 77 K to 200 ns at 298 K. In contrast, the lifetimes of the binuclear rhodium systems all display pronounced temperature dependences. In the case of $\text{Rh}_2(\text{TMB})_4^{2+}$ the lifetime changes from 25 ns (298 K) to 8 μs (77 K). Milder *et al.*²² have studied the temperature dependences of the rhodium systems in considerable detail and found that they can be fit to an Arrhenius-type equation; the activation energy for $\text{Rh}_2(\text{TMB})_4^{2+}$ is $\sim 2000 \text{ cm}^{-1}$. This activation barrier is believed to correspond to the energy required to populate another state which then rapidly relaxes (non-radiatively) to the ground state. The most likely candidate for this state is the 3B_2 or 3B_1 ligand field state having the following configuration: $(xy)^2(yz)^2 - (xz)^2(z^2)^1(d_{x^2-y^2})^1$. Gray and Ballhausen³⁹ have suggested that a similar configuration in d^6 monomers is unstable with

Figure 8. Transient difference spectrum of $\text{Ir}_2(\text{TMB})_4(\text{BPh}_4)_2$.



respect to a D_{2d} distortion, a distortion which would result in intersection with the ground state potential surface and account for the efficient intersystem crossing. The fact that the iridium system does not show this behavior provides strong support for this theory because the ligand field states are thermally inaccessible.

Although $\text{Ir}_2(\text{TMB})_4^{2+}$ is indefinitely stable to irradiation in the visible region, the unbridged dimer $\text{Ir}_2(\text{CNMe})_8^{2+}$ and the higher oligomers based on $\text{Ir}(\text{CNMe})_4^+$ are exceedingly photosensitive. Two investigators^{40,41} have reported the following photochromic reaction



The forward reaction is believed to proceed by initial dissociation to form $\text{Ir}(\text{CNMe})_4^+$ followed by association with a solvent molecule. The dissociation step, however, appears to be in direct contradiction with the concept of a bound excited state. It is also interesting to note that the analogous unbridged rhodium oligomers are photostable.²¹ There are two explanations which can account for these observations. The first possibility is that the dissociative pathway is operative for both iridium and rhodium unbridged systems but only in the case of iridium is association with a solvent molecule competitive with

reformation of oligomers. The evidence supporting this contention is as follows: 1) the prevalence of five coordinate complexes of iridium(I) suggests that there is little energy difference between four and five coordination, whereas five coordinate rhodium(I) is much rarer;⁴² 2) although emission is observed from the unbridged rhodium systems, indicating a bound excited state, the quantum yield for fluorescence is an order of magnitude lower than that for $\text{Rh}_2(\text{B})_4^{2+}$, demonstrating that non-radiative processes are much more important in the unbridged systems; 3) flash photolysis studies on the rhodium oligomers indicate that more than one transient is generated.

The most likely mechanism for the dissociation of oligomers is very rapid internal conversion from the $\text{A}_2(^1\text{A}_2)$ excited state, producing a vibrationally hot ground state which breaks the weak metal-metal bonds. Another possible mechanism is prompt bond fission.⁴³ The choices are rather limited because of the limited number of states found for the iridium system at these energies.

The alternative explanation for the dissociation of iridium oligomers is that there is some iridium(II) present, possibly from the starting materials or by adventitious oxidation. This allows for formation of mixed-valent oligomers similar to those discussed in Chapter 1. In this case the transition would be expected to be dissociative in nature

as it would involve redistribution of electrons from bonding orbitals to antibonding orbitals. We view this the less likely possibility because there is no direct evidence for iridium(II), but it cannot be entirely discounted because the spectra of the iridium oligomers are very sensitive to the method of preparation; the absorption maxima vary from 605 nm to 650 nm. Furthermore, the extinction coefficients are quite high, between 16,000 - 20,000 $\text{M}^{-1} \text{cm}^{-1}$ per rhodium, possibly more consistent with the extremely intense $\sigma \rightarrow \sigma^*$ transition.

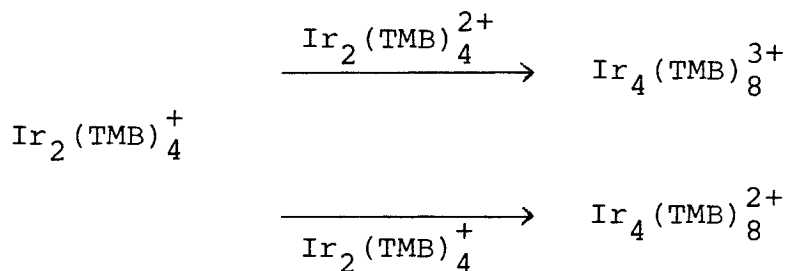
Preliminary experiments indicate that the $E(^3A_2)$ excited state of $\text{Ir}_2(\text{TMB})_4^{2+}$ undergoes electron transfer reactions. In the presence of N,N,N',N'-tetramethyl-p-phenylenediamine (TMPD), the phosphorescence/fluorescence ratio shows a marked decrease. Proof that reductive quenching is occurring comes from flash photolysis experiments, indicating the presence of $\text{TMPD}^{\cdot+}$. Two common oxidative quenchers, chloranil and methylviologen, react with the ground state molecule.

ELECTROCHEMISTRY

The electrochemistry of iridium(I) complexes has not been extensively studied,^{44,45} and there are no reports on iridium isocyanide complexes. Najdzionek,⁴⁶ however, has investigated a series of monomeric and dimeric rhodium(I) isocyanides. The most intensely investigated of these complexes was $\text{Rh}_2(\text{TMB})_4^{2+}$. A cyclic voltammogram of this complex was not very informative, revealing only one irreversible reduction wave which peaked at -1.55 V (*vs.* SCE). Bulk electrolysis, however, yielded at least two metal-containing products, one of which has been crystallographically identified as $\text{Rh}_2(\text{TMB})_3$ (3,3,6,6-tetramethylcyclohexylimine)⁺. This product results from loss of cyanide from one of the TMB ligands, followed by ring formation, and involves no change in the oxidation state of the metal. Unfortunately, the other product eluded full characterization. It is noteworthy that no anodic waves were observed at reasonable potentials, despite the rich oxidation chemistry exhibited by this complex.

We have performed a cursory examination of the electrochemistry of three iridium complexes, $\text{Ir}_2(\text{TMB})_4^{2+}$, $\text{Ir}_2(\text{DMB})_4^{2+}$, and $\text{Ir}(\text{CN-t-Bu})_4^+$, employing cyclic voltammetry. The cyclic voltammogram of the monomer exhibits only one irreversible wave, $E_{\text{peak}} = -1.48$ V (*vs.* SCE), and is quite similar to the wave observed in the rhodium systems. The cyclic voltammogram of $\text{Ir}_2(\text{DMB})_4^{2+}$ possesses a well-shaped

wave $E_{1/2} = -1.44$ V (*vs.* SCE) with a 70 mv separation (Figure 9). The behavior found for $\text{Ir}_2(\text{TMB})_4^{2+}$ is more complex; at slow scan rates (*e.g.* 100 mv/scc) a cathodic wave is observed at -1.20 V (*vs.* SCE) and an anodic feature is observed at -1.00 V (*vs.* SCE) on the return scan; however, at fast scan rates (*e.g.* 20 V/sec) two waves are observed on the return scan. The new wave at -1.10 V (*vs.* SCE) is believed to be the reversible component of the cathodic wave (*i.e.* $\text{Ir}_2(\text{TMB})_4^+ \rightarrow \text{Ir}_2(\text{TMB})_4^{2+} + e^-$). The wave at -1.10 V (*vs.* SCE) increases in intensity at the expense of the other anodic feature (Figure 10) as the scan rate is increased. When the solution is cooled the reversible wave is essentially the only anodic feature. Furthermore, if the concentration of $\text{Ir}_2(\text{TMB})_4^{2+}$ is decreased the wave at -1.10 V (*vs.* SCE) is once again favored. These experiments indicate that a chemical reaction follows electron transfer and that it involves another iridium species. The two most likely possibilities are shown below.



At this point, we have no experimental basis on which to decide between these two possibilities.

Figure 9. Cyclic voltammogram for $\text{Ir}_2(\text{DMB})_4(\text{BPh}_4)_2$.

CURRENT

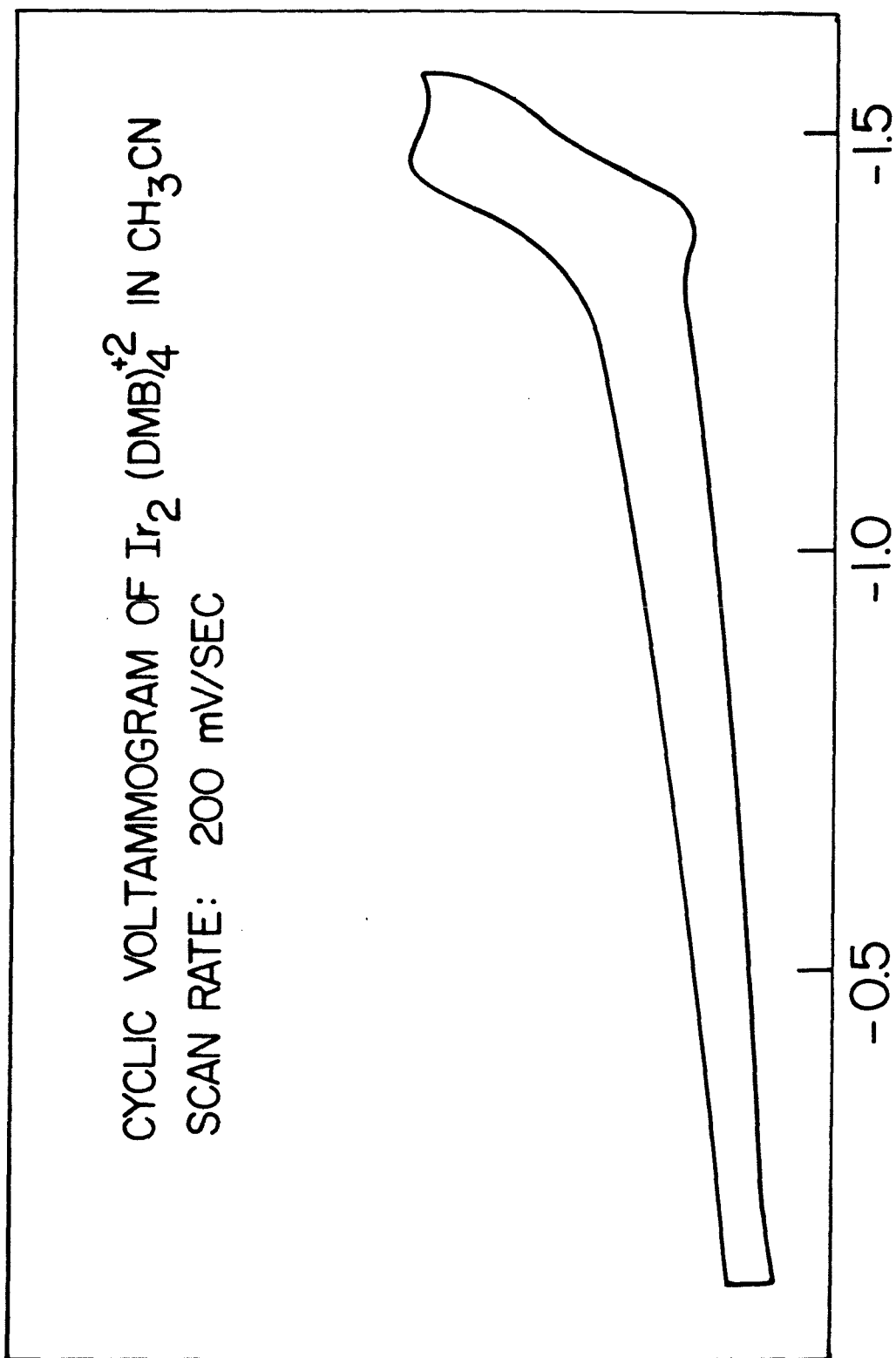
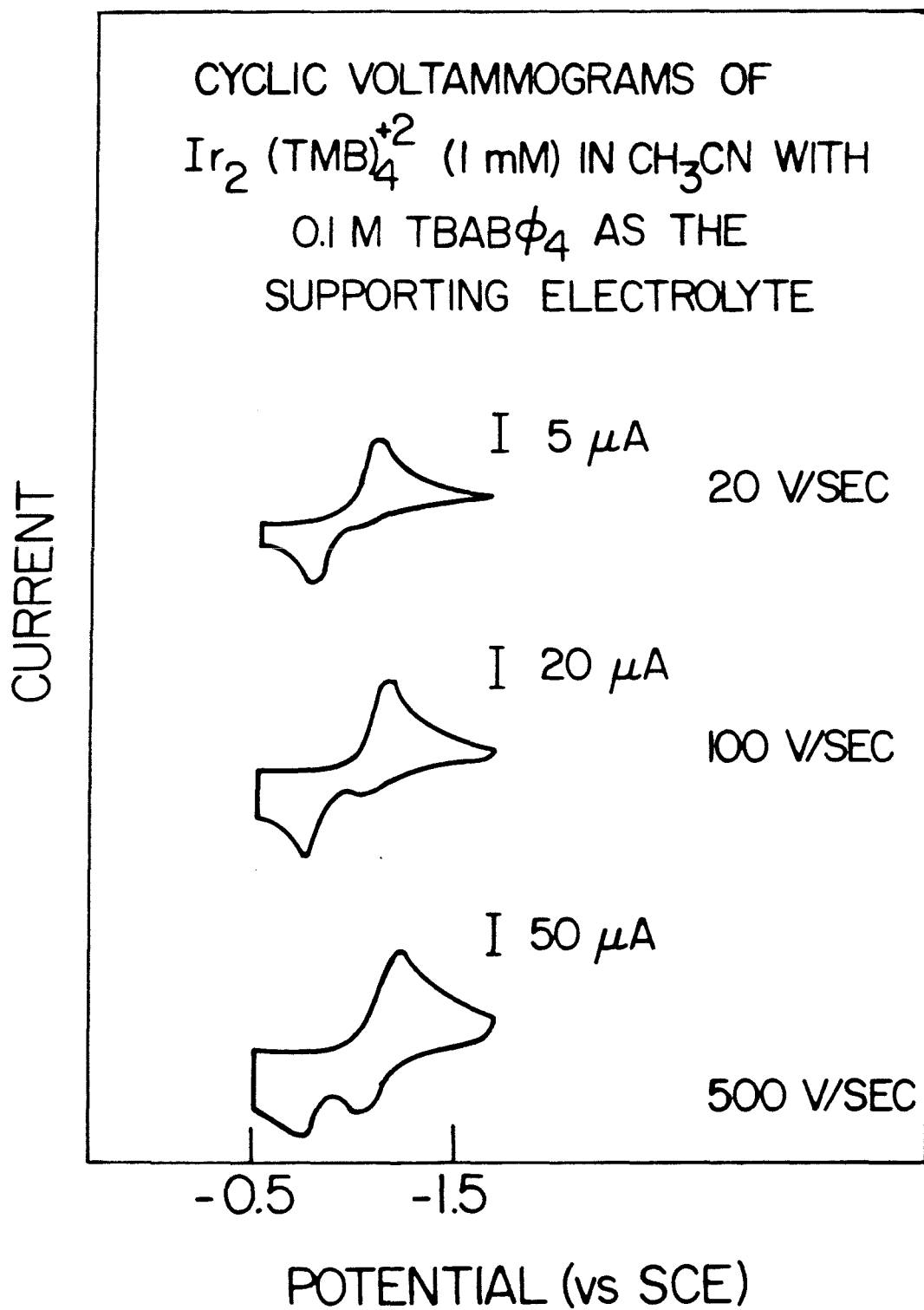


Figure 10. Cyclic voltammograms for $\text{Ir}_2(\text{TMB})_4(\text{BPh}_4)_2$
at three scan rates.



The reduction potential reflects the position of the LUMO in most chemical systems; and the observed trend in the iridium system is in compliance with molecular orbital considerations (based on extent of interaction). Assuming that electron transfer is adiabatic and that minimal geometric distortions are occurring for these systems, we can say that the LUMO of $\text{Ir}_2(\text{TMB})_4^{2+}$ is stabilized by ~ 8 kcal/mole by the metal-metal interaction.⁴⁷

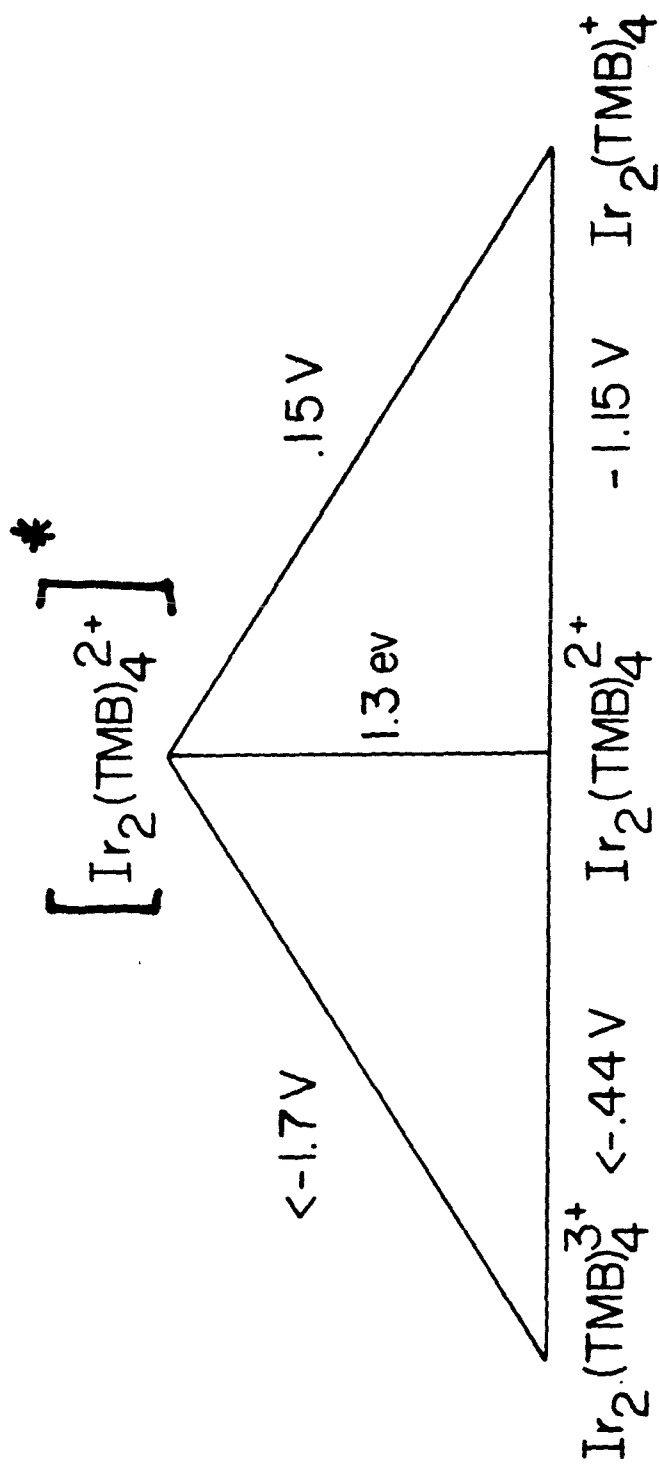
CONCLUSIONS AND PROSPECTS

A modified Latimer diagram is a convenient method of summarizing the relationship between the ground state and excited state redox potentials (Figure 11). It is readily apparent from this diagram that both $\text{Ir}_2(\text{TMB})_4^{+2*}$ and $\text{Ir}_2(\text{TMB})_4^+$ are powerful reductants; future experiments should be designed with this aspect in mind. The chemistry of $\text{Ir}_2(\text{TMB})_4^+$ is of particular interest because it is capable of transferring up to $3e^-$. The reactivity of the reduced species with small molecules (*e.g.* CO or CO_2) is also worthy of consideration.

The binuclear d^8-d^8 systems possess a number of important properties which make them an important class of photoreceptors. Firstly, the absorption maxima may be varied throughout the entire visible region by appropriate choice of metal and ligand; the binuclear iridium species has the longest wavelength absorption. Secondly, electron transfer from the excited state, produced by $\sigma^* \rightarrow \sigma$ excitation appears to be quite general. Finally, the availability of an open coordination site provides a means of inhibiting the ordinarily very rapid back electron transfer reaction.^{48,49}

Figure 11. Modified Latimer diagram for $\text{Ir}_2(\text{TMB})_4(\text{BPh}_4)_2$.

MODIFIED LATIMER DIAGRAM FOR $\text{Ir}_2(\text{TMB})_4^{2+}$



POTENTIAL MEASURED vs SCE

CHAPTER 3 (PART A)Reactions of $\text{Ir}_2(\text{TMB})_4^{2+}$

INTRODUCTION

There has been a great deal of interest in low-valent d^8 complexes because of the facility with which they undergo oxidative addition reactions. Because of this ability these complexes have become very important in catalytic processes, ranging from the small scale syntheses of drugs to the large scale production of basic chemical feedstocks.⁵⁰

Recently, it has been demonstrated that d^8 complexes, in particular those of iridium, are able to insert into non-aromatic carbon-hydrogen bonds. The first example of this involved the reaction of $\text{Ir}(\text{PMe}_3)_4^+$ with activated carbon-hydrogen bonds (*e.g.* CH_3CN).⁵¹ However, the most exciting development in this area is the reactions of $\text{Ir}(\text{Me}_5\text{C}_5)(\text{PMe}_3)^{52}$ (photochemically generated from $\text{Ir}(\text{Me}_5\text{C}_5)(\text{PMe}_3)(\text{H}_2)$) and $\text{IrH}_2\text{S}_2\text{L}_2^{+53}$ ($\text{L} = \text{PPh}_3$; $\text{S} = \text{acetone}$ or H_2O) with unactivated alkanes. In principle, this reactivity could be utilized to synthesize important chemicals from petroleum reserves.

Since the electronic structure of the binuclear systems is dramatically altered from that of the monomers, a corresponding change in reactivity might be expected as well. Also, the fact that a metal-metal bond is formed upon oxidation might be expected to lower activation barriers to oxidative addition. For these

reasons, a general investigation of the reactivity of $\text{Ir}_2(\text{TMB})_4^{2+}$ has been initiated. One aspect of this study of particular interest is the reaction with acid which has been extended to include the analogous binuclear rhodium system as well.

EXPERIMENTAL

Materials

Solvents were prepared in the same fashion as in Chapter 2. Iodine, bromine, chlorine, and hydrogen chloride were obtained from commercial sources and used without further purification. Methyl iodide was purified by repeated chromatography on an alumina column until all traces of iodine disappeared. Malononitrile was washed with diethyl ether to remove a brown surface impurity. Deuterated solvents, d_2 -dichloromethane and d_3 -acetonitrile were obtained from Bio-Rad Laboratories; the d_3 -acetonitrile was distilled from P_2O_5 and stored on activated sieves; the d_2 -dichloromethane was stored on activated sieves.

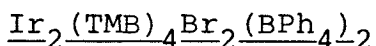
Metal Complexes

$Rh_2(B)_4(triflate)_2$, $Rh_2(B)_4(BPh_4)_2$, and $Rh_2(TMB)_4(triflate)_2$ were purified by published procedures.¹⁹

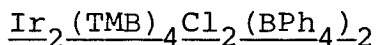
 $Ir_2(TMB)_4I_2(BPh_4)_2$

An acetonitrile solution containing 0.05g of $Ir_2(TMB)_4(BPh_4)_2$ was titrated with an iodine solution of acetonitrile until the blue color disappeared. The solvent was removed and the resulting yellow solid was slurried in methanol and then filtered; the accumulated solid was collected and a solution containing 0.05g of sodium tetraphenyl borate was then added to the filtrate, resulting in formation of a

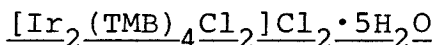
precipitate which was also filtered and collected. The two solids were combined and then crystallized from either acetonitrile or acetone. Anal. Calc. for $\text{Ir}_2\text{I}_2\text{C}_{88}\text{H}_{104}\text{N}_8\text{B}_2$: C, 54.66; H, 5.42; N, 5.79. Found: C, 54.82; H, 5.42; N, 5.80.



This compound was prepared in an analogous fashion to the iodide adduct. Anal. Calcd. for $\text{Ir}_2\text{Br}_2\text{C}_{88}\text{H}_{104}\text{N}_8\text{B}_2$: C, 57.45; H, 5.70; N, 6.12; Br, 8.69. Found: C, 57.05; H, 5.89; N, 6.49; Br, 8.53.

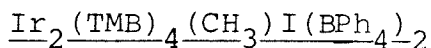


This compound was prepared as above. Anal. Calcd. for $\text{Ir}_2\text{Cl}_2\text{C}_{88}\text{H}_{104}\text{N}_8\text{B}_2$: C, 60.37; H, 5.99; N, 6.40; Cl, 4.05. Found: C, 59.71; H, 6.17, N, 6.39, Cl, 4.60.

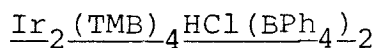


One arm of a photolysis cell was charged with 0.1 g of $[\text{IrCODCl}]_2$ and 0.1 g of TMB. Acetonitrile was distilled on to the solids and the resulting solution was stirred. After an hour, argon was placed over the deep blue solution and then chlorine was admitted which rapidly bleached the solution. Diethyl ether was then added, resulting in precipitation of an off-white solid which was collected on a sintered glass filter. The presence of water was confirmed by IR (in nujol). Anal. Calcd. for

$\text{Ir}_2\text{Cl}_4\text{C}_{40}\text{H}_{74}\text{N}_8\text{O}_5$: C, 37.74; H, 5.86, N, 8.80. Found:
C, 37.51; H, 5.36; N, 8.81.



Excess methyl iodide was distilled into a flask containing an acetonitrile solution of $\text{Ir}_2(\text{TMB})_4(\text{BPh}_4)_2$. The solution was stirred for 5 minutes and then the solvent and excess methyl iodide were removed. The solid was crystallized from acetone. Anal. Calcd. for $\text{Ir}_2\text{IC}_{89}\text{H}_{107}\text{N}_8\text{B}_2$: C, 58.69; H, 5.92; N, 6.15. Found: C, 58.28; H, 6.00; N, 6.03.



A one-hundred milliliter round bottom flask equipped with a vacuum stop-cock was charged with 0.1 g of $\text{Ir}_2(\text{TMB})_4(\text{BPh}_4)_2$. The flask was evacuated and 25 ml of acetonitrile was distilled onto the solid. The resulting solution was warmed to $\sim 0^\circ\text{C}$ and excess hydrogen chloride gas was added, then the solvent and excess gas were immediately removed at reduced pressure at $\sim 0^\circ\text{C}$; oily crystals were isolated.

Methods

The ^1H NMR experiments were performed on a JEOL FX-90Q spectrometer; all tubes were sealed under vacuum. The presence of hydrogen gas was verified by Toepler pump experiments. All other methods were the same as given in Chapter 2.

REACTIVITY OF $\text{Ir}_2(\text{TMB})_4^{2+}$ WITH HALOGENS
AND METHYL IODIDE

The reactions of halogens and methyl iodide with $\text{Ir}_2(\text{TMB})_4^{2+}$ occur upon mixing, yielding yellow, air-stable products. The crude yields generally exceeded 70%, although repeated recrystallizations were necessary to obtain analytically pure samples. The spectroscopic characterization, along with an X-ray diffraction study on one of the addition products are reported in Part B of this chapter.

The methyl iodide reaction was examined in the most detail. The ^1H NMR spectrum of the reaction mixture revealed peaks in the methyl and methylene region which were considerably broadened from that of the analytically pure samples, possibly indicating that $\text{Ir}_2(\text{TMB})_4\text{CH}_3\text{I}^{2+}$ was not the exclusive product. The most likely by-product of this reaction is $\text{Ir}_2(\text{TMB})_4\text{I}_2^{2+}$, whose existence is supported by the fact that the ratio of TMB protons (1 to 1.6 δ) to iridium methyl protons (.91 δ) is twice that expected for pure $\text{Ir}_2(\text{TMB})(\text{CH}_3)\text{I}^{2+}$. This suggests that free radicals are probably involved in this reaction.

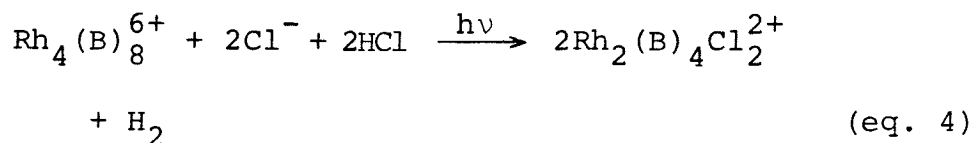
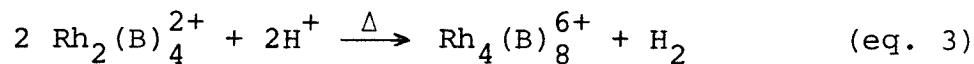
REACTIONS OF BINUCLEAR ISOCYANIDE COMPLEXES OF RHODIUM
AND IRIDIUM WITH HCl

The photochemical decomposition of water into molecular hydrogen and oxygen by sunlight is an attractive means of storing energy.^{54,55} However, since there is insufficient energy in a solar photon to break two oxygen-hydrogen bonds directly, it has been necessary to develop systems which can accomplish this task in a step-wise manner, taking advantage of the following energetically less demanding redox reactions (equations 1 and 2).



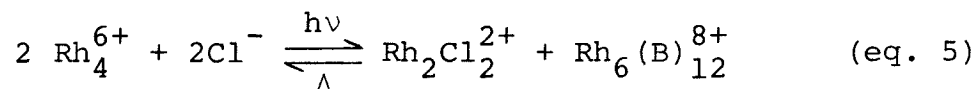
Many excited state inorganic systems are thermodynamically capable of carrying out these processes but substantial kinetic barriers often exist which generally result in very low efficiencies in the absence of heterogeneous catalysts. The rhodium isocyanide system, briefly discussed in Chapter 1, is an exception in this regard and understanding the detailed mechanism of H₂ evolution may be quite important in arriving at new systems which do not depend on expensive catalysts.

The stoichiometries of the thermal and photochemical reactions of Rh₂(B)₄²⁺ and Rh₄(B)₈⁶⁺ with 12 M HCl are shown in equations 3 and 4.¹⁸

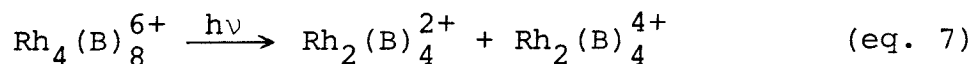
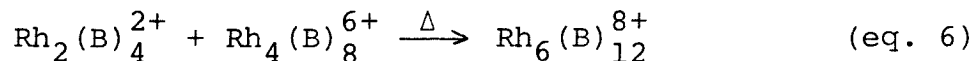


Unfortunately, these reactions provide no indication of the actual details of H_2 production. However, some insight into the photochemical mechanism has been obtained by studying the photochemistry of $\text{Rh}_4(\text{B})_8^{6+}$ under conditions where no net H_2 production occurs.

Mann et al. have previously observed that in 6 M HCl at 240 K,¹⁸ prolonged photolysis of $\text{Rh}_4(\text{B})_8^{6+}$ results not in H_2 production but rather in the following disproportionation reaction (equation 5).



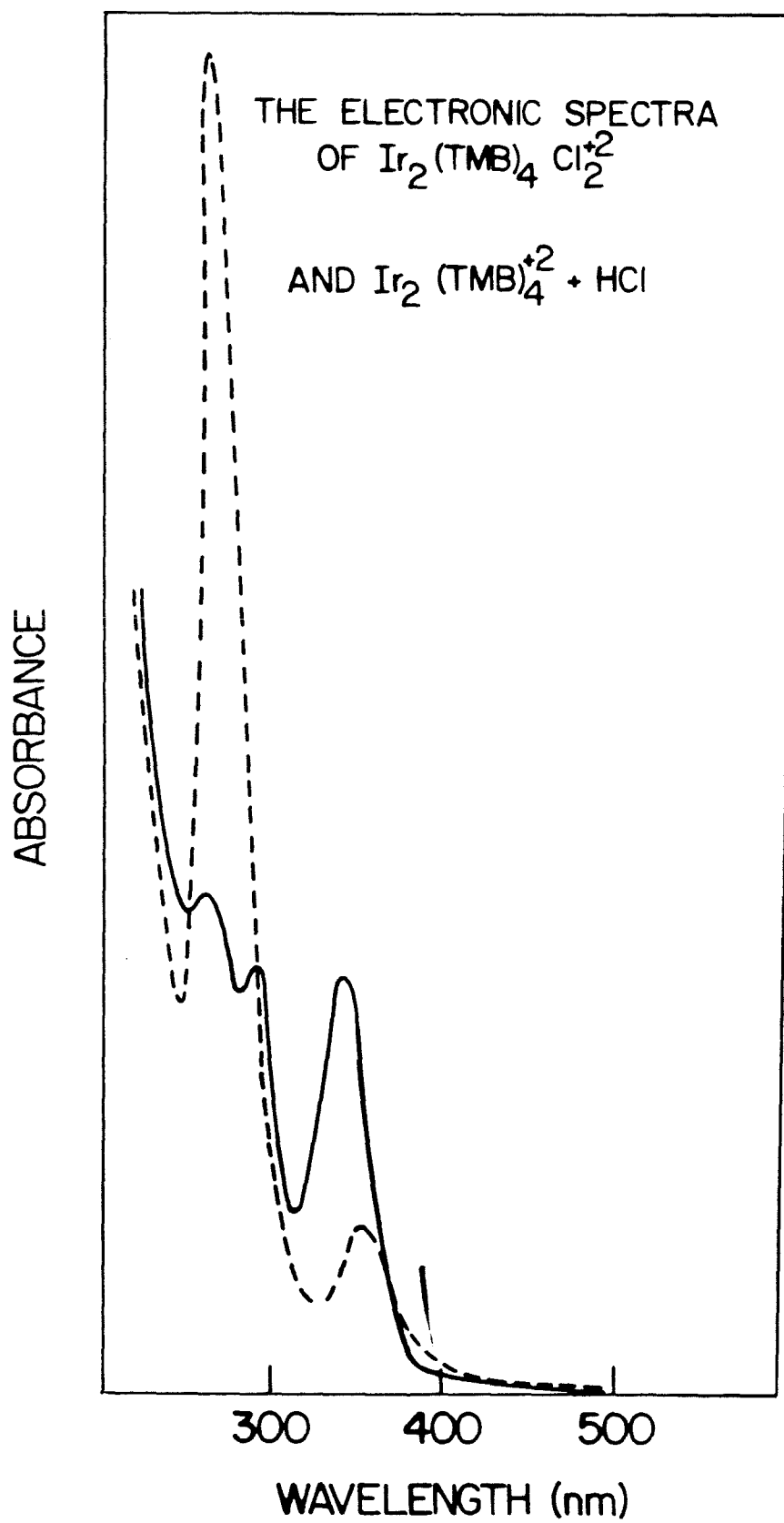
Since the hexanuclear species is known to form as shown in equation 6, it has been postulated that the initial step in the photochemical reaction involves heterolytic cleavage of the tetranuclear ion (equation 7).



This, of course, ties the thermal mechanism of H_2 production with the photochemical mechanism. In view of this, it seemed appropriate to investigate the reactions of other binuclear isocyanide complexes with gaseous and aqueous hydrogen chloride with the goal of discovering possible intermediate steps in the hydrogen-producing mechanism.

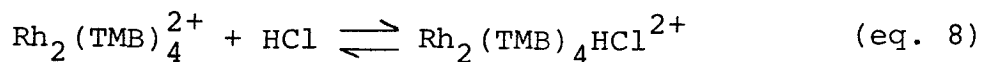
The deep blue binuclear iridium ion, $Ir_2(TMB)_4^{2+}$, reacts thermally with 6 M HCl forming a pale yellow product. The color change suggests that the metal center has been oxidized; however, unlike other oxidation products previously discussed, the new species is quite air sensitive. The UV-VIS spectral changes observed upon air oxidation of the new species (solid line) are shown in Figure 12. The final product (dashed line) has been identified as $Ir_2(TMB)_4Cl_2^{2+}$ as the spectrum is identical to that of an authenticated sample produced by chlorine oxidation of $Ir_2(TMB)_4^{2+}$. This implies that the initial product formed by the reaction of $Ir_2(TMB)_4^{2+}$ with protons is only partially oxidized; the most likely formulation of this species is either as a mixed valent ion (*i.e.* $Ir_2(TMB)_4^{3+}$) or possibly as a hydride-chloride adduct. To differentiate between these two possibilities, a 1H NMR spectrum was taken of a rigorously dried d_3 -acetonitrile solution containing $Ir_2(TMB)_4^{2+}$ and ~ 10 equivalents of HCl gas. The spectrum

Figure 12. The electronic absorption spectra of $\text{Ir}_2(\text{TMB})_4\text{Cl}_2^{2+}$ (dashed line) and $\text{Ir}_2(\text{TMB})_4 + \text{HCl}$ (solid line) in 6 M HCl.



(Figure 13) reveals a new feature at -13.1δ which is not present in the spectrum of $\text{Ir}_2(\text{TMB})_4^{2+}$. The position of this resonance is a strong indication of the presence of a terminal iridium hydride. Further support for a hydride-chloride adduct is found in the IR spectrum of the yellow solid which exhibits a peak at 2040 cm^{-1} (Figure 14) which can be assigned to a terminal iridium-hydrogen stretch. Interestingly, when argon is bubbled through an acetonitrile solution of $\text{Ir}_2(\text{TMB})_4\text{HCl}^{2+}$, the reduced iridium species, $\text{Ir}_2(\text{TMB})_4^{2+}$, is formed.

It has been previously noted that $\text{Rh}_2(\text{TMB})_4^{2+}$ is unreactive towards 6 M HCl in the absence of air. However, when air is admitted to the solution $\text{Rh}_2(\text{TMB})_4\text{Cl}_2^{2+}$ is rapidly produced. The addition of small amounts of PtO_2 also results in formation of $\text{Rh}_2(\text{TMB})_4^+\text{Cl}_2^{2+}$ and H_2 is evolved as well. These reactions suggest that the equilibrium shown in equation 8 is operative.



However, unlike the iridium system the equilibrium lies far to the left.

The room temperature ^1H NMR of a d_2 -dichloromethane solution of $\text{Rh}_2(\text{TMB})_4^{2+}$ with ~ 10 equivalent of hydrogen chloride gives no indication of a rhodium hydride. However, when the deep red solution is cooled to -85°C the solution becomes yellow; accompanying this color change is the

Figure 13. ^1H NMR spectrum of $\text{Ir}_2(\text{TMB})_4(\text{triflate})_2$ with ~ 10 equivalents of HCl gas in CD_3CN .

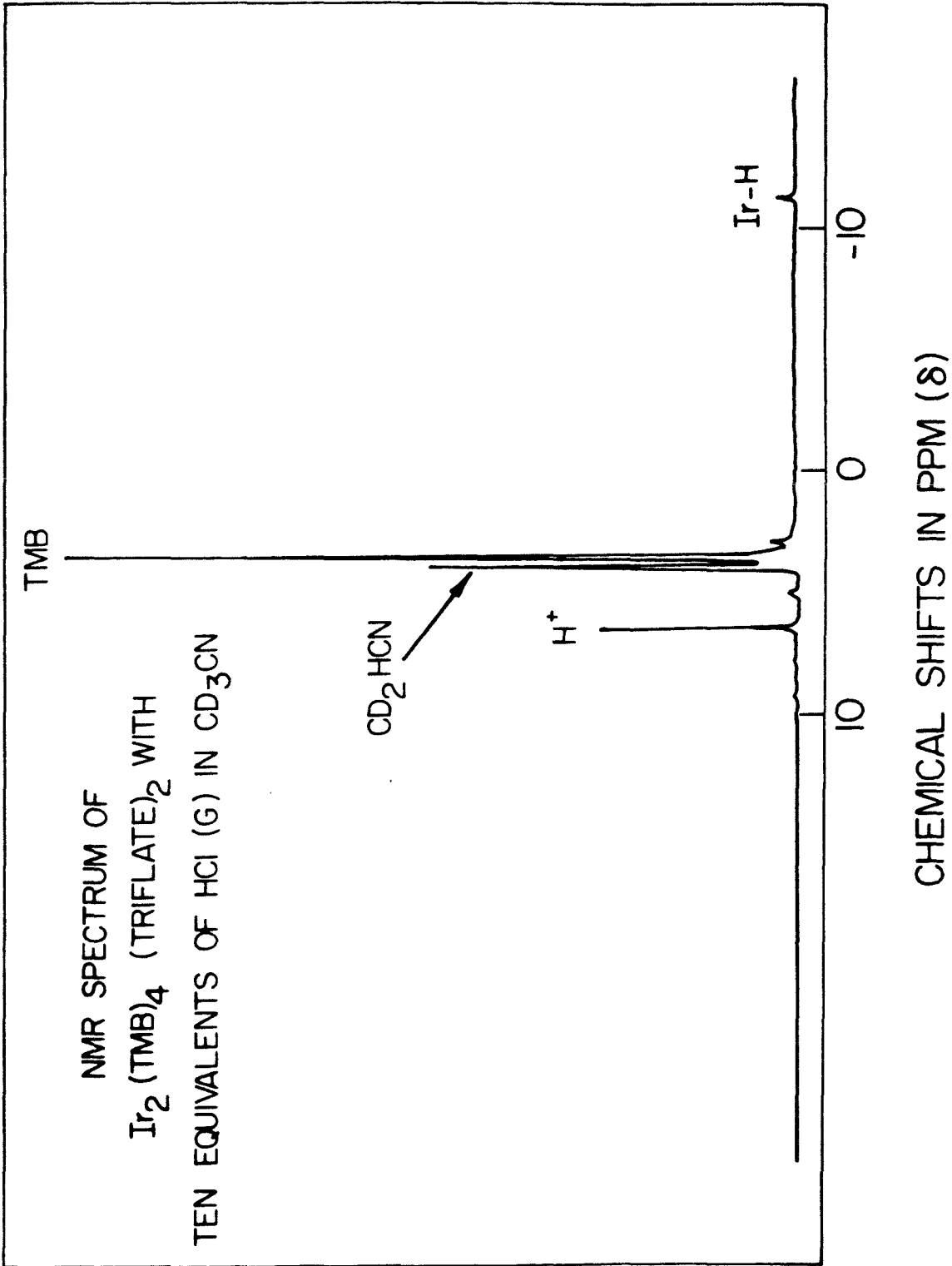
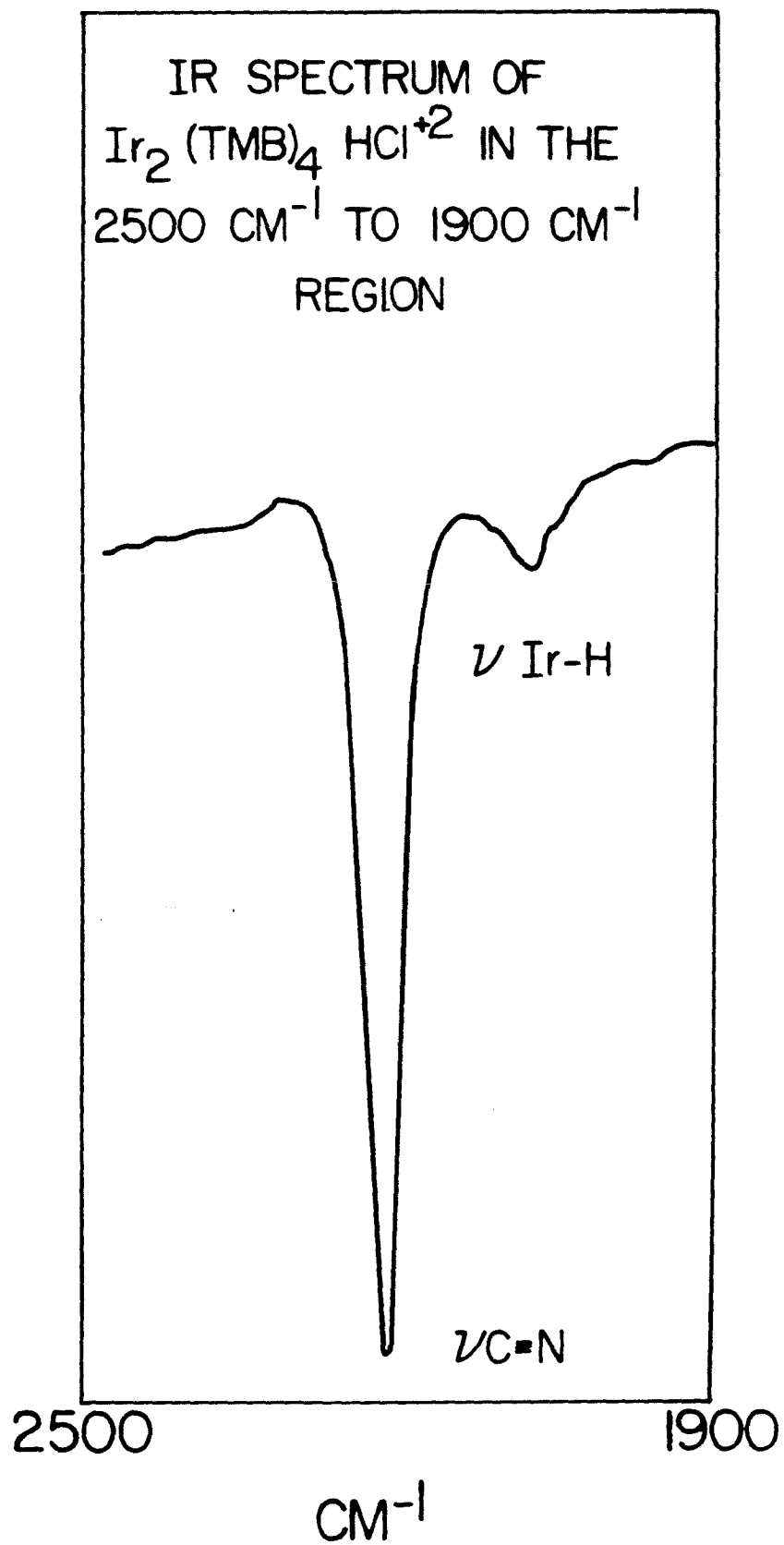


Figure 14. IR spectrum of $\text{Ir}_2(\text{TMB})_4\text{HCl}^{2+}$ in the 2500 cm^{-1} to 1900 cm^{-1} region.

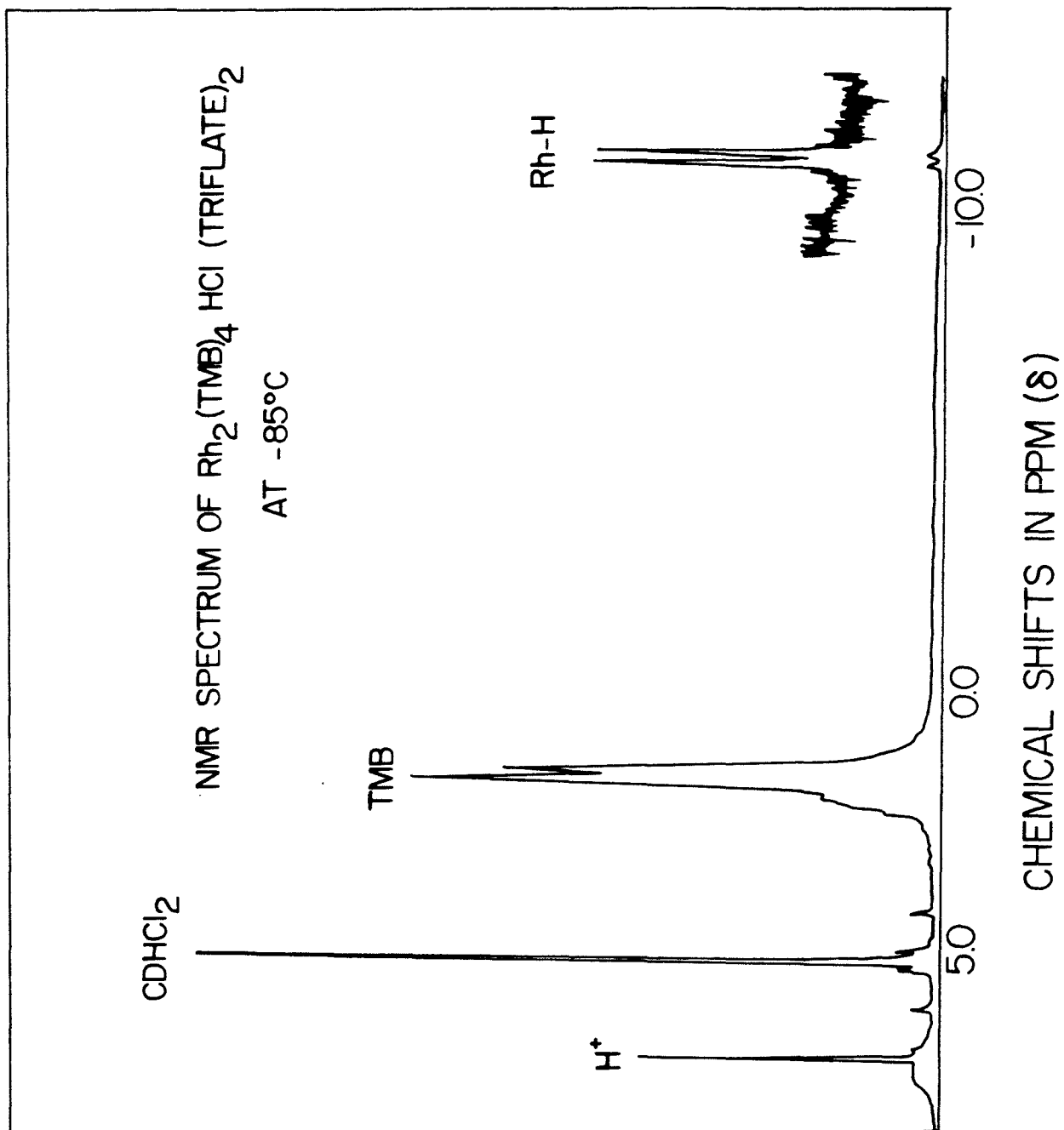


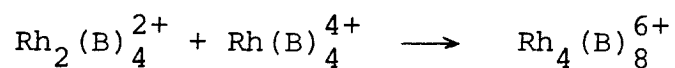
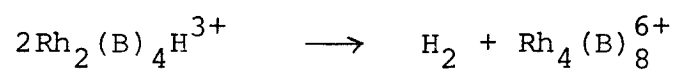
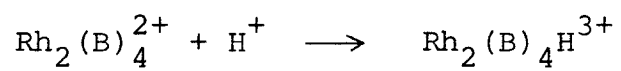
appearance of a doublet centered at -11.02δ (Figure 15). This feature can be ascribed to a terminal rhodium hydride with a coupling constant ($J_{\text{Rh-H}}$) of 19.5 hz. The pattern of the methyl and methylene region provides strong evidence that the $\text{Rh}_2(\text{TMB})_4^{2+}$ moiety is still intact. The spectrum of the reheated sample is identical to the original spectrum. This cycle can be repeated but eventually (~ 2 days) the solution becomes irreversibly oxidized if left at room temperature.

When hydrogen chloride is added to a propionitrile solution of $\text{Rh}_2(\text{B})_4^{2+}$ at -80°C , the purple solution immediately becomes yellow. If the solution is allowed to warm to $\sim -50^\circ\text{C}$, $\text{Rh}_4(\text{B})_8^{6+}$ is formed, and immediately precipitates. Unfortunately, the low solubility of $\text{Rh}_2(\text{B})_4^{2+}$ (with any counter ion) prevented observation of a hydride signal in the ^1H NMR. Nonetheless, it is apparent that a hydride is formed at low temperature.

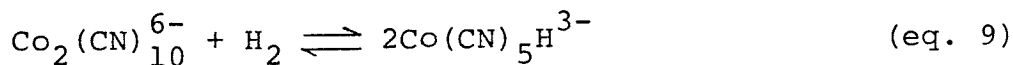
The hydride, $\text{Rh}_2(\text{B})_4\text{H}^{3+}$, is almost certainly involved in the thermal evolution of hydrogen; two possible mechanisms are shown in Schemes 1 and 2. The hydrogen producing step in Scheme 1 involves the reaction of the rhodium hydride with acid, whereas in Scheme 2 it involves the reaction of two hydrides. Unfortunately, preliminary kinetic studies on this system were ambiguous, indicating that the reaction was between first and second order in dimer concentration.

Figure 15. ^1H NMR spectrum of $\text{Rh}_2(\text{TMB})_4\text{HCl}(\text{triflate})_2$
at -85°C in CD_2Cl_2 .



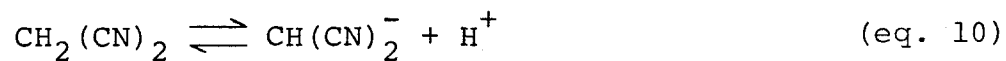
Scheme IScheme II

In lieu of good kinetic data, distinguishing between the two mechanisms is difficult. There are certainly precedents for the reactivity of a metal hydride with excess acid to form H_2 .⁵⁵ Although, if Scheme 1 is the actual mechanism, the reasons why hydrogen is not produced at approximately the same rate in the $Rh_2(TMB)_4^{2+}$ system are not clear, since the two hydrides are expected to be quite similar in hydridity and the H_2 producing step appears to be thermodynamically favored. So, on this basis, the most appealing mechanism for H_2 evolution appears to be Scheme 2 because the hydrogen producing step involves a bimolecular reaction between two rhodium dimers; a reaction which involves a transition state which is sterically unfavorable for $Rh_2(TMB)_4H^{+3}$. Halpern and Pribonić⁵⁶ favor a similar transition state in the hydrogenation of $Co_2(CN)_{10}^{6-}$ (equation 9), thus providing a precedent for this type of process (actually the microscopic reverse of this process).



REACTIVITY OF $\text{Ir}_2(\text{TMB})_4^{2+}$ WITH OTHER SMALL MOLECULES

Malononitrile ($\text{pK}_a = 11.1$)⁵⁶ reacts with $\text{Ir}_2(\text{TMB})_4^{2+}$ in acetonitrile solution. The ^1H NMR spectrum of the product is consistent with $\text{Ir}_2(\text{TMB})_4(\text{CH}(\text{CN})_2)\text{H}^{2+}$ with new resonances at -12.8δ ($\text{Ir}-\underline{\text{H}}$) and 5.21δ ($\text{Ir}-\text{C}(\text{CN})_2\underline{\text{H}}$). Interestingly, other molecules with similar acid strengths (*e.g.* acetylacetone ($\text{pK}_a = 13.4$) and benzoic acid ($\text{pK}_a = 10.7$))⁵⁶ are unreactive. This suggests that the reaction with malononitrile does not proceed by the reaction of free protons provided by the acid-base equilibrium shown in equation 10.



Prior coordination, through the nitrile, may be an important step in this reaction. Unfortunately, this complex could not be purified.

No reactions were observed with acetonitrile, hydrogen, or carbon monoxide.

CONCLUSIONS

Despite the large changes in the absorption spectrum which occur upon dimerization, the reactivity of the binuclear complexes of iridium(I) and rhodium(I) appear to be quite similar to that of the corresponding monomeric complexes. This is consistent with conclusions reached from a spectroscopic study⁵⁷ on $\text{Rh}_2(\text{B})_4^{2+}$ which state that the changes in electronic structure are predominantly associated with the stabilization of the LUMO, and that the energy level of the HOMO is not altered significantly. Alternatively, the similar reactivity of monomers and dimers might be rationalized by considering their respective transition states. If a substrate is added side-on to a monomer, a six coordinate transition state is formed. Moreover, the equatorial ligands can adopt a new geometry because they are not constrained. Side-on addition to dimers results in a seven coordinate transition state with an unfavorable geometry which is compensated for by the formation of a metal-metal bond.

CHAPTER 3 (PART B)

Physical Studies on $\text{Ir}_2(\text{TMB})_4\text{X}_2^{2+}$

INTRODUCTION

In the past decade, an increasing number of complexes containing a linear M_2X_2 core have been synthesized; examples of this structural unit have been found for every metal in the cobalt, nickel, and copper triads.^{58,59} In many cases bridging ligands are present; among the bridging ligands that appear to promote this structural type are: sulfates, phosphates, carboxylates, ylides, bis-phosphines, bis-arsines and diisocyanides. The most common route to these complexes involves transannular oxidative addition to binuclear d^8-d^8 or $d^{10}-d^{10}$ systems by halogens.

Many trends are evident in complexes containing the M_2X_2 moiety. For example, both the energy of the lowest energy transition, and the metal-metal stretching frequency for a given metal, decrease in the following order: $Cl > Br > I$. The metal-metal bond distances appear to parallel the observed trend in van der Waals radii. In this chapter, the Ir_2X_2 core is examined by a variety of spectroscopic methods and some attempt is made to correlate the various spectroscopic parameters.

EXPERIMENTAL

All of the metal complexes were made by established procedures (see Experimental sections of previous chapters) except for $\text{Rh}_2(\text{TMB})_4\text{Br}_2(\text{BPh}_4)_2$ which was prepared by bromine oxidation of $\text{Rh}_2(\text{TMB})_4(\text{triflate})_2$ in methanol, followed by precipitation with excess NaBPh_4 and then recrystallization from acetone. The general spectroscopic methods have already been discussed.

Raman spectra were recorded on a Spex instrument consisting of the following components: two 1.25 M monochromaters with gratings containing 2400 lines/mm, a photon counting device, and a strip recorder. The slits were set at $200 \mu/400 \mu/400 \mu/200 \mu$; the resolution at these settings is approximately 2 cm^{-1} . The vibrational frequencies were calibrated *vs.* acetonitrile and are accurate to $\pm 1 \text{ cm}^{-1}$. All experiments were performed using the 5145 \AA line of an argon ion laser. All the samples were crystalline obtained by cooling, hot saturated solutions in capillary tubes. Solution spectra were unobtainable. The force field calculations were done on the VAX in the Department of Chemistry, California Institute of Technology, using the program GMAT.⁶⁰

The variable temperature ^1H NMR experiments were performed on either the FX-90Q or Brücker 500 spectrometers. In both cases the temperatures were calibrated using neat methanol. The error in coalescence temperature is $\pm 2^\circ\text{C}$.

The X-ray diffraction studies were carried out on crystals of $\text{Ir}_2(\text{TMB})_4\text{I}_2(\text{BPh}_4)_2$ grown from acetone. The crystals grew as columnar parallelepipeds and were mounted along the long direction which corresponded to the a-axis in the unit cell. It was necessary to coat the crystals with epoxy to prevent solvent loss. The dimensions of crystals chosen for detailed analysis were .22 mm x .27 mm x .12 mm. Preliminary precession and Weissenberg photographs indicated that the unit cell had mmm symmetry. The following systematic absences were noted on the zero layer and first layer Weissenberg photographs: okl , $l \neq 2n$; $hh\ell$, $\ell \neq 2n$; hko , $h + k \neq 2n$; hoo , $h \neq 2n$; oko , $k \neq 2n$; ool , $l \neq 2n$; $hk\ell$, $\ell \neq 2n$. These conditions uniquely define the space group as Pccn .⁶¹ Furthermore, the intensity pattern along ool indicated that the IrIrI units were parallel to the c axis. The unit cell dimensions were determined by least squares analysis on 15 centered reflections; $a = 15.141(8)$, $b = 28.104(14)$ and $c = 23.877(12)$. The intensity data were collected at room temperature on a $\text{P}2_1$ automated full-circle diffractometer using graphite monochromatized MoK_α radiation. The density of the crystals were determined by flotation using a number of solvent combinations, the average value was $1.35(1) \text{ g/cm}^{-3}$ in good agreement with the calculated value of $1.340(1) \text{ g/cm}^{-3}$, which assumes four dimers, eight tetraphenylborates and eight acetones.

Two data sets were collected, the first set was collected out to $2\theta = 50^\circ$, the second set was collected out to $2\theta = 20^\circ$. In both sets the scan ranged from $.8^\circ$ below K_{α_1} to $.9^\circ$ above K_{α_2} ; the scan rate for the first data set was $2.02^\circ/\text{min}$ whereas the rate for the second data set was $1.01^\circ/\text{min}$. Background counts were taken before and after each scan; the total counting time equalled the scan time (per reflection) for the first set and half the scan time for the second set. The two sets were averaged for refinement purposes. Three standard reflections were collected every 97 reflections to monitor crystal decomposition. The decrease in intensity was essentially monotonic and amounted to $\sim 4\%$; the intensities of the reflections were corrected for this decay. The faces of the crystal were identified in order to apply an absorption correction, however, at the current stage of refinement the absorption correction ($\mu = 32.15 \text{ cm}^{-1}$)⁶² has been ignored. The data were corrected for Lorentz and polarization effects. The data were scaled by Wilson's method. The reflections with $2\theta > 30^\circ$ have been excluded because they lead to unrealistic thermal parameters. The current refinement has been carried out on 2433 independent reflections.

UV-VIS SPECTROSCOPY

There has been a great deal of interest in the electronic structure and photochemistry of binuclear complexes containing metal-metal single bonds. The most extensively investigated series of complexes has been the group VII binuclear carbonyls (*i.e.* $M_2(CO)_{10}$, $M = Mn, Tc,$ and Re) and their phosphine substituted derivatives.^{63,64}

The electronic spectrum of these complexes is dominated by an intense feature in the ultraviolet region which corresponds to a transition from a metal-metal bonding orbital to a metal-metal antibonding orbital ($\sigma \rightarrow \sigma^*$). Excitation into this transition results in efficient homolytic cleavage (*i.e.* formation of two 17 electron fragments). The energy of this transition has been found to correlate well with the activation energy associated with homolytic cleavage, thereby providing a qualitative indication of metal-metal bond strength.^{65,66}

The binuclear complexes, M_2 (diisocyanoalkane) $_4X_2^{2+}$ ($M = Co, Rh, \text{ or } Ir; X = Cl, Br \text{ or } I$), also have a d^7-d^7 configuration but the axial ligands are π -donors rather than π -acceptor acceptors (*vide supra*). This section deals specifically with the electronic structure of $Ir_2(TMB)_4X_2^{2+}$, however, general aspects pertaining to the isostructural rhodium system are also discussed.

A simplified MO diagram for $\text{Ir}_2(\text{TMB})_4\text{X}_2^{2+}$, assuming D_4 symmetry, is shown in Figure 16. The major result of changing halides will obviously be to move the energies of the $X\sigma$ and the $X\sigma^*$ orbitals; the greater the electron affinity, the farther these orbital will be from the metal d orbitals. Based on this diagram we expect the two lowest lying allowed transitions to be $A_1(^1A) \rightarrow A_2(^1A_2)$ ($\sigma \rightarrow \sigma^*$) and $A_1(^1A_1) \rightarrow E(^1E)$ ($d\pi \rightarrow \sigma^*$). Table 2 lists the relevant spectral data for the iridium series, and Figures 17 and 18 show the spectra of two of these complexes. The extinction coefficients, shapes, and energies of these bands allow the higher energy intense feature and the low energy feature in each case to be assigned as $\sigma \rightarrow \sigma^*$ and $d\pi \rightarrow \sigma^*$, respectively. Interestingly, there is no evidence for the $A_1(^1A_1) \rightarrow E(^3A_2)$ or the $A_1(^1A) \rightarrow E(^3E)$ transitions. Although it is possible that they are obscured by the intense bands, another possibility is that they lie at much lower energies because of substantially different electron repulsion terms and as a result cannot gain much intensity from allowed transitions of appropriate symmetry and are therefore simply too weak to be observed.

In order to gain some insight into the factors responsible for the trend in the energies of the $\sigma \rightarrow \sigma^*$ transitions it is pertinent to point out that the maxima in the chloride and the iodide adducts differ by 17 kcals for the iridium system whereas in the analogous rhodium system they differ by only

Figure 16. Molecular orbital diagram for $M_2(TMB)_4X_2^{2+}$.

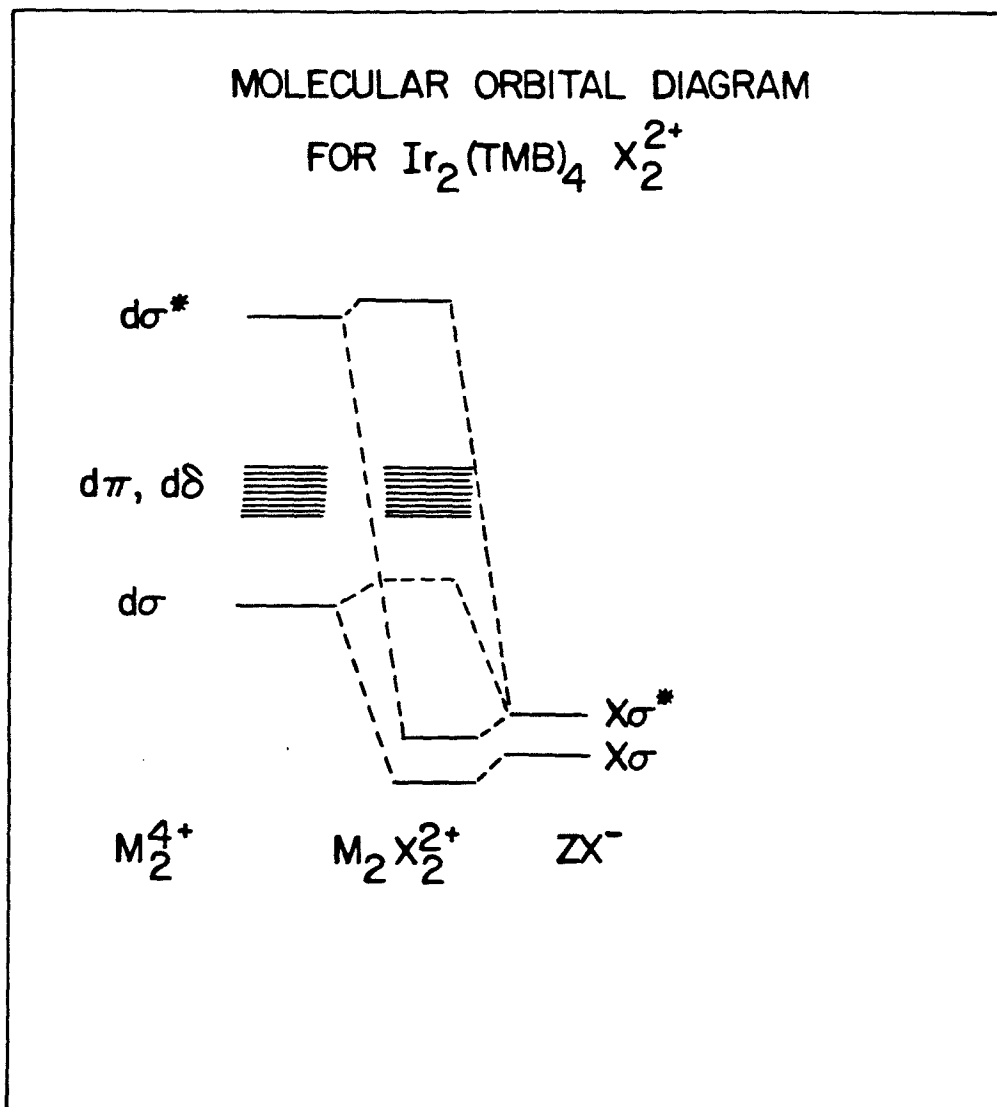


Table 2. Electronic absorption data for $\text{Ir}_2(\text{TMB})_4\text{X}_2(\text{BPh}_4)_2$

	λ_{max} (ϵ)		λ_{max} (ϵ)	
	nm	$\text{cm}^{-1} \text{ M}^{-1}$	nm	$\text{cm}^{-1} \text{ M}^{-1}$
$\text{Ir}_2(\text{TMB})_4\text{Cl}_2(\text{BPh}_4)_2$	274	(50,520)	349	(5910)
$\text{Ir}_2(\text{TMB})_4\text{Br}_2(\text{BPh}_4)_2$	297	(52,569)	330	(4510)
$\text{Ir}_2(\text{TMB})_4\text{I}_2(\text{BPh}_4)_2$	330	(49,800)	375	(8110)

Figure 17. Electronic absorption spectrum of $\text{Ir}_2(\text{TMB})_4\text{Cl}_2^{2+}$
in acetonitrile solution.

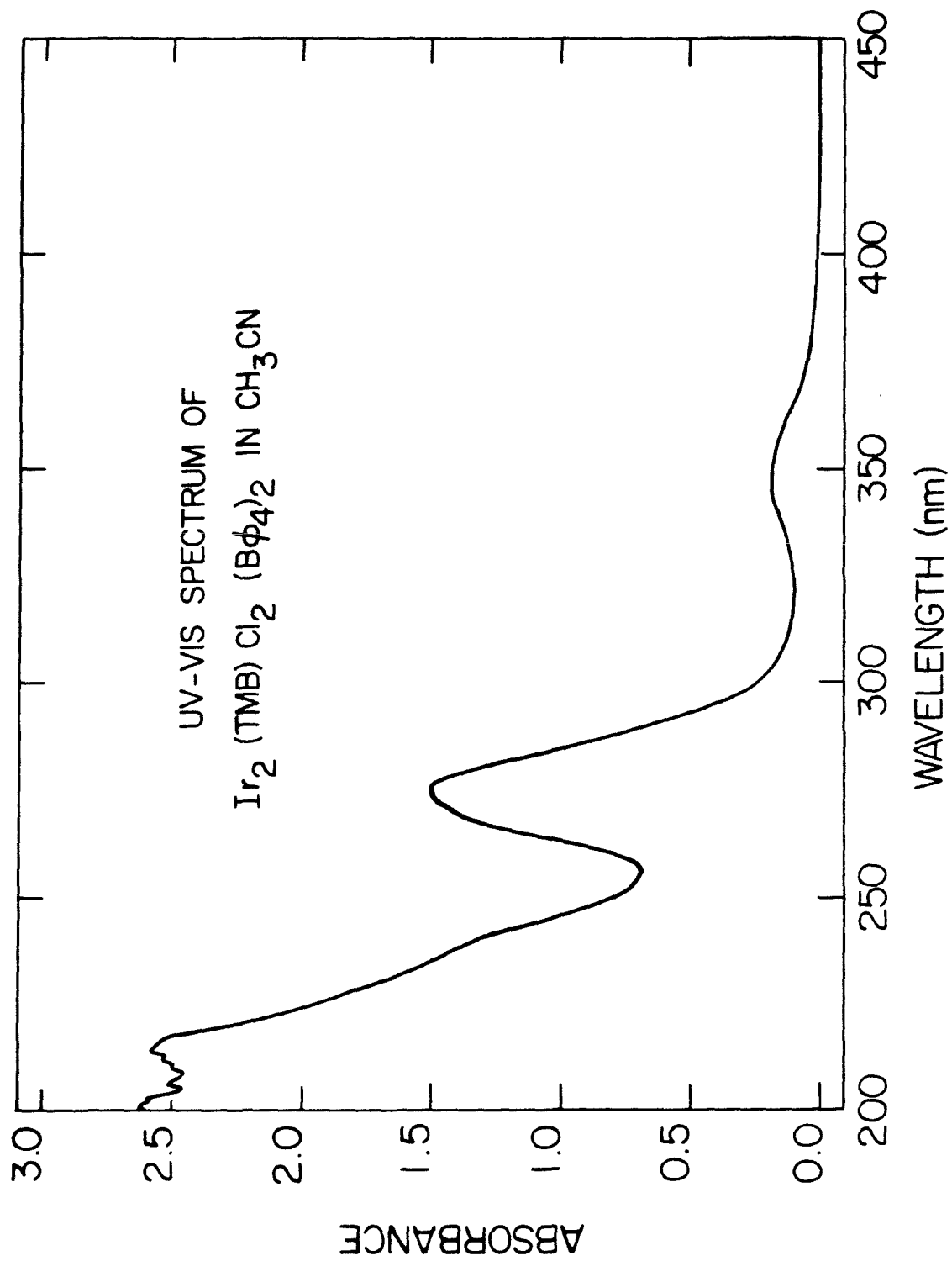
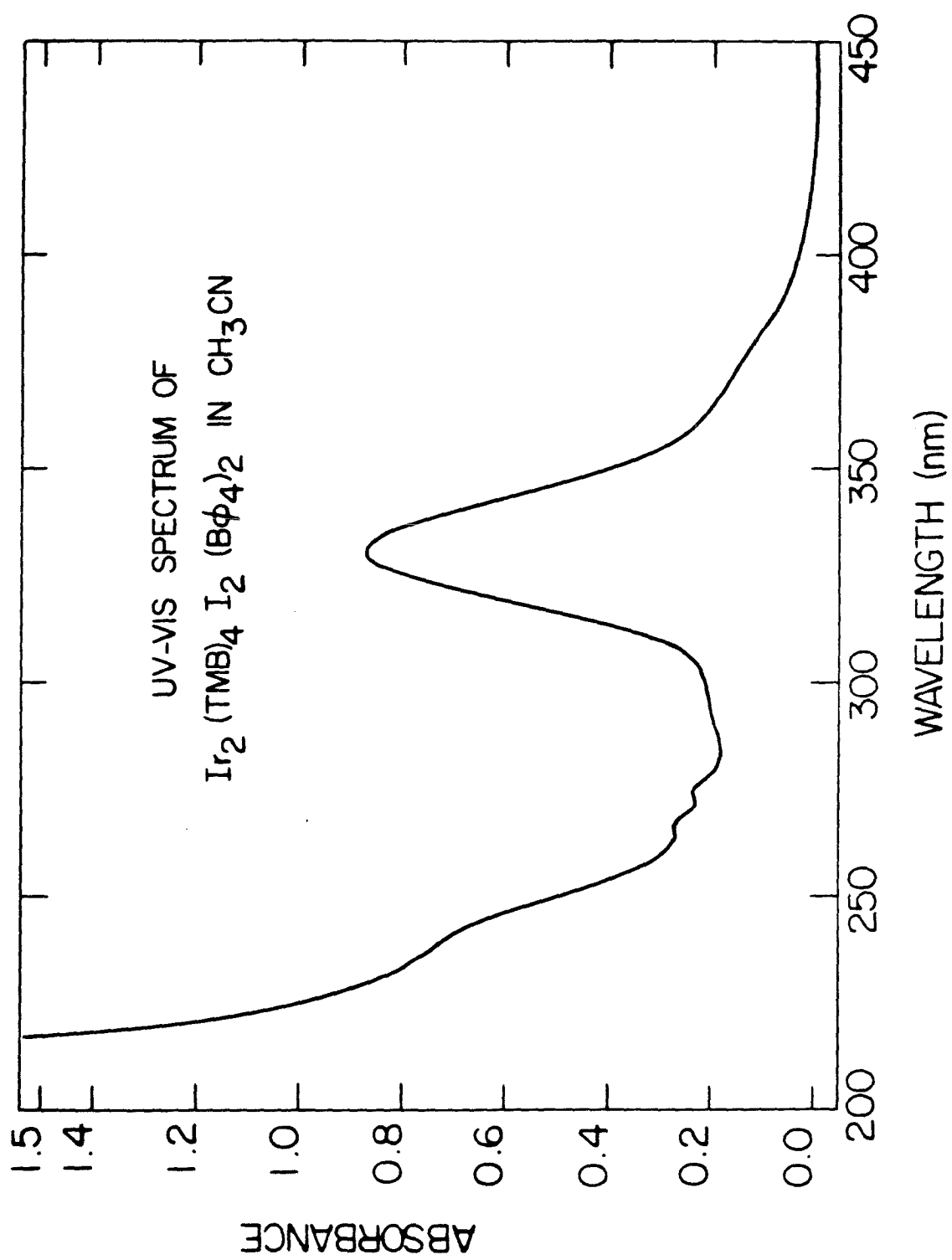


Figure 18. Electronic absorption spectrum of $\text{Ir}_2(\text{TMB})_4\text{I}_2^{2+}$
in acetonitrile solution.



8 kcals. Also, since the iridium-iridium bond strength is expected to be stronger, it is not clear why it would be more affected by axial ligation. If these differences actually reflected a change in the metal-metal bond strength, a substantial variation in metal-metal bond distance would be expected by changing the halide.

There are only two pertinent binuclear systems that have been studied by single crystal X-ray diffraction methods: the mercurous salts^{67,68} and the binuclear rhodium isocyanides.^{69,70} The mercury(I) complexes, where the axial ligands are OH_2 , F^- , Cl^- , or Br^- , have intermetallic distances of $2.51 \pm .02 \text{ \AA}$ and $\text{Rh}_2(\text{TMB})_4\text{Cl}_2^{2+}$ and $\text{Rh}_2(\text{CN-tolyl})_8\text{I}_2^{2+}$ have intermetallic distances of 2.770 \AA and 2.785 \AA , respectively. These structures suggest that the metal-metal bond strength is not varying a great deal as a result of halide substitution.

The most reasonable interpretation of this trend is that the $\sigma \rightarrow \sigma^*$ transition acquires some halide-to-metal charge transfer character. Consistent with this argument is the fact that the $\sigma \rightarrow \sigma^*$ transition for $\text{Rh}_2(\text{TMB})_4(\text{OH}_2)_2^{4+}$ lies at higher energy than the chloride adduct. This implies that for the binuclear complexes with axial π -donor ligands the $\sigma \rightarrow \sigma^*$ transition is not a valid indication of metal-metal bond strength.

Although the photochemistry of the $M_2(\text{diisocyanoalkanes})_4^{2+}$ complexes has not been examined in great detail, some interesting observations have been made. Miskowski and Gray⁷¹ have reported that photolysis of the binuclear rhodium complexes in the presence of radical traps results in the production of the corresponding rhodium(I) complexes. Similarly, irradiation ($\lambda = 256 \text{ nm}$) of $\text{Ir}_2(\text{TMB})_4\text{Cl}_2$ in the solid state results in the formation of $\text{Ir}_2(\text{TMB})_4^{2+}$, presumably with loss of chlorine. On the other hand, irradiation of a 6 M HCl solution of $\text{Ir}_2(\text{TMB})_4\text{HCl}^{2+}$ results in formation of $\text{Ir}_2(\text{TMB})_4\text{Cl}_2^{2+}$. Unfortunately, however, prolonged photolysis leads to disappearance of both species. The photochemistry reflects the metal-halide antibonding character in the σ^* orbital and also the fact that the ligand effectively prevents homolytic cleavage of the metal-metal bond.

FAR INFRARED AND RAMAN STUDIES

The first reported assignment of a feature in a vibrational spectrum to a metal-metal stretch was made in 1934 by Woodward while studying aqueous mercurous ions.⁷² Since this time, Raman spectroscopy has become a powerful tool and great strides have been taken in understanding the relationship between observed frequencies and in the strength of metal-metal interactions.

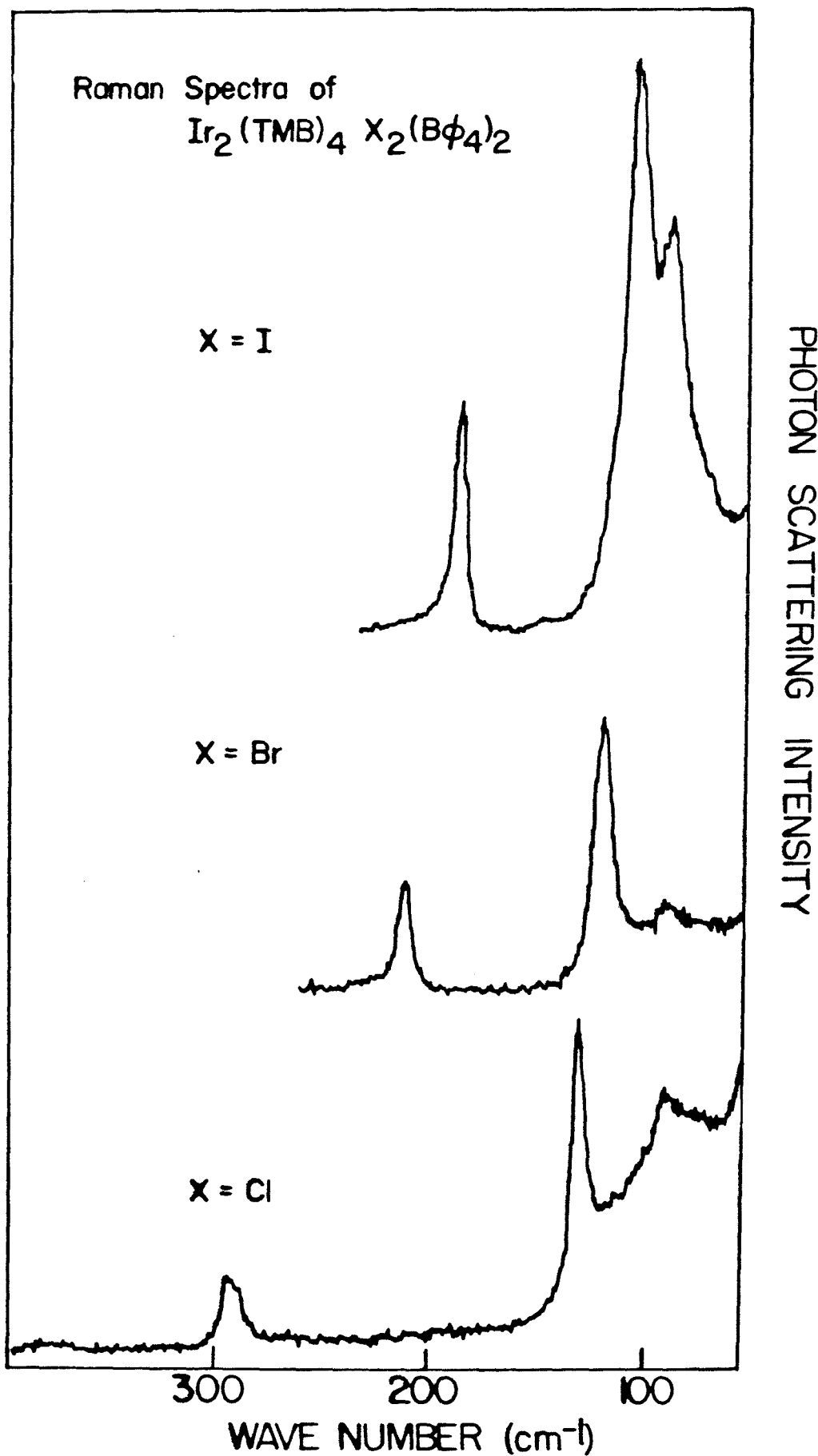
In principle, vibrational spectroscopy can yield a considerable amount of information not only about the strength of metal-metal bonds but also about the dynamics of the bonding (*i.e.* how the electron density changes as the atoms are displaced from their vibrational ground state equilibrium positions). This information is obtained by fitting the observed frequencies to an appropriate force field and deriving a set of force constants. In practice, however, a complete and unique description for a given molecule is rarely realized because the number of force constants necessary to describe a system generally exceeds the number of observed frequencies. This problem can be alleviated by careful studies on isotopically substituted systems, but for most cases this is an expensive and tedious task. In lieu of isotope data, the most common approach in dealing with complex systems is to make certain assumptions (*e.g.* set some of the non-principal force constants equal to zero). Although this tends to lead to values for the other force

constants which may not be absolutely correct, the relative values often reflect important trends.⁷³

The $\text{Ir}_2(\text{TMB})_4\text{X}_2^{2+}$ system is extremely complex, possessing 342 possible degrees of vibrational freedom. Fortunately, however, most of these modes are localized on the ligands and have little effect on the modes associated with the $\text{Ir}_2\text{X}_2^{2+}$ core. Studies on the group VII carbonyls have been particularly useful in demonstrating that the equatorial ligands do not have a great effect on the metal-metal mode. In fact, for the third row dimer, $\text{Re}_2(\text{CO})_{10}$, the value for the metal-metal force constant using the diatomic approximation was the same as the value obtained from a detailed force field calculation. The fact that the $\text{Ir}_2\text{X}_2^{2+}$ core is a visible chromophore greatly simplifies the process of identifying which modes are associated with this unit because of the large preresonance enhancement. In this section, a number of force fields are applied to $\text{Ir}_2(\text{TMB})_4\text{I}_2^{2+}$.

Considering just the $\text{M}_2\text{X}_2^{2+}$ core, group theory⁷⁴ predicts three stretching modes: two totally symmetric modes, Σ_g^+ (Raman allowed) and one asymmetric mode, Σ_u^+ (infrared allowed). Figure 19 shows the Raman spectra of the three halide adducts. Three distinct features are clearly resolved. The lowest energy, essentially invariant feature cannot be rigorously assigned; it may be an Ir-Ir-C deformation. In any case, this assignment is unimportant in the ensuing discussion. The

Figure 19. Raman spectra of $\text{Ir}_2(\text{TMB})_4\text{X}_2^{2+}$.



energies of the two higher energy features in the Raman spectra (ν_1 and ν_2) and the energy of the asymmetric stretch (ν_3) in the IR are presented in Table 3. The most intense feature in each Raman spectrum can be tentatively assigned as predominantly due to a metal-metal stretch and the higher energy feature can be assigned to a metal-halide stretch; similar assignments have been made for the more extensively studied mercurous halide.⁷⁵

The most trivial force field which can be considered for this system is obtained by assuming that the $M_2X_2^{2+}$ core is a hypothetical diatomic system, $XM-MX^{2+}$. The frequency (ν) of the "metal-metal" stretch can be expressed as $\nu = (f_d/4\pi^2\mu)^{1/2}$, where f_d is the force constant and μ is the reduced mass $\frac{(MW_{Ir-X})^2}{2MW_{Ir-X}}$. Since crystallographic information on similar systems (see previous section) suggests that the bond strengths are roughly equal, to a first approximation the value of f_d can be considered constant in the series. So using the frequency of 140 cm^{-1} and the appropriate reduced mass for $Ir_2(TMB)_4Cl_2^{2+}$ a value of $1.31\text{ md/\AA}^{\circ}$ is obtained for f_d . The frequencies for the bromide and iodide adducts can then be predicted. They are 128 cm^{-1} and 118 cm^{-1} , respectively, in excellent agreement with observed values. Unfortunately, this same analysis performed on similar systems does not adequately account for the changes in frequency, so the agreement found for the iridium system is probably somewhat fortuitous.

Table 3. Frequencies of $\text{Ir}_2(\text{TMB})_4\text{X}_2^{2+}$ in the 100 cm^{-1} to 400 cm^{-1} region

X	$\frac{\nu_1}{\text{cm}^{-1}}$	$\frac{\nu_2}{\text{cm}^{-1}}$	$\frac{\nu_3}{\text{cm}^{-1}}$
Cl	140	297	274
Br	128	217	196
I	116	193	149

Nonetheless, the effective reduced mass undoubtedly plays a significant role in determining the frequency of the vibration. In this context, the iridium system shows the least variation in metal-metal stretch.

There are a number of deficiencies in the above force field; the most serious of these is the neglect of the interaction between the other totally symmetric mode. A more realistic force field has to take into account the mixing of the metal-metal and metal-halide vibrations because they are coupled not only mechanically but electronically as well. Thus, a more general expression must be used to describe the potential energy of the system. The equation for the general force field for a linearly symmetric tetraatomic molecule is given below (equation 9).⁷⁶

$$2V = f_d (Q_{23}^2) + f_r (Q_{12}^2 + Q_{34}^2) + f_{dr} (Q_{12}Q_{23} + Q_{23}Q_{34}) + f_{44} (Q_{12}Q_{34}) \quad (\text{eq. 9})$$

V is the potential energy; f_d and f_r are the valence metal-metal and metal-halide force constants, respectively; and f_{dr} and f_{rr} are interaction constants between adjacent and non-adjacent bonds respectively; and Q_{ij} are normal coordinates in the system.

Since there are only three observed frequencies and four force constants, the system possesses an infinite

number of solutions. The extreme values for the principal force constants can be calculated. These calculations were performed employing F and G matrixes (shown in Table 4) using symmetry coordinates. The relationships between symmetry coordinates and internal coordinates are given in Table 5.⁷⁷

Two force fields, FFI, and FFII are shown in Tables 6 and 7. These force fields represent limiting values for the symmetry force constant F_{11} . The assumption in FFI is that ν_2 is the stretching frequency of an isolated Ir-X symmetry coordinate and therefore $f_{rr} = \frac{1}{2}(F_{11} + F_{22})$. The assumption involved in FFII is that $F_{11} = F_{33}$ and therefore $f_{rr} = 0$. FFI appears to be a more reasonable force field for the halide series as the metal-metal force constants are reasonably constant. Also, the potential energy distribution and values of f_{dr} reflect expected increases in mixing of the metal-metal and metal-halide modes as the weight of the halide approaches that of the metal.

FFII, on the other hand, predicts large variations in the metal-halide and metal-metal bond strengths, in particular, the dramatic increase in f_d seems unreasonable. An interesting feature of FFII is that the potential energy distribution for the iodide adduct actually indicates that the character of ν_1 and ν_2 have been interchanged (*i.e.* ν_1 is mainly an iridium-iodide stretch whereas ν_2 is mainly

Table 4. F and G matrixes, and equations relating symmetry force constants to valence force constants

Symmetry force constant: F

$$\Sigma_g^+ \begin{vmatrix} F_{11} & F_{12} \\ F_{12} & F_{22} \end{vmatrix} \qquad \Sigma_u^+ \begin{vmatrix} F_{33} \end{vmatrix}$$

$$F_{11} = f_r + f_{rr}$$

$$F_{33} = f_r - f_{rr}$$

$$F_{22} = f_d$$

$$F_{12} = \sqrt{2} f_{rd}$$

Symmetry kinetic energy matrix: G

$$\Sigma_g^+ \begin{vmatrix} G_{11} & G_{12} \\ G_{12} & G_{22} \end{vmatrix} \qquad \Sigma_u^+ \begin{vmatrix} G_{33} \end{vmatrix}$$

$$G_{11} = g_r + g_{rr}$$

$$G_{33} = g_r - g_{rr}$$

$$G_{22} = g_d$$

$$G_{12} = \sqrt{2} g_{rd}$$

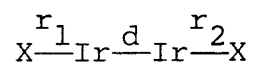
$$g_r = 1/M_x + 1/M_{Ir},$$

$$g_{rr} = 0, g_{rd} =$$

$$-1/M_{Ir} \text{ and}$$

$$g_d = 2/M_{Ir}$$

Table 5. Internal coordinates and symmetry coordinates of X-M-M-X core.



$$\begin{array}{ll} s_1 = 1/\sqrt{2} (\Delta r_1 + \Delta r_2) & \Sigma_g^+ \\ s_2 = \Delta d & \\ s_3 = 1/\sqrt{2} (\Delta r_1 - \Delta r_2) & \Sigma_u^+ \end{array}$$

Table 6. Force Field I

	F_{11}	F_{22}	F_{33}	F_{12}	f_r	f_d	f_{rr}	f_{rd}
					(md/Å)			
Ir_2Cl_2	1.56	1.32	1.33	.16	1.44	1.32	.115	.226
Ir_2Br_2	1.57	1.38	1.28	.321	1.42	1.38	.145	.454
Ir_2I_2	1.68	1.37	1.00	.434	1.35	1.37	.340	.614

Potential energy distributions for FFI:

Ir_2Cl_2	ν_2 (297 cm^{-1}):	$99.9 \nu_1 + 5.2 \nu_2 - 5.1 \nu_1 \nu_2$
	ν_1 (140 cm^{-1}):	$1.4 \nu_1 + 96.0 \nu_2 + 2.6 \nu_1 \nu_2$
	ν_3 (274 cm^{-1}):	$100 \nu_3$
Ir_2Br_2	ν_2 (217 cm^{-1}):	$97.7 \nu_1 + 23.1 \nu_2 - 20.8 \nu_1 \nu_2$
	ν_1 (128 cm^{-1}):	$7.3 \nu_1 + 81.9 \nu_2 + 10.7 \nu_1 \nu_2$
	ν_3 (196 cm^{-1}):	$100 \nu_3$
Ir_2I_2	ν_2 (193 cm^{-1}):	$95.1 \nu_1 + 40.3 \nu_2 - 35.4 \nu_1 \nu_2$
	ν_1 (116 cm^{-1}):	$13.8 \nu_1 + 68.5 \nu_2 + 17.6 \nu_1 \nu_2$
	ν_3 (149 cm^{-1}):	$100 \nu_3$

Table 7. Force Field II

	F_{11}	F_{22}	F_{33}	F_{12}	f_r	f_d	f_{rr}	f_{rd}
	(md/Å)							
Ir_2Cl_2	1.33	1.56	1.33	-.19	1.33	1.56	0	-.269
Ir_2Br_2	1.28	1.62	1.28	.148	1.28	1.62	0	.209
Ir_2I_2	1.10	2.09	1.00	.427	1.05	2.09	.05	.604

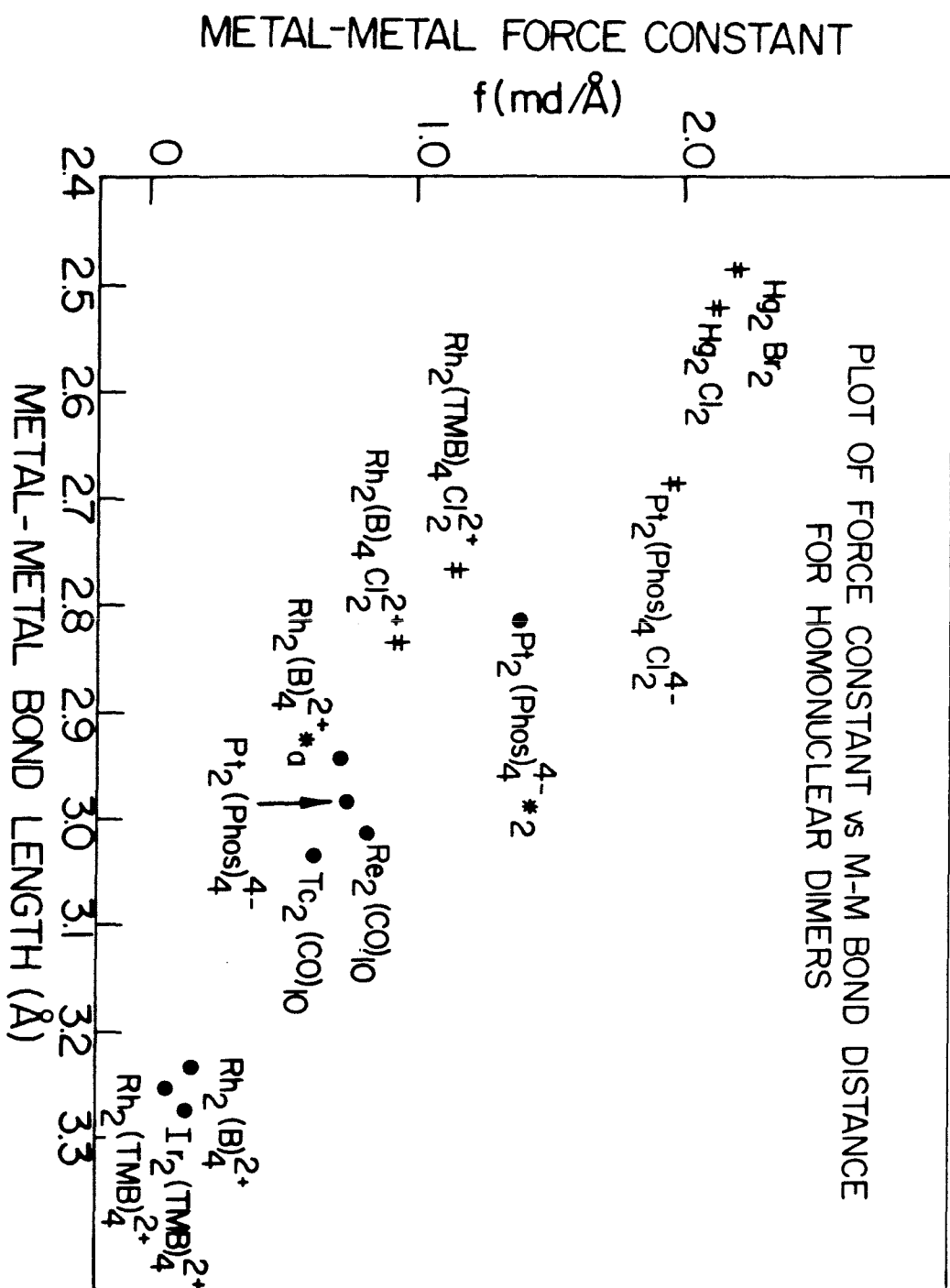
Potential energy distribution for FFII

Ir_2Cl_2	ν_2 (297 cm^{-1}):	$80.8 \nu_1 + 11.2 \nu_2 + 8.0 \nu_1 \nu_2$
	ν_1 (140 cm^{-1}):	$20.9 \nu_1 + 90.6 \nu_2 + 11.5 \nu_1 \nu_2$
	ν_3 (274 cm^{-1}):	$100 \nu_3$
Ir_2Br_2 :	ν_2 (217 cm^{-1}):	$71.4 \nu_1 + 39.5 \nu_2 - 10.9 \nu_1 \nu_2$
	ν_1 (128 cm^{-1}):	$29.6 \nu_1 + 61.6 \nu_2 + 8.8 \nu_1 \nu_2$
	ν_3 (196 cm^{-1}):	$100 \nu_3$
Ir_2I_2 :	ν_2 (193 cm^{-1}):	$41.3 \nu_1 + 93.8 \nu_2 - 35.0 \nu_1 \nu_2$
	ν_1 (116 cm^{-1}):	$67.3 \nu_1 + 14.9 \nu_2 - 17.8 \nu_1 \nu_2$
	ν_3 (149 cm^{-1}):	$100 \nu_3$

an iridium-iridium stretch). Based on the relative intensities exhibited in the spectrum of the complex, this interchange seems highly unlikely because the metal-metal stretch should result in the greatest polarization and therefore greatest intensity. Interestingly, constraining the value of $f_{rr} \sim 0$ has a dramatic effect on the iodide adduct whereas the force constants for the chloride and bromide adducts seem reasonable.

Metal-Metal bond lengths are inversely proportional to the metal-metal force constants. Figure 20 illustrates this relationship for 2nd and 3rd row binuclear complexes. For complexes containing a M_2 core, the diatomic approximation was used, whereas for complexes containing an M_2X_2 core the approximate equations found in Hertzberg were employed.⁷⁶ (The equations in Hertzberg are similar to FFII which assumes $f_{rr} = 0$. Unfortunately, these equations are invalid for the iodide adducts). Despite the shortcomings of these force fields, the correlation is quite impressive throughout the effective metal-metal single bond range. Importantly, the equatorial ligands and the presence of bridging ligands have little effect, suggesting that the metal-metal stretch is essentially isolated. Most surprising is the fact that the correlation is linear even though the formal bonding is quite different. Perhaps this reflects the hybrid character of the metal-metal bond (*e.g.* it may be better to describe the bonding

Figure 20. Plot of metal-metal force constant *vs.* metal-metal bond length. (Compiled from references 10, 11, 14, 67, 68, 69, 71, 75, 76-86.)



in $\text{Re}_2(\text{CO})_{10}$ as $\text{Sd}^7\text{-Sd}^7$ or $\text{pd}^7\text{-pd}^7$ as opposed to simply $d^7\text{-d}^7$).

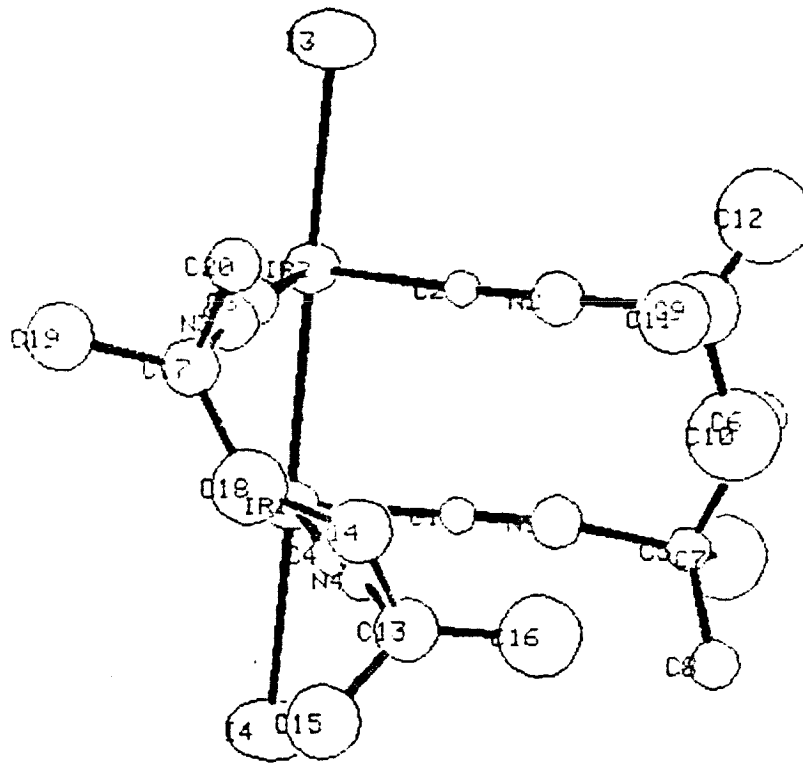
Theoretically, the force constant should be proportionate to the inverse sixth power of the bond length,⁸⁷⁻⁸⁹ and in many organic systems, this relationship or similar ones have been borne out.^{90,91} Reasons for the linear relationship between metal-metal distance and the force constants are not obvious. However, it should be noted that even in the organic systems there are substantial portions of the plot of force constant *vs.* bond distances which can be fit to a straight line. In any case, the correlation is significant as it allows a reasonably accurate indication of the metal-metal bond length from spectroscopically obtained parameters.

STEREODYNAMICS OF $M_2(TMB)_4^{2+}$ AND
 $M_2(TMB)_4X_2^{2+}$ COMPLEXES

The low temperature (-60°C) ^1H NMR spectrum of $\text{Rh}_2(\text{TMB})_4^{2+}$ reveals two resonances associated with the methyl protons on the TMB ligand. At room temperature only one resonance is observed which indicates that some process is rapidly interconverting the two types of methyl groups. Over approximately the same temperature range that this process is frozen out, the lifetime of the $E(^3A_2)$ excited state is observed to rapidly increase. The possibility that these phenomena were related prompted us to study the ligand dynamics and determine the activation energies for this process. To examine the effect of changes in metal and oxidation state, three other complexes were also examined.

The TMB ligand, along with the two metal atoms, form a ten atom ring. Because the $M-C\equiv N-C$ unit is essentially linear, it is valid to view the ring as a six-sided figure, thereby allowing the conformational changes to be discussed in terms of the more familiar six membered ring system. Just as in cyclohexane, a number of conformations can be adopted by the M_2 TMB ring. The most common conformer in the solid state corresponds approximately to a skew boat (conformer A).⁹² This conformation is illustrated in the ORTEP drawing of $\text{Ir}_2(\text{TMB})_4^{2+}$ (Figure 21). Two types of

Figure 21. ORTEP showing conformation of crystallographically inequivalent ligands.



methyl groups are clearly distinguished: axial and equatorial. A similar conformation¹⁰ is found in the structure of $\text{Rh}_2(\text{TMB})_4\text{Cl}_2^{2+}$. Another conformer which possesses distinct axial and equatorial methyl groups corresponds to a distorted chair (conformer B); however, there is no precedent for this structural type in the solid state. Although crystal packing forces may influence the conformation of the ligand, for the purpose of discussion, conformer A will be assumed to be the low energy conformation in solution as well.

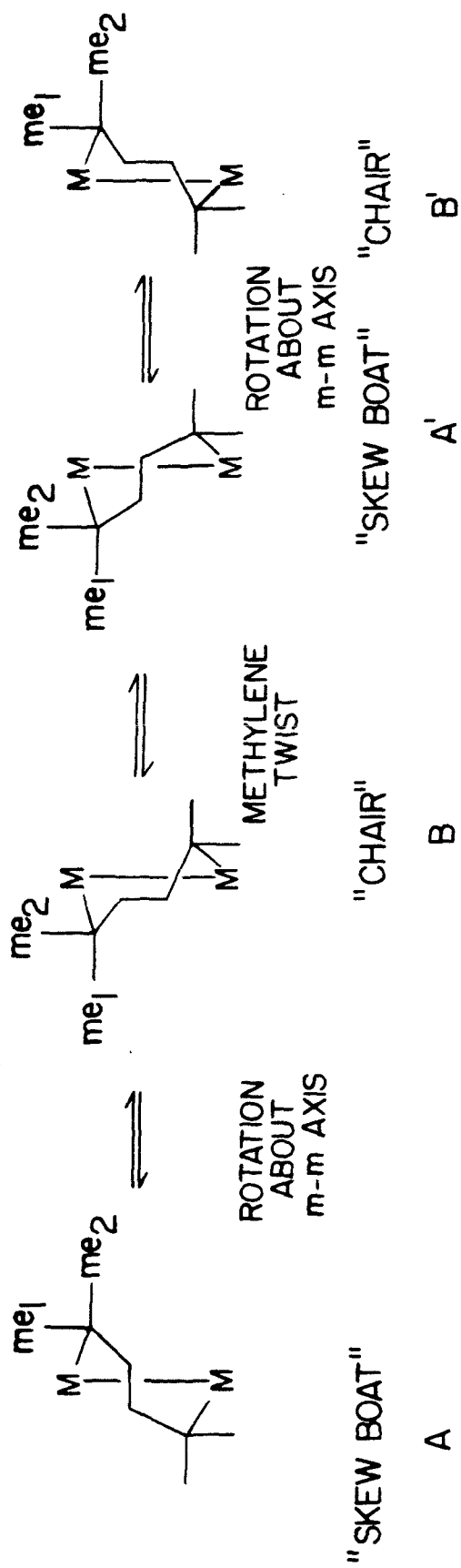
Examination of molecular models of $\text{M}_2(\text{TMB})_4^{2+}$ indicates that conformers A and B can be easily interconverted by rotation about the metal-metal axis. This motion converts the axial groups of conformer A to equatorial groups of conformer B and vice versa. It is, however, quite unlikely that this motion is responsible for the methyl interchange observed in the ^1H NMR experiment because it would require that conformers A and B not only be isoenergetic but also have identical chemical shifts for the axial and equatorial groups. In order to completely interchange the axial and equatorial methyl groups of conformer A, it is necessary to first rotate about the metal-metal axis to conformer B and then twist the methylene groups 90° . These motions give conformer A', the mirror image of conformer A. This

process is shown in Figure 22. Of course, this rearrangement could conceivably be accomplished by a concerted, one-step rearrangement, but in view of the other studies on ring inversion processes, this seems highly unlikely.

The variable temperature ^1H NMR spectra of $\text{Rh}_2(\text{TMB})_4^{2+}$ at 90 MHz and 500 MHz in d_2 -dichloromethane are shown in Figure 23 and 24, respectively. At ambient temperature only one peak is observed for the methyl protons. As the solution is cooled the peak broadens, coalescence occurs at $-20 \pm 2^\circ\text{C}$, further cooling results in resolution of two distinct methyl resonances. The asymmetry in the methyl region in the 90 MHz spectrum is due to overlap with the methylene resonances. At low temperature in the 500 MHz spectrum methylene resonance is clearly split and some coupling is resolved. The analogous d^8 - d^8 iridium dimer, $\text{Ir}_2(\text{TMB})_4^{2+}$ behaves quite similarly; however, the coalescence temperature is much higher ($15 \pm 2^\circ\text{C}$).

The actual spectra of the two oxidized species, $\text{Ir}_2(\text{TMB})_4\text{I}_2^{2+}$ and $\text{Rh}_2(\text{TMB})_4\text{Br}_2^{2+}$, are slightly different than those of the reduced dimers in that the resonance due to the methylene protons are clearly separated from resonances due to the methyl protons. Figure 25 shows the spectrum of $\text{Rh}_2(\text{TMB})_4\text{Br}_2^{2+}$. The coalescence temperatures for $\text{Ir}_2(\text{TMB})_4\text{I}_2^{2+}$ and $\text{Rh}_2(\text{TMB})_4\text{Br}_2^{2+}$ are at -14°C and -11°C , respectively, nearly identical. The NMR data for all these complexes are summarized in Table 8.⁹³

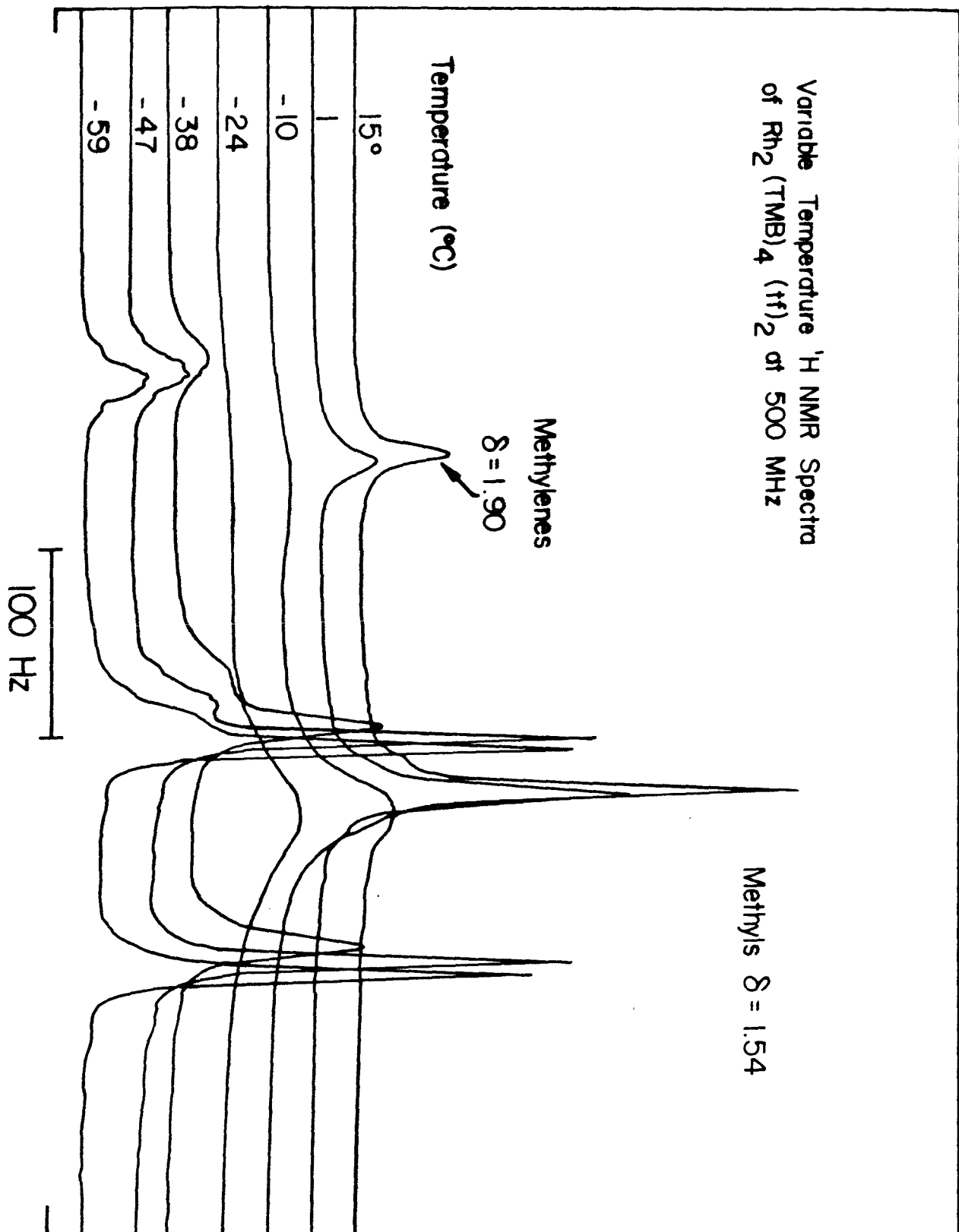
Figure 22. Ligand motions in two TMB binuclear complexes.



LIGAND MOTIONS IN TMB BINUCLEAR COMPLEXES

Figure 23. Variable temperature ^1H NMR spectra of $\text{Rh}_2(\text{TMB})_4^{2+}$ at 90 MHz.

Figure 24. Variable temperature ^1H NMR spectra of $\text{Rh}_2(\text{TMB})_4^{2+}$ at 500 MHz.



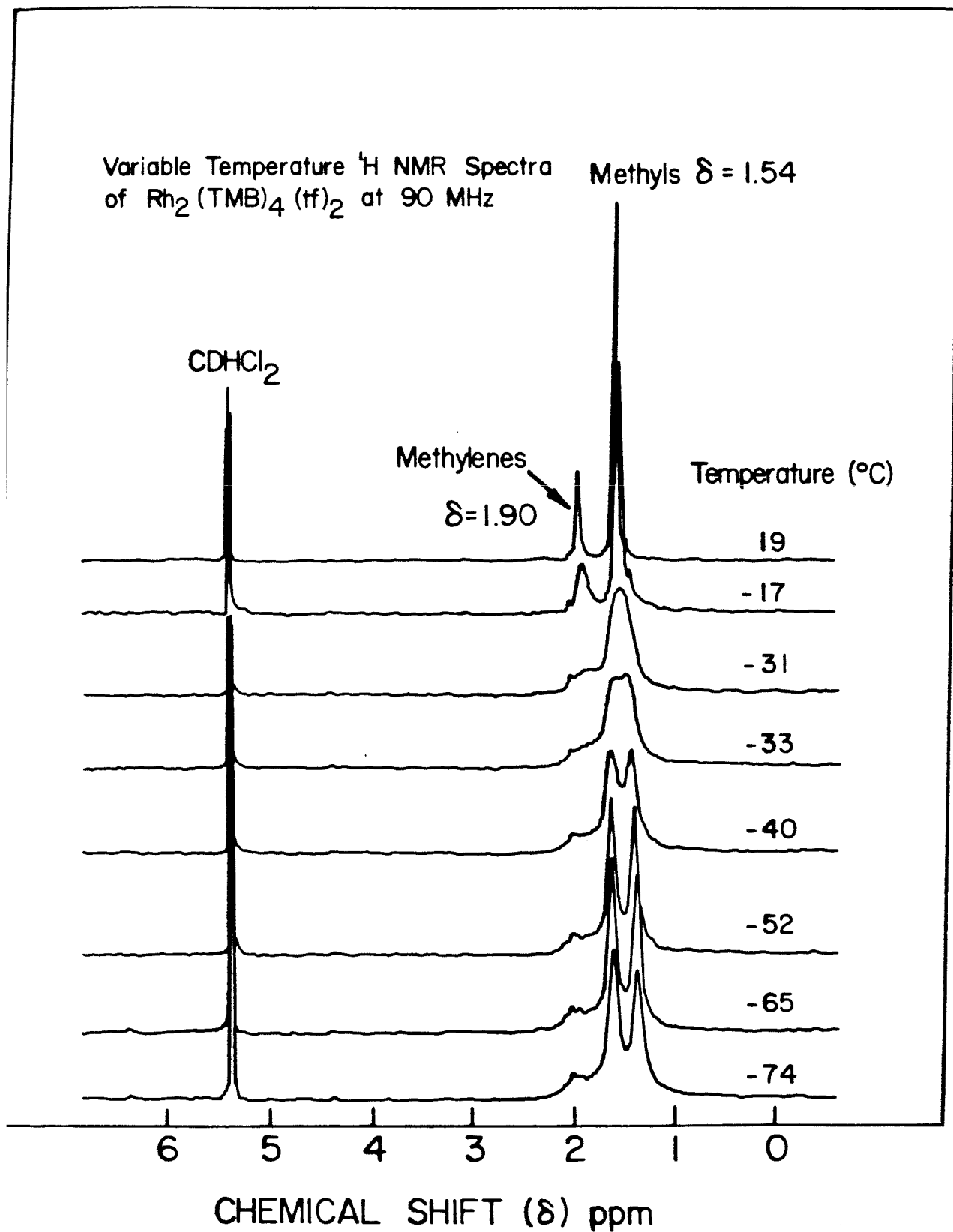


Figure 25. Variable temperature ^1H NMR of the oxidized species, $\text{Rh}_2(\text{TMB})_4\text{Br}_2^{2+}$.

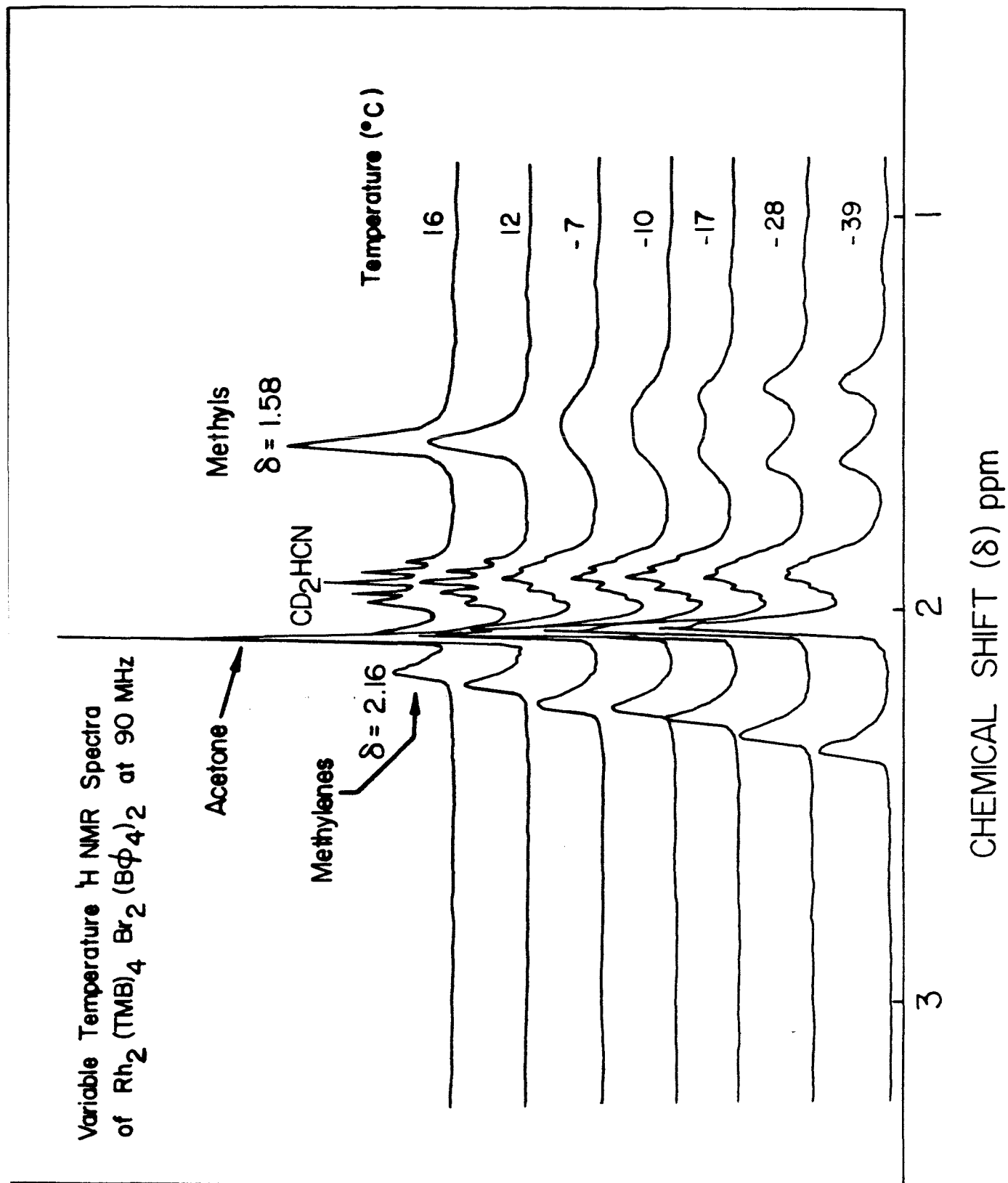


Table 8. NMR Data for $M_2(TMB)_4^{2+}$ and $M_2(TMB)_4X_2^{2+}$ Complexes

Complex	ν MHz	CHEMICAL SHIFTS				T_c C	\dagger Kcal/ mole
		Stopped Exchange methylenes	Fast Exchange methylenes	Fast Exchange methyls			
$Rh_2(TMB)_4(tf)_2$	90	1.93 multiplet	1.58	1.90	1.54	-32	12.1
			1.34				
$Rh_2(TMB)_4(tf)_2$	500	1.99	1.59	1.90	1.54	-19	12.0
		1.97	1.35				
$Rh_2(TMB)_4Br_2^-$ (BPh ₄) ₂	90	2.39	1.63	2.16	1.58	-11	13.3
			1.42				
$Ir_2(TMB)_4^-$ BPh ₄) ₂	90	1.78	1.58	1.72	1.46	15	14.7
			1.33				
$Ir_2(TMB)_4I_2^-$ (BPh ₄) ₂	90	2.36	1.63	2.11	1.54	-14	13.0
			1.33				

The behavior exhibited by the methyl protons is an example of two site exchange of an AB uncoupled system,⁹⁴ and the free energy of activation (ΔG^\ddagger) can be calculated using

$$\Delta G^\ddagger = -RT_c \ln \frac{h\pi \Delta\nu}{\sqrt{2} kT_c} ,$$

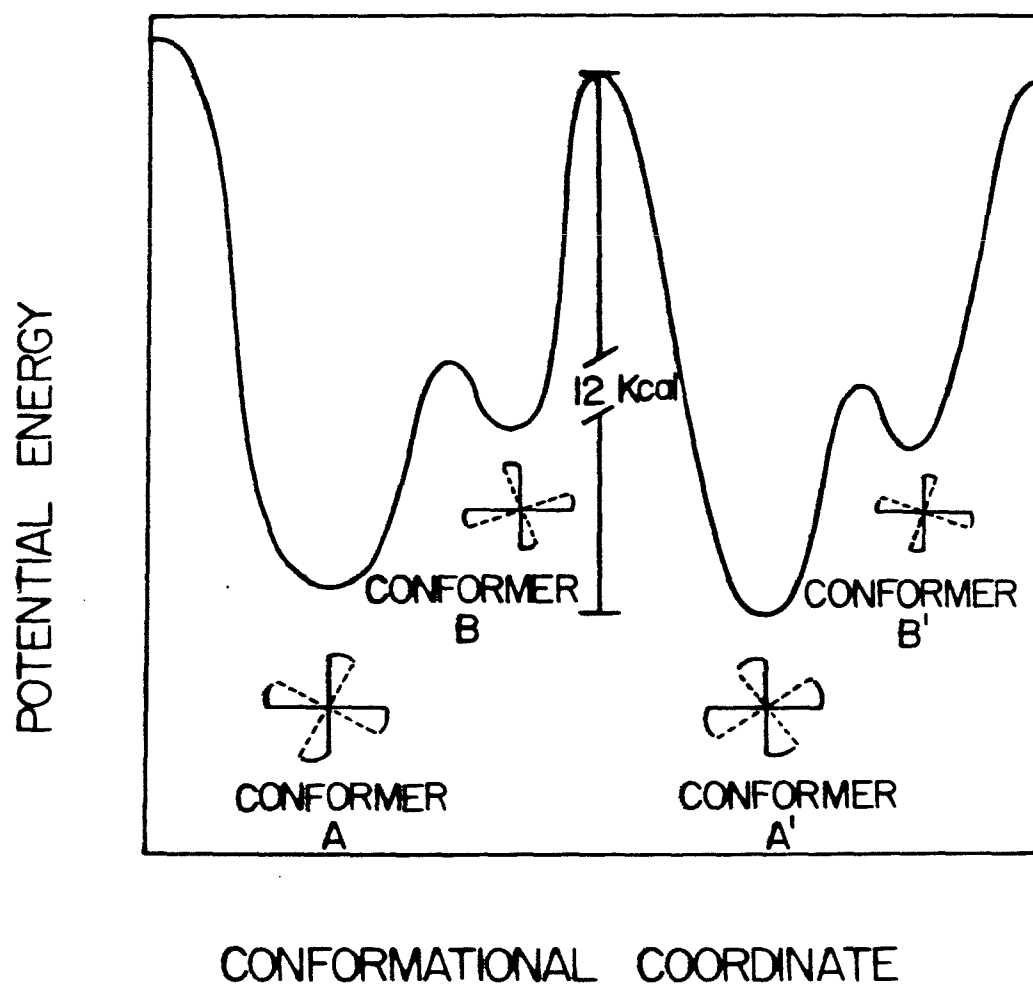
where ΔG^\ddagger is the free energy of activation, $\Delta\nu$ is the separation in Hertz between the A and B resonances in the stopped exchange limit, T_c is the coalescence temperature, k is Boltzmann's constant, h is Planck's constant, and R is the universal gas constant.⁹⁵

The values of ΔG^\ddagger for the $M_2(\text{TMB})_4$ complexes are listed in Table 8. They are quite similar to the free energy of activation observed for the chair-chair interconversion in cyclohexane (11 kcal/mole).⁹⁶ Although the ΔG^\ddagger values are very sensitive to the configuration of the ligand, there is no apparent correlation with metal-metal bond distance. However, the similar spectral data for $\text{Rh}_2(\text{TMB})_4\text{Br}_2^{2+}$ and $\text{Ir}_2(\text{TMB})_4\text{I}_2^{2+}$ suggest a very similar ligand configuration. Interestingly, the chemical shifts for the methyl protons indicate that the shielding is only slightly dependent on the metal and oxidation state.

A simplified potential energy profile for $\text{Rh}_2(\text{TMB})_4^{2+}$ is shown in Figure 26. A few points are worthy of mention:

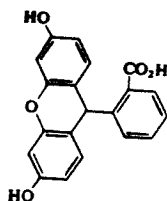
Figure 26. Potential energy diagram for $\text{Rh}_2(\text{TMB})_4^{2+}$.

POSSIBLE POTENTIAL ENERGY RELATIONSHIP
AMONG CONFORMATIONS IN $\text{Rh}_2(\text{TMB})_4^{2+}$

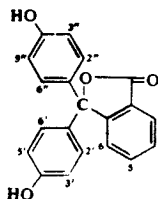


1) the measured activation energy represents the height of the highest barrier which is assumed on the basis of models to be the methylene twist; 2) the lowest energy conformer appears to be at least 2 to 3 kcal/mole more stable than the other conformers because there is no indication of another species in the NMR spectrum; 3) if the interchange process proceeds by maintaining square planar geometry about each metal center, the motions of all of the ligands must be coupled.

A well established tenet of organic photophysics is that the less rigid a chromophore is, the more likely the excited state will decay by non-radiative processes.³⁸ For example,⁹⁷ consider the two molecules below, fluorescein(I) and phenolphthalein(II):



1



11

Both molecules possess the same degree of conjugation and yet I is strongly fluorescent while II is virtually non-fluorescent. A similar situation appears to exist for $\text{Rh}_2(\text{B})_4^{2+}$ and $\text{Rh}_2(\text{TMB})_4^{2+}$ in which phosphorescence at room temperature are 4.0 μs and 25 ns, respectively.²² The shorter lifetime in $\text{Rh}_2(\text{TMB})_4^{2+}$ is due to deactivation by

thermal population of a nearby ligand field state which is unstable with respect to a D_{2d} distortion. The more flexible ligand, TMB, can accommodate this type of distortion whereas 1,3-diisocyanopropane essentially prohibits it. It is likely that this distortion (for $Rh_2(TMB)_4^{2+}$) will be particularly facile when the isocyanide groups are eclipsed because the ligand backbone is compressed in this configuration. It should be pointed out that the activation barrier associated with the decrease in lifetime is only ~ 6 kcal.

There are a number of reasons why the energy of activation (E_a) associated with the lifetime dependence and the free energy of activation (ΔG^\ddagger) for the conformational process cannot be directly compared. First, although motions of the ligand are necessarily involved in both processes, it is not clear that they involve the same motions. Second, the ΔG^\ddagger is for the ground state complex not for the excited state complex. Third, E and ΔG are different thermodynamic state functions.⁹⁸ The Arrhenius energy (E_a') for the conformation process is related to ΔG^\ddagger by the following equation, $E_a' = \Delta G^\ddagger + T\Delta S^\ddagger + RT$, where ΔS^\ddagger is the entropy of activation. But without specific knowledge of the entropy term, any quantitative comparison is virtually meaningless.

X-RAY DIFFRACTION STUDY ON $\text{Ir}_2(\text{TMB})_4\text{I}_2(\text{BPh}_4)_2 \cdot 8 \text{ ACETONE}$

While over a dozen square planar tetrakisocyanide rhodium complexes have been examined by single crystal X-ray diffraction, no work has been reported on the analogous iridium systems. This section discusses the structure of $\text{Ir}_2(\text{TMB})_4\text{I}_2(\text{BPh}_4)_2$ at its current stage of refinement. Considerable difficulties have plagued the refinement process. In part, this is viewed as a consequence of the alignment of the heavier scatters. Emily Maverick is credited with locating the tetraphenylborates and solvent molecules. The scattering factors were obtained from the following sources: Cromer and Weber (iridium and iodine),⁹⁹ International Tables (carbon, nitrogen, boron),¹⁰⁰ and Stewart et al. (hydrogen).¹⁰¹

A Patterson map was generated to locate the positions of the heavy atoms. However, the solution was ambiguous. Fortunately, the use of direct methods with upweighted, $l = \text{odd}$ reflections, indicated that the iridiums were at (.25 .25 .4433) and (.25 .25 .3259). The initial agreement factor (R) was $\sim 32\%$. Many successive Fourier syntheses were necessary to locate the rest of the non-hydrogenic atoms on the dimer and the counteranion. Only at this point were the solvent molecules observable on the difference Fourier maps. The solvents were ill-defined and were refined with large thermal parameters.

The occupancy was also refined and found to be .75 (*i.e.* six acetones/unit cell). The phenyl rings of the tetraphenylborate were refined as rigid bodies and finally hydrogen atoms were added as riding atoms at .95 Å. No intermolecular close contacts appear to exist. In spite of the difficulties, the structure did converge at this point. The agreement factors are: $R_w = 11\%$, $R = 13\%$.

An ORTEP of the dimer is shown in Figure 27 and select bond distances and angles are listed in Table 9. The error in heavy atom distances (.004 Å) is approximately an order of magnitude better than for the error in the distances between the lighter atoms ($\sim .04$ Å). The average values for the distances seem reasonable within the large error limits. The distances between Ir(1)-C(4) and C(4)-N(4) appear unreasonable. The overall configuration of the ligand is very similar to that of $\text{Rh}_2(\text{TMB})_4\text{Cl}_2^{2+10}$. In both cases the ligands are staggered by $\sim 31^\circ$. The only meaningful comparisons to be pointed out are the iridium-iodide distance and the iridium-iridium distance. The distance of 2.73 Å for the iridium-iodide distance falls within the wide range (2.67 Å - 2.79 Å),^{102,103} exhibited for terminal iridium-iodide bond lengths, indicating that the metal-metal trans-influence is not exceptional. The iridium-iridium bond distance (2.80 Å) is somewhat longer ($\sim .1$ Å) than that found for

Figure 27. ORTEP of $\text{Ir}_2(\text{TMB})_4\text{I}_2^{2+}$.

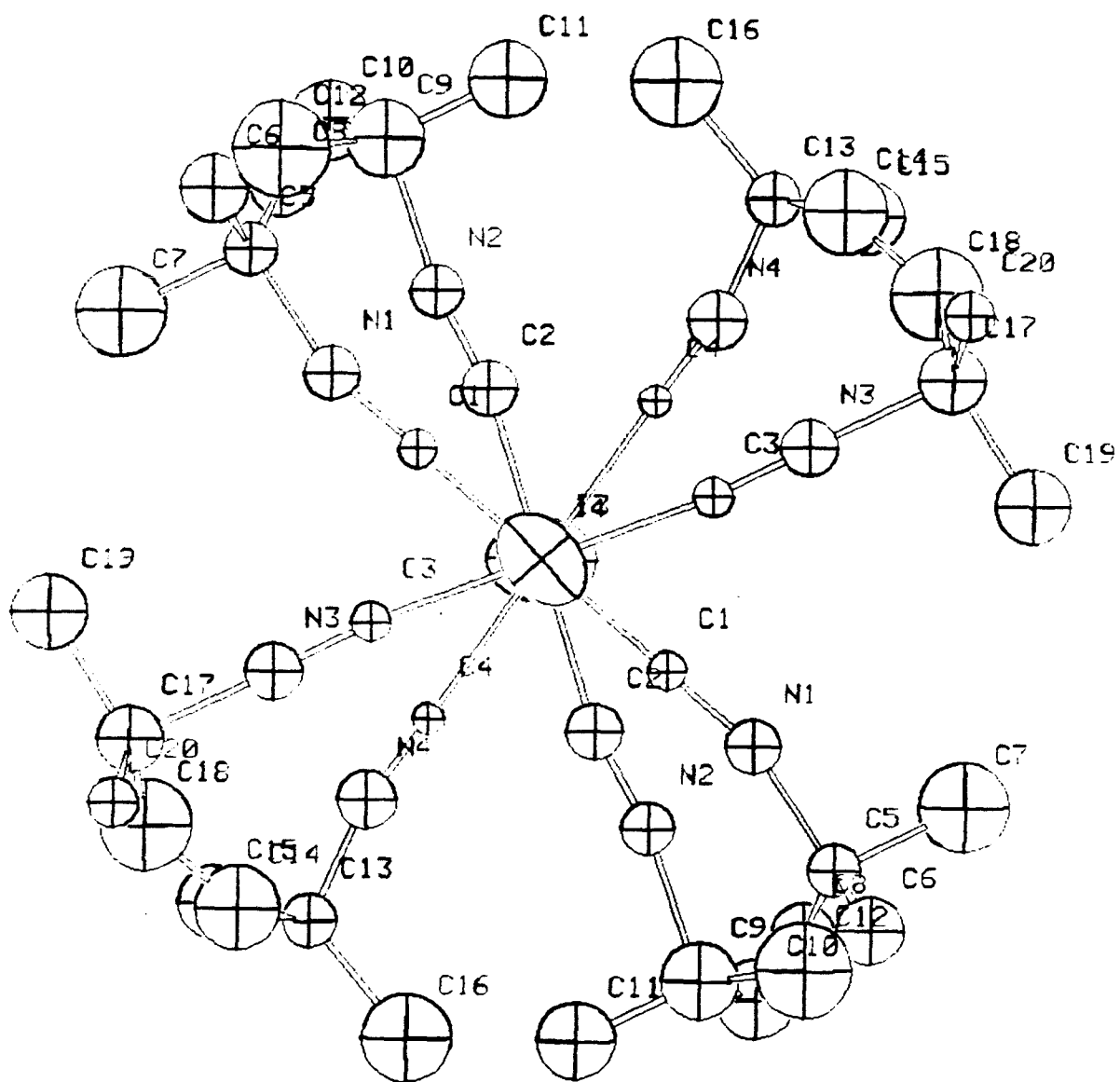


Table 9.

<u>Dimer Distances (Å)</u>					
Ir(1)-Ir(2)	2.803(4)	2.802	C(1)-N(1)	1.180(42)	
Ir(1)-I(4)	2.723(6)	2.726	C(2)-N(2)	1.106(43)	1.158
Ir(2)-I(3)	2.730(6)		C(3)-N(3)	1.211(45)	
			C(4)-N(4)	1.134(63)	
Ir(1)-C(1)	1.902(41)		N(1)-C(5)	1.597(43)	
Ir(1)-C(4)	2.106(66)	1.971	N(2)-C(9)	1.663(59)	1.573
Ir(2)-C(2)	2.030(30)		N(3)-C(17)	1.564(47)	
Ir(2)-C(3)	1.845(45)		N(4)-C(13)	1.468(56)	
C(5)-C(6)	1.593(48)		C(5)-C(7)	1.544(50)	
C(9)-C(10)	1.503(57)	1.521	C(5)-C(8)	1.407(49)	
C(13)-C(14)	1.407(55)		C(9)-C(11)	1.538(62)	
C(17)-C(18)	1.583(50)		C(9)-C(12)	1.466(58)	1.488
C(14)-C(18)	1.432(52)	1.420	C(13)-C(15)	1.538(55)	
C(6)-C(10)	1.408(54)		C(13)-C(16)	1.480(61)	
			C(17)-C(19)	1.546(51)	
			C(17)-C(20)	1.387(47)	

Dimer Angles in Ir(CN)₈I₂ Unit

(in degrees)

I(4)Ir(1)-Ir(2)	180.0(0)
I(3)Ir(2)-Ir(1)	180.0(0)
Ir(2)-Ir(1)-C(1)	91.3(1.1)
Ir(2)-Ir(1)-C(4)	93.3(1.5)
Ir(1)-Ir(2)-C(2)	89.4(.9)
Ir(1)-Ir(2)-C(3)	90.7(1.2)
Ir(1)-C(1)-N(1)	170.5(3.5)
Ir(1)-C(4)-N(4)	165.9(5.7)
Ir(2)-C(2)-N(2)	164.5(3.8)
Ir(2)-C(3)-N(3)	171.3(3.9)
C(1)-Ir(1)-C(4)	88.7(1.9)
C(2)-Ir(2)-C(3)	96.9(1.6)

other Ir(II)-Ir(II) systems.¹⁰⁴⁻¹⁰⁶ Interestingly, the value is very similar to the rhodium-rhodium distance (2.77 Å) found in $\text{Rh}_2(\text{TMB})_4\text{Cl}_2^{2+}$.

Better models for the disordered solvent molecules, application of an absorption correction, and elimination of some of the low angle data are important future considerations. It is viewed unlikely, however, that this will result in much change in the overall quality of the structure, and therefore large changes in the important features (*i.e.* iridium-iridium distance and ligand conformation) are not expected. A list of atomic coordinates and structure factors will be made available as supplementary material.

APPENDIX

In this section, preliminary results on another class of binuclear iridium(I) complexes are reported. This work is being carried out in collaboration with Stephen Stobart who has supplied us with samples of the compounds. The general formula for these complexes is $[\text{Ir}_2\text{L}_1\text{L}_2\text{Pz}']_2$, where L_1 and L_2 are π -acceptors (*e.g.* CO, PPh_3 , and C_2H_4) and Pz' is either a pyrazolyl or substituted pyrazolyl. The structure of $[\text{IrCOD Pz}]_2$ ¹⁰⁷ has recently been determined and is shown in Figure 28. The molecule has C_{2v} symmetry with each iridium atom coordinated by four ligands, distributed in a square planar fashion. The intermetallic distance is 3.2 Å.

Stobart has demonstrated that these complexes react with a variety of small molecules, including halogens, hydrogen and substituted acetylenes.^{107,108} All of these substrates add across the two iridium centers, forming symmetric adducts. The fact that the substrate molecules can interact with both metal centers probably accounts for the more diverse reactivity exhibited as compared to $\text{Ir}_2(\text{TMB})_4^{2+}$.

An MO diagram is shown in Figure 29. In this particular diagram, C_{2v} symmetry is assumed; however, the ordering of the d orbitals in a lower symmetry molecules will be the same, only the symmetry designations will be

Figure 28. ORTEP of [Ir PZ COD]₂.

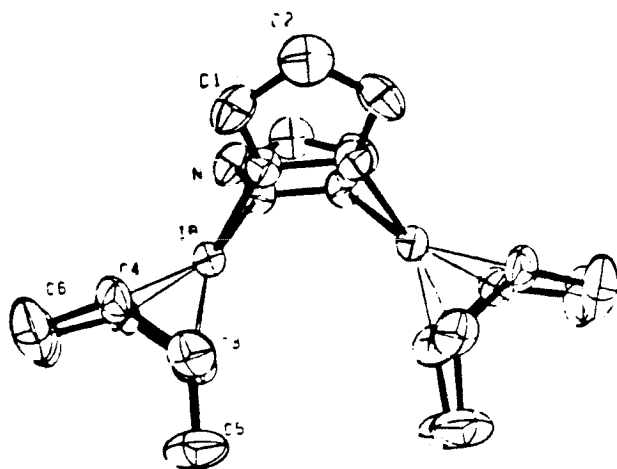
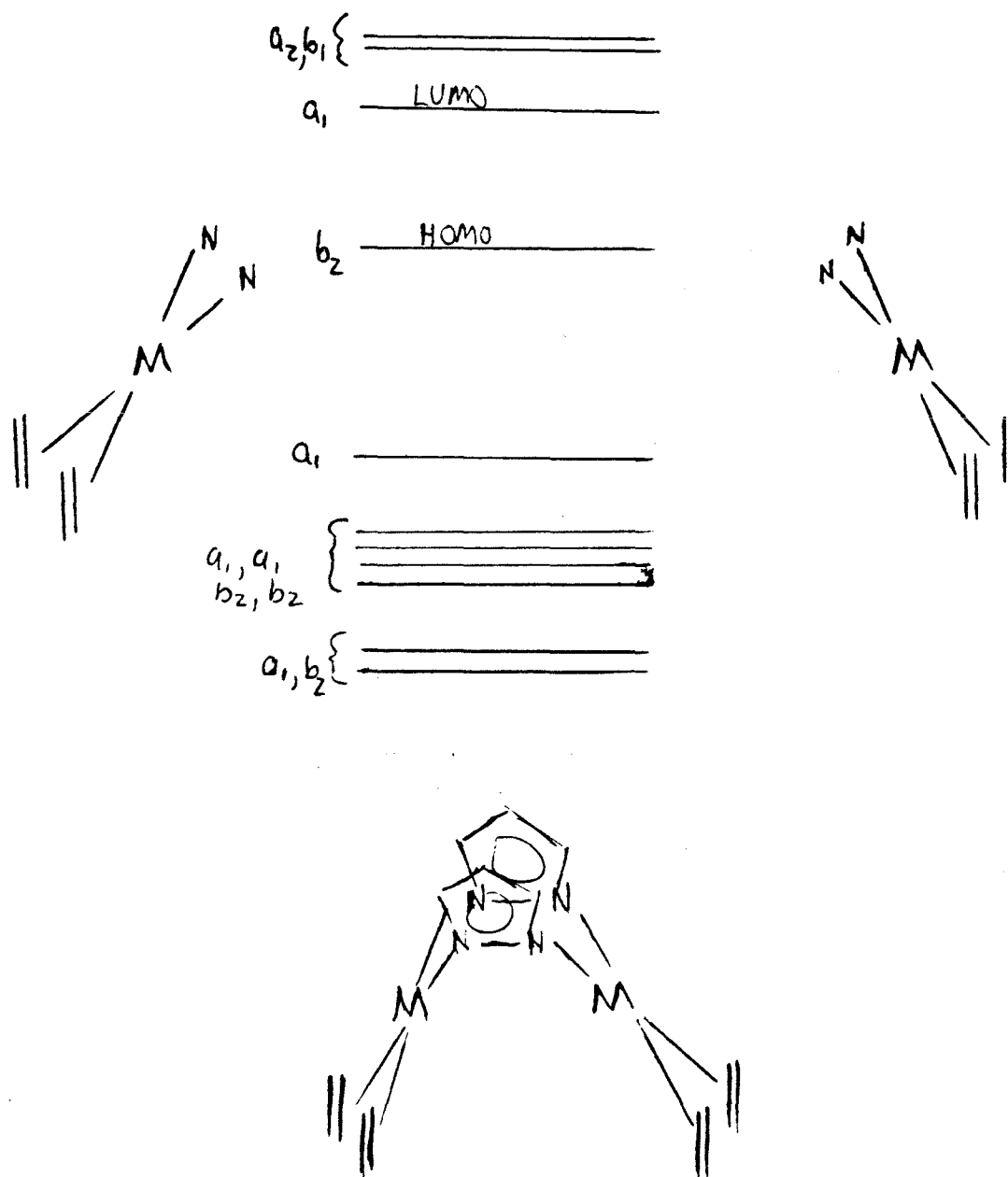


Figure 29. Molecular orbital diagram for $[\text{Ir PZ COD}]_2$ or $[\text{Ir Me}_3\text{PZ COD}]_2$.

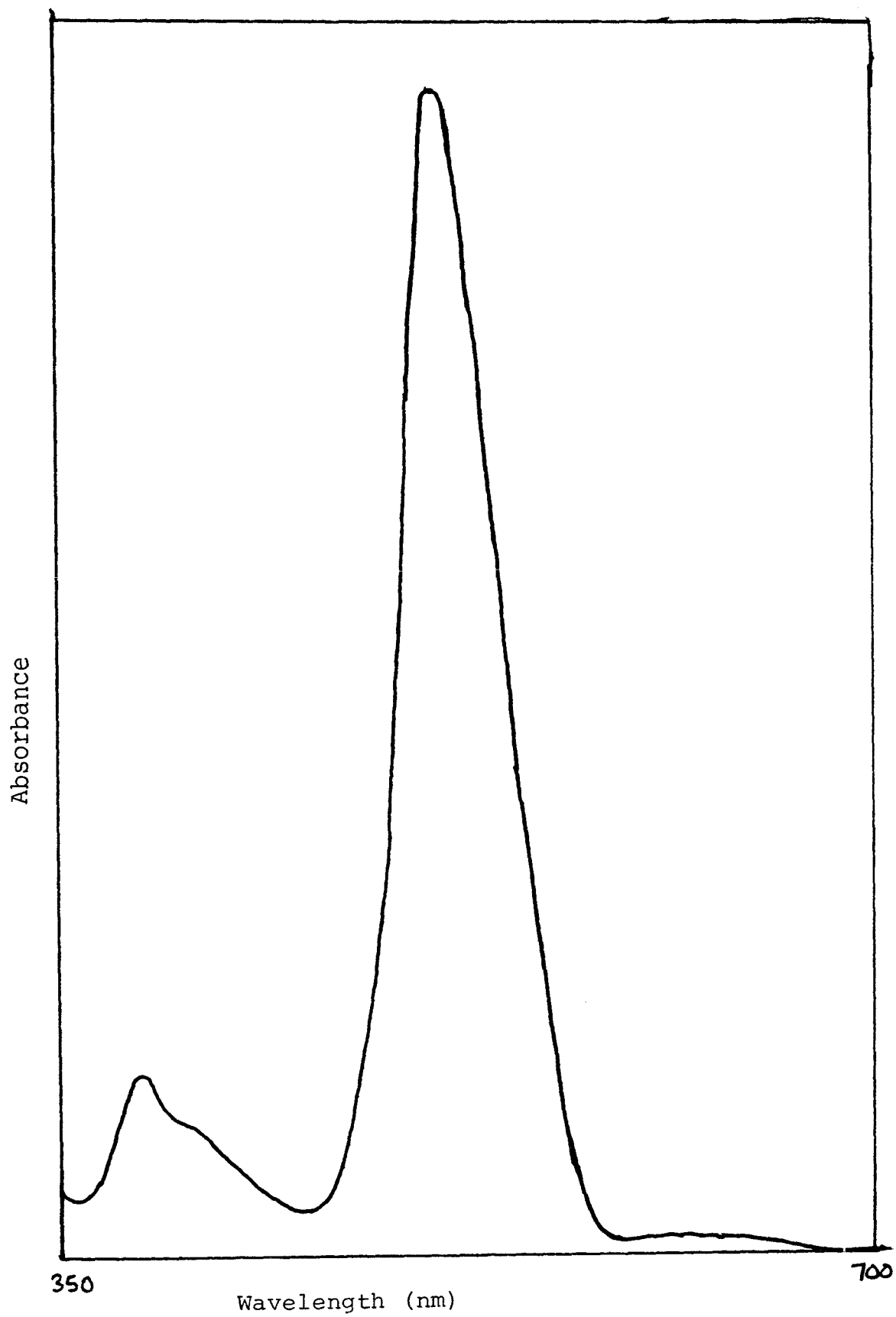


different. Interestingly, the metal-metal interaction can have an angular dependence, as well as a distance dependence. The binuclear complex which has been examined in the most detail is $[\text{Ir}(\text{Me}_3\text{PZ})\text{COD}]_2$. The electronic spectrum of this complex is shown in Figure 30. The intense band at 529 nm is logically assigned to the $A_1(^1A_1) \rightarrow B_2(^1B_2)$ ($d_{z^2}^* \rightarrow \text{Pz}$) transition; the weak feature at lower energy can be assigned to the corresponding triplet transition, $A_1(^1A_1) \rightarrow B_2(^3B_2)$.

The spectra of all the binuclear complexes are qualitatively quite similar. Substitution of the pyrazolyl ligand results in slight changes in the absorption maxima of the lowest energy intense feature (*e.g.* $[\text{IrPZCOD}]_2$; $\lambda_{\text{max}} \sim 498$ nm, $[\text{Ir}(\text{CF}_3\text{PZ})\text{COD}]_2$; $\lambda_{\text{max}} = 518$ nm; $[\text{Ir}(\text{Me}_3\text{PZ})\text{COD}]_2$; $\lambda_{\text{max}} = 530$ nm). On the other hand, changes in the ancillary ligands result in considerably larger changes. For instance, the lowest energy intense feature in $[\text{IrPZ}(\text{CO})-(\text{PPh}_3)]_2$ is at 442 nm. Since the metal-metal distance in this complex is .1 Å shorter than $[\text{IrPZ COD}]_2$, clearly, the energy of the transition is not solely determined by intermetallic distance.

All of the binuclear complexes of this type exhibit both phosphorescence and fluorescence at room temperature. The lifetimes of the two complexes examined in the most detail $[\text{IrPZ CO PPh}_3]_2$ and $[\text{IrMe}_3\text{PZ}(\text{COD})]_2$ are strongly dependent on temperature. The corrected luminescence

Figure 30. Absorption spectrum of $[\text{Ir}(\text{Me}_3\text{Pz})\text{COD}]_2$



spectra of these complexes are shown in Figures 31 and 32. The spectral data are listed in Table 10. Curiously, while the emission spectrum of $[\text{Ir}_2\text{Me}_3\text{PZ COD}]_2$ changes very little, the spectrum of $[\text{Ir PZ CO PPh}_3]_2$ changes considerably. The reason for this difference is not clear and warrants further investigation. One possibility is that nearby ligand field states play a crucial role in deactivating the excited state. A crude estimate of the radiative lifetime based on the oscillator strength of the $A_1(^1A_1) \rightarrow B_2(^3B_2)$ transition,¹⁰⁹ assuming quantum efficiency ($\bar{\phi}_{p=1}$) for the phosphorescence, predicts a value of 3.8 μs in satisfactory agreement with the low temperature value of 1.9 μs considering the approximations involved. The long-lived excited state is a powerful reductant and is quenched at diffusion controlled by a variety of pyridinium salts. These systems are ideally suited for electron transfer studies. The prospect of channeling the energy provided by a photon to enhance reactivity is quite exciting. For example, with the appropriate ligands the excited state may be capable of activating carbon-hydrogen bonds. Another possibility would be to sensitize organic molecules, such as diazoalkanes to induce nitrogen extrusion with visible light. One can envision the two nitrogens of the substrate interacting with the two metal centers, an ideal situation for energy or electron transfer.

Figure 31. Emission spectra of $[\text{Ir}(\text{Me}_3\text{PZ})\text{COD}]_2$ at room temperature.

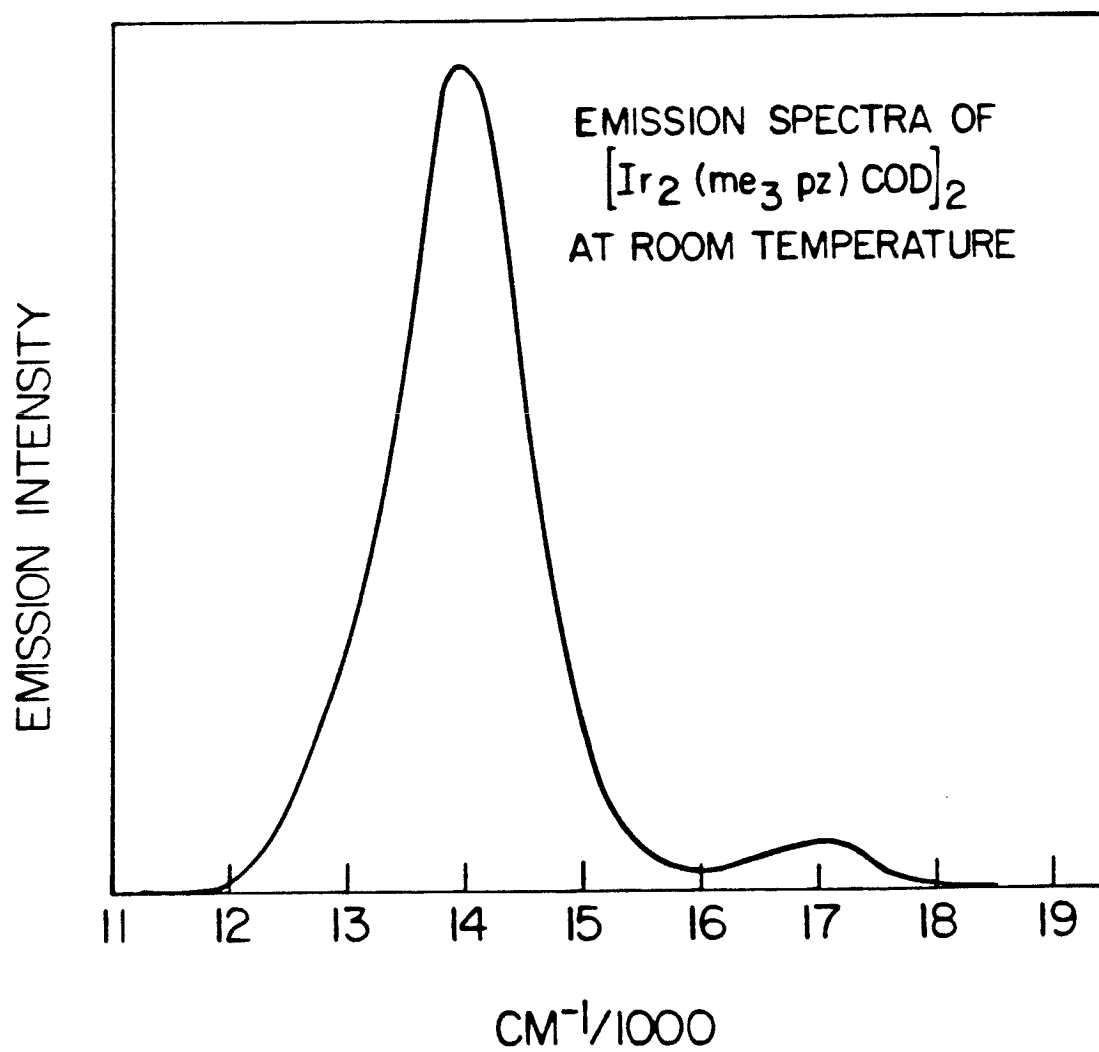


Figure 32. Emission spectra of $[\text{Ir}(\text{PZ CO})\text{PPh}_3]_2$ at room temperature

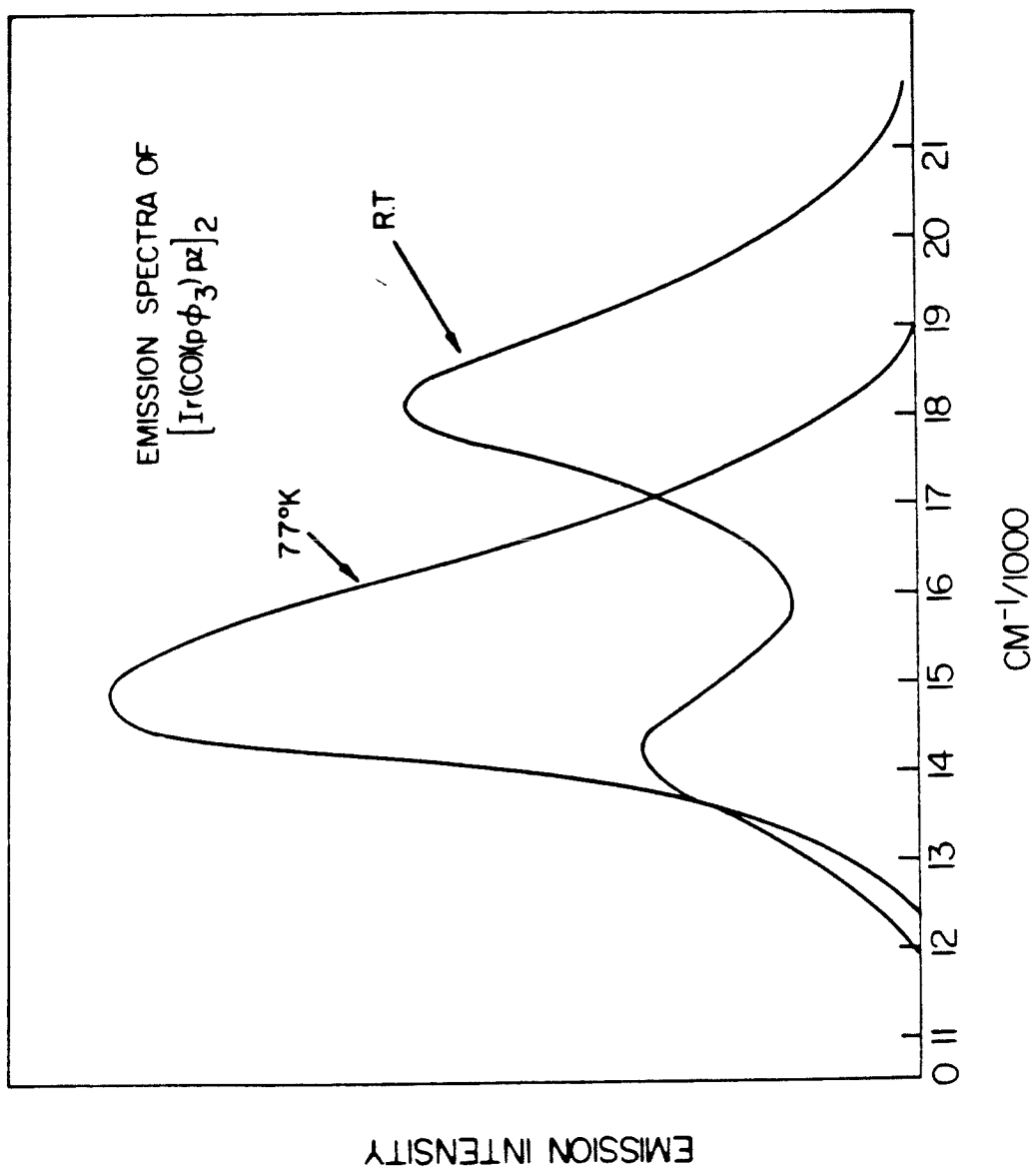


Table 10.

	λ_{max} (nm)	ϵ ($\text{cm}^{-1}\text{M}^{-1}$)	Emission Maxima (nm)			Lifetimes		
			Fluorescence Phosphorescence			Phosphorescence		
			298°K	77K	298	77K	τ 77	τ 298
[IrMe ₃ PZCOD] ₂	627	189	590	-	704	704	1.84 μs	98.5 ns
	529	10,240						
	422	1,194						
	390	1,788						
	324	4,448						
	276	10,375						
[IrPZCODPPH ₃] ₂	442	9,400	552	-	672	701	8.0 μs	< 8 ns
	348	8,600						
	283	4,100						

Unraveling the photophysics and photochemistry of these complexes are certainly worthwhile endeavors. The first step in understanding the photophysics will be to explore the lifetime's dependence on temperature. Also, the lifetimes should be determined in solids, films, and other solvents to determine media effects. Quantum yields should also be measured. Since these molecules are neutral, gas phase studies are also possible. This system affords a rather rare opportunity to examine complex transition metal complexes in molecular beams.

REFERENCES AND NOTES

1. J.S. Miller and A.J. Epstein, *Prog. Inorg. Chem.* 20, 1, 1976.
2. L. Interrante in "Extended Interactions Between Metal Ions in Transition Metal Complexes", L. Interrante, ed., American Chemical Society, Washington, D.C., 1974.
3. C.D. Cowman and H.B. Gray, *Inorg. Chem.* 15, 2823, 1976.
4. C.D. Cowman, C.J. Ballhausen, and H.B. Gray. *J. Amer. Chem. Soc.*, 95, 7873, 1973.
5. K. Kawakami, M. Haga, and T. Tanaka, *J. Organomet. Chem.* 60, 363, 1973.
6. L. Malatesta and F. Bonati, *Isocyanide Complexes of Metals*, Wiley, New York, 1969.
7. K.R. Mann, J.G. Gordon III, and H.B. Gray, *J. Amer. Chem. Soc.* 97, 3553, 1975.
8. K. R. Mann, N.S. Lewis, R.M. Williams, H.B. Gray, and J.G. Gordon II, *Inorg. Chem.* 17, 828, 1978.
9. J.D. Buhr, unpublished results.
10. K.R. Mann, J.R. Thich, R.A. Bell, C.L. Coyle, and H.B. Gray, *Inorg. Chem.* 19, 2462, 1980.
11. K.R. Mann, R.A. Bell, and H.B. Gray, *Inorg. Chem.* 18, 2671, 1979.
12. A.W. Maverick, Ph.D. Thesis, California Institute of Technology, 1977.

13. N.S. Lewis, K.R. Mann, J.G. Norman and H.B. Gray, *J. Amer. Chem. Soc.* 98, 7461, 1976.
14. V.M. Miskowski, T. Loehr, and H.B. Gray, unpublished results.
15. K.R. Mann, N.S. Lewis, V.M. Miskowski, D.K. Erwin, G.S. Hammond, and H.B. Gray, *J. Amer. Chem. Soc.* 99, 5525, 1977.
16. K.R. Mann and H.B. Gray, *Adv. Chem. Ser.* 173, 225, 1979.
17. V.M. Miskowski, C.S. Sigal, K.R. Mann, H.B. Gray, S.J. Milder, G.S. Hammond, and P.R. Rasason, *J. Amer. Chem. Soc.* 101, 4383, 1979.
18. K.R. Mann, M.J. DiPierro, and T.P. Gill, *J. Amer. Chem. Soc.* 102, 3965, 1980.
19. I.S. Sigal, K.R. Mann, and H.B. Gray, *J. Amer. Chem. Soc.* 102, 7252, 1980.
20. I.S. Sigal and H.B. Gray, *J. Amer. Chem. Soc.* 103, 2220, 1981.
21. V.M. Miskowski, G.L. Nobinger, D.S. Kligei, G.S. Hammond, N.S. Lewis, K.R. Mann, and H.B. Gray, *J. Amer. Chem. Soc.* 100, 485, 1978.
22. S.J. Milder, R.A. Goldbeck, D.S. Kliger, and H.B. Gray, *J. Amer. Chem. Soc.* 102, 6761, 1980.
23. S.F. Rice, Ph.D. Thesis, California Institute of Technology, 1972.

24. S.F. Rice and H.B. Gray, *J. Amer. Chem. Soc.* 103, 1594, 1981.
25. A.W. Adamson and P.D. Fleischauer, *Concepts of Inorganic Photochemistry*, Wiley-Interscience, New York, 1975.
26. M. Chou, T.L. Netzel, M. Okumura, and N. Sutin, *J. Amer. Chem. Soc.* 102, 1809, 1980.
27. B. Brunschwig and N. Sutin, *J. Amer. Chem. Soc.* 100, 7568, 1978.
28. E.M. Kober, B.P. Sullivan, J.W. Dressick, J.V. Casper, and T.J. Meyer, *J. Amer. Chem. Soc.* 102, 1383, 1980.
29. D.D. Perrin, W.L.F. Armarego and D.R. Perrin, *Purification of Laboratory Chemicals*, Pergamon Press, New York, 1980.
30. W.P. Weber, G.W. Oobel, and I.K. Ugi, *Angew. Chem. Int. Ed. Engl.* 11, 350, 1972.
31. J.L. Herde, J.C. Lambert, and C.V. Seroff, *Inorg. Synth.* 15, 18, 1974.
32. G.L. Geoffroy, M.G. Bradley, and M.E. Keeney, *Inorg. Chem.* 17, 777, 1978.
33. D.G. Nocera, Candidacy Report, California Institute of Technology, 1980.
34. R.J. Watts, J.J. van Houfen, *J. Amer. Chem. Soc.* 98, 4853, 1976.
35. J.N. Demas and F.G. Crosby, *J. Phys. Chem.* 75, 991, 1971.

36. R. Brady, B.R. Flynn, G.L. Geoffroy, H.B. Gray, J. Peone, Jr., and L. Vaska, *Inorg. Chem.* 15, 1485, 1976.
37. G.L. Geoffroy, H. Isci, J. Litrenti, and W.R. Mason, *Inorg. Chem.* 16, 1950, 1977.
38. N.J. Turro, *Modern Molecular Photochemistry*, Benjamin/Cummings, Menlo Park, 1978.
39. H.B. Gray and C.J. Ballhausen, *J. Amer. Chem. Soc.* 85, 200, 1963.
40. W.M. Bedford and G. Rouschias, *J. Chem. Soc. Chem. Commun.* 1224, 1972.
41. A.R. Sanger, *J. Chem. Soc. Dalton Trans*, 120, 1977.
42. L. Vaska and D.L. Catone, *J. Amer. Chem. Soc.* 88, 53, 5324, 1966.
43. V. Balzani and V. Carassiti, *Photochemistry of Coordination Compounds*, Academic Press, London, 1970.
44. W.A. Fordyce, K.H. Pool and G.A. Crosby, submitted for publication.
45. B.K. Teo, A.P. Ginsberg, and J.C. Calabrese, *J. Amer. Chem. Soc.* 98, 3027, 1976.
46. J.S. Najdzionek, Ph.D. Thesis, California Institute of Technology, 1982.
47. A source of error in this estimation results from the fact that the electron transfer occurs at an intermediate geometry between $\text{Ir}_2(\text{TMB})_4^{2+}$ and $\text{Ir}_2(\text{TMB})_4^+$, unfortunately the magnitude of this distortion is unknown.

48. D.G. Nocera has noted similar results for the back electron transfer rate with $\text{Re}_2\text{Cl}_8^{2-}$.
49. C.M. Che and H.B. Gray, unpublished results.
50. G. W. Parshall, *Homogeneous Catalysis*, Wiley-Interscience, New York, 1980.
51. A.D. English and T. Herskovits, *J. Amer. Chem. Soc.* 99, 1648, 1977.
52. A.H. Janowicz and R.G. Bergman, *J. Amer. Chem. Soc.* 104, 352, 1982.
53. R.H. Crabtree, M.F. Mellea, J.M. Mihelcic, and J.M. Quick, *J. Amer. Chem. Soc.* 99, 1648, 1977.
54. J. Kiwi, K. Kalyanasundoram, and M. Grätzel, *Structure and Bonding* 49, 37, 1982.
55. J. Basset, L.J. Farrugia, F.G.A. Stone, *J. Chem. Soc. Dalt.*, 1789, 1980.
56. J. Halpern and M. Pribonić, *Inorg. Chem.* 9, 2616, 1970.
57. W.S. Matthews, J.E. Bares, J.E. Bartmess, F.G. Bondwell, F.J. Cornforth, G.E. Drucker, Z. Margolin, R.J. McCallum, G.J. McCallum and N.R. Vanier, *J. Amer. Chem. Soc.* 97, 7006, 1975. And refs. therein.
58. H. Schmidbaur, *Acc. Chem. Res.* 10, 62, 1975.
59. A. Balch, *J. Amer. Chem. Soc.* 98, 8049, 1979.
60. G. Overend and J.R. Scherer, *J. Chem. Phys.* 32, 1289, 1960.
61. *International Tables for X-Ray Crystallography*, Kynoch Press, Birmingham, Vol. I, 144, 1962.

63. G.L. Geoffrey and M.S. Wrighton, *Organometallic Photochemistry*, Academic Press, New York, 1979.
64. R.A. Levenson, H.B. Gray, and G.P. Ceasar, *J. Amer. Chem. Soc.* 92, 3053, 1970.
65. L.I.B. Haines, D. Hopgood and A.J. Poë, *J. Chem. Soc. A* 421, 1968.
66. D. Dewitt, J.P. Fawcett, A.J. Poë, and M.V. Twigg, *Coord. Chem. Rev.* 8, 81, 1972.
67. E. Dorm, *Chemical Communications*, 466, 1971.
68. E. Dorm, *Acta Chem. Scand.* 21, 2745, 1967.
69. B. Lindh, *Acta Chem. Scand.* 21, 2745, 1967.
70. M.M. Olmstead and A.L. Balch, *J. Organomet. Chem.* 148, C15, 1978.
71. V.M. Miskowski and H.B. Gray, unpublished results.
72. L.A. Woodward, *Phil. Mag.*, 18, 823, 1934.
73. C.S. Kraihanzel and F.A. Cotton, *Inorg. Chem.* 2, 533, 1963.
74. F.A. Cotton, *Chemical Applications of Group Theory*, Wiley-Interscience, New York, 1971.
75. D.M. Adams, M. Goldstein, and E.F. Mooney, *Trans. Faraday Soc.* 59, 2228, 1963.
76. G. Herzberg, *Infrared and Raman Spectra*, Vol. 2, Van Nostrand Reinhold, New York, 1950, pp. 180-189.
77. J.R. Durig, K.K. Lau, G. Nagarajan, M. Walker, and J. Bragin, *J. Chem. Phys.* 50, 2130, 1969.
78. C.M. Che, H.B. Gray, and M. Roundhill, submitted for publication.

79. M.A. Filomena Dos Remadios Pinto, P.J. Sadler, S. Naible, M.R. Sanderson, and A. Subbiah, *J. Chem. Soc. Chem. Commun.* **13**, 1980.
80. C.O. Quicksall and T.G. Spiro, *Inorg. Chem.* **8**, 2363, 1969.
81. M.F. Bailey and L.F. Dahl, *Inorg. Chem.* **4**, 1140, 1965.
82. L.F. Dahl, E. Ishishi, and R.E. Rundle, *J. Chem. Phys.* **26**, 7150, 1957.
83. L. Butler and T.P. Smith, unpublished results.
84. L. Butler, private communication.
85. T.P. Smith and B. Santarsiero. unpublished results.
86. L. Loerh, private communication.
87. P.M. Morse, *Phys. Rev.* **34**, 57, 1929.
88. R.M. Badger, *J. Chem. Phys.* **2**, 128, 1934.
89. R.M. Badger, *J. Chem. Phys.* **3**, 710, 1935.
90. C.H.D. Clark, *Phil. Mag.* **19**, 476, 1935.
91. J.A. Ladd, W.J. Orville-Thomas and B.C. Cox, *Spectrochim. Acta.* **20**, 1971, 1964.
92. J.B. Hendrickson, *J. Amer. Chem. Soc.* **83**, 4537, 1961.
93. Chemical shifts are measured relative to the solvent chemical shifts; CH₂Cl₂ (5.32 ppm) and CH₃CN (1.87 ppm).
94. W.W. Paudler, *Nuclear Magnetic Resonances*, Allyn and Bacon, 173, 1971.
95. D. Kost, E.H. Carlson, and M. Raban, *J. Chem. Soc., Chem. Comm.*, 656, 1971.

96. F.A.L. Anet, M. Ahmed, and L.D. Hall, *Proc. Chem. Soc.* 145, 1964.
97. E.C. Lim, *Excited States*, Vol. 1, Academic Press, New York, 257, 1974.
98. W.J. Moore, *Physical Chemistry*, Prentice-Hall, Inc., Englewood Cliffs, New Jersey, 381, 1972.
99. D.T. Cromer and J.T. Weber, *Acta Crystallogr.* 18, 104, 1965.
100. *International Tables for X-Ray Crystallography*, Kynoch Press, Birmingham, Vol. III, 201, 1962.
101. R.F. Stewart, E.R. Davidson, and W.T. Simpson, *J. Chem. Phys.* 42, 3175, 1965.
102. D.J. Hodson and J.A. Ibers, *Inorg. Chem.* 8, 1282, 1969.
103. V.G. Albano, R.L. Bellow, and M. Sansoni, *Inorg. Chem.* 8, 298, 1969.
104. M. Angoletta, G. Ciani, M. Manassero, and M. Sansoni, *J. Chem. Soc., Chem. Commun.*, 182, 1979.
105. R.H. Crabtree, H. Felkin, G.E. Morris, T.J. King, and J.A. Richards, *J. Organomet. Chem.* 113, C7, 1976.
106. R. Mason, I. Sptofte, S.D. Robinson, and M.F. Uttley, *J. Organomet. Chem.* 46, C61, 1972.
107. K.A. Beveridge, G.W. Bushnell, K.R. Dixon, D.T. Eddie, S.R. Stobart, J.L. Atwood, and M.J. Zaworotko, *J. Amer. Chem. Soc.* 104, 920, 1982.

108. A.W. Coleman, D.T. Eadie, S. Stobart, M.J. Zaworotko, and J.L. Atwood, *J. Amer. Chem. Soc.* 104, 922, 1982.
109. S.J. Strickler and R.A. Berg, *J. Chem. Phys.* 37, 814, 1962.